Dynamics on Spatially Extended Systems

Promit Moitra

A thesis submitted in partial fulfillment of

the requirements for the degree of Doctor of Philosophy

Department of Physical Sciences

Indian Institute of Science Education and Research (IISER) Mohali

May, 2019

Certificate of Examination

This is to certify that the dissertation titled *"Dynamics on Spatially Extended Systems"* submitted by **Mr. Promit Moitra** (Reg. No. MP12012) for the partial fulfillment of Doctor of Philosophy programme of the Institute, has been examined by the thesis committee duly appointed by the Institute. The committee finds the work done by the candidate satisfactory and recommends that the report be accepted.

Dr. Ananth Venkatesan Dr. Kamal Priya Singh Professor Sudeshna Sinha

(Supervisor)

Declaration

The work presented in this dissertation has been carried out by me under the guidance of Prof. Sudeshna Sinha at the Indian Institute of Science Education and Research Mohali.

This work has not been submitted in part or in full for a degree, a diploma, or a fellowship to any other university or institute. Whenever contributions of others are involved, every effort is made to indicate this clearly, with due acknowledgment of collaborative research and discussions. This thesis is a bona-fide record of original work done by me and all sources listed within have been detailed in the bibliography.

Promit Moitra

(Candidate)

In my capacity as the supervisor of the candidate's doctoral thesis, I certify that the above statements by the candidate are true to the best of my knowledge.

Professor Sudeshna Sinha

(Supervisor)

Acknowledgements

Seven years is a long time. Especially going from 21 to 28, there is a lot of growing up to do. So first and foremost, I am thankful that the journey has been one to cherish. And it wouldn't have been, if not for the people I met along the way.

I am extremely thankful to Prof. Sudeshna Sinha, for her incredible patience and constant support in my academic life. I have learned my entire approach to research from illuminating and insightful discussions with her. She has been a source of inspiration in dire times, and she has opened doors to wonderful opportunities which I greatly appreciate. I honestly cannot imagine a better guide than Sudeshna ma'am for taking my first steps in academics.

I thank Manaoj Aravind V., my oldest friend and neighbour. I am grateful to him for giving me quite a few much needed timely reality checks. But most of all, I thank him for turning the sad into funny-sad.

From the first couple of years, I have a lot of gratitude for my batchmates Ashish, Srikant, Pankaj and Imran, for keeping me grounded and on my toes. I thank Zeeshan, Vikesh and Shiv, for keeping my reading habit and the debater in me alive and kicking. I thank the MS09 batch for the unforgettable experience of organizing the first cultural fest. I especially thank Vrinda, for questioning every one of my thoughts and words, letting me look beyond them.

I thank the MS10 batch for the mad times at and around the seventh floor of H5. We shared courses as well, but the most memorable times were between the exams. I thank Neeeraj, Manas and Arul, for everything from music to arguments (and more recently, yoga). I thank Geetananda, for teaching me the art of zen, and Nishant Malik, for practising the art of anarchy. I thank Tj, for being a rock right till my last few days here.

I thank Anubhuti, for showing me how people can stay friends while everything around them changes. I thank Priyanka, for being the reason for my best days here, and being there throughout.

I thank the colourful patchwork of old and new friends since then - Himanshu, Ruchika, Panda, Sanjay, Dewra, Divanshu and especially Soumitro da, for showing me the true meaning of the mountain soul. I thank Saurav, for epic times at Bob's cafe.

I thank the juniors, across batches from MS12 to MS18, for making the last couple

of years unexpectedly exciting and dynamic. I thank our band, Somak, Varun, Nilotpal and Parth, for bringing one of my childhood dreams to life. I thank the debsoc group, especially Misha for being the convener and bringing it back to life. I thank Dhruv and Deesha for their constant friendship.

I thank IISER Mohali for the infrastructure and funding for the duration of my stay, being the platform of this enriching experience. I sincerely hope the institute continues to disseminate the kind of experience I had to future generations of researchers.

I thank my parents for being the material and emotional safety net I can fall back on in times of crisis. Without that kind of support, such uncertain endeavours like research cannot be undertaken, and I consider myself blessed for having Pallav Moitra and Runa Moitra as my Baba and Ma.

Promit

Preface

The study of dynamical systems can be broadly classified in terms of the spatial and temporal characteristics of the system under consideration. Mathematical models of systems can be continuous or discrete, in both space and time. If the description of the system's behaviour involves many connected dynamical elements, then apart from the individual dynamics of each element, the form and topology of coupling between these elements becomes an important consideration as well. Such collective descriptions of systems have become fundamental in order to model (and perhaps predict) the emergent behaviour of real-world complex systems, which consist of interacting dynamical units, which constitute many physical, biological, chemical or socially engineered systems, ranging from ecosystems to social networks, from atmospheric flows to traffic flows, from infection spreading through a population to cascading failures on a power grid. The research work in this thesis provides analysis and characterization of emergent behaviour, arising from the interplay of local dynamics and the form and topology of coupling, in such connected dynamical systems. Specifically, the spatially extended systems under consideration in this thesis are motivated by biological phenomena. Thus the work of this thesis is inter-disciplinary in nature.

In the first three sections of the thesis, the dynamics of infection spreading across a population is modeled, and the emergence of persistent infection in a closed region is explored. In this system, the disease progression of an individual is given by the SIRS model, with an individual becoming infected on contact with another infected individual. Specifically, the disease cycle consists of three compartments of discrete states: the susceptible state (S), which is an absorbing phase; the infected states (I), which triggers any nearby susceptible individuals to become infected as well; and the refractory states (R), which is a temporarily immune phase. An individual remains susceptible until infected by a nearest neighbour, and then goes through the cyclical sequence of states described above, returning to the susceptible state. Such excitation-relaxation dynamics can also be used to model systems arising in various other contexts, such as neural or cardiac tissues.

The persistence of contagion is qualitatively and quantitatively investigated, under increasing heterogeneity in the partitioning of the population into different disease compartments, as well as increasing heterogeneity in the phases of the disease among individuals within a compartment. It is observed that when the initial population is uniform, consisting of individuals at the same stage of disease progression, infection arising from a contagious seed does not persist. However when the initial population consists of ran-

domly distributed refractory and susceptible individuals, a single source of infection was found to cause sustained infection in the population. It is concluded that heterogeneity facilitates the de-synchronization of the phases in the disease cycle of the individuals, leading to steady state dynamics, or persistence, of the infection in the population. It is also observed that the average extent of the window of persistence of infection depends on the degree of heterogeneity in the initial composition of the population.

The next aspect that is focused on is the *role of synchronization in the persistence of infection* in such a closed region. The following key result is observed: higher degree of synchronization in the individual states, both globally in the population and locally in the neighbourhoods, hinders persistence of infection. Importantly, it is demonstrated that early short-time asynchrony appears to be a consistent precursor to future persistence of infection, and can potentially provide valuable early warnings for sustained contagion in a population patch. It is then found that *transient synchronization can help anticipate the long-term persistence of infection*. It is also found that when the range of influence of an infected individual is wider, the infection persists for a smaller window of initially infected individuals. This counter-intuitive observation can also be understood through the relation between synchronization and infection burn-out.

In a subsequent study, it is established that a population structured into communities yields a persistently infected sub-population, in contradistinction to an equivalent population where the same initial fractions of susceptible, refractory and infected individuals are homogeneously distributed in space. So populations where the initial distribution of the disease cycle is strongly compartmentalized leads to persistent infection in the complete region. Even after transience, the patterns of disease spreading in the two communities may be completely dissimilar, even though both communities settle down to the same average infected sub-population size. The time evolution of the total number of infected individuals in the two communities displays distinct periodic wave forms, with different amplitudes, but same frequency.

In the last section of the thesis we study a collection of populations modeled by the prototypical chaotic Ricker map. Such chaotic maps are widely utilized to model the population growth of species with non-overlapping generations. The feedback received by each population patch is modeled to be influenced by the local mean field of its neighbourhood. Specifically, we separate the terms of the dynamical map into two parts: the growth term and the regulation term. The growth term consists of a positive feedback, and the regulation term contains a negative feedback, from the variable that represents the population at each time step, leading to the characteristic unimodal shape of such

population maps. Now, instead of the commonly-used diffusive interactions among coupled populations, here we consider networks of populations where the rate of population growth at a site is influenced by neighbouring populations. We find that such parametrically coupled networks of populations yield very interesting and non-intuitive collective behaviour.

The dynamics and distribution of the local populations, as well as the total biomass, in the coupled system described above, is examined. The significant observation is the following: When the range of coupling is sufficiently large, namely when enough neighbouring populations influence the growth rate of a population, the system yields remarkably large biomass values that are very far from the mean. These extreme events are relatively rare and uncorrelated in time. It is also found that at any point in time, exceedingly large population densities emerge in a few patches, analogous to an extreme event in space. It is important to note that the isolated dynamics of an individual Ricker map does not result in extreme values, even asymptotically. These results indicate a *new mechanism in coupled chaotic systems that naturally yield extreme events in both time and space.*

The study above presents further scope of research on the mechanisms that generate extreme events in networked systems, by implementing different forms of coupling. Complex networks such as ecosystems may have connections between individual dynamical constituents, which are not obvious, perhaps influencing each other in indirect ways, such as via the environment, or in terms of resource availability. Sudden population explosions and extinctions have been widely observed, but the attempts to model such phenomena have largely been concentrated on refining the single species model in isolation. This study provides the insight that the emergent behaviour of a unit should be considered, not only in terms of its isolated dynamics, but also as a result of the collective influence of its neighbourhood of similar dynamical units.

In summary, the problems explored in this thesis have led us to find interesting and unexpected phenomena, such as the early warning of long-term persistence of infection from transient local synchronization, and the emergence of extreme events in space and time in a complex network of parametrically coupled populations. So our studies potentially lend more understanding to the emergence of spatiotemporal patterns in complex systems, arising from the interplay of local dynamics and non-local connections.

List of Publications

1. Emergence of Persistent Infection due to Heterogeneity
   Vidit Agrawal, **Promit Moitra** and Sudeshna Sinha
   Scientific Reports, **7**:41582, 2017.

2. Anticipating Persistent Infection
   Promit Moitra, Kanishk Jain and Sudeshna Sinha
   Europhysics Letters, **121**:60001, 2018.

3. Emergence of Extreme Events in Networks of Parametrically coupled Chaotic Populations
   Promit Moitra and Sudeshna Sinha
   Chaos, **29**:023131, 2019.

4. Effect of Community Structure on the Persistence of Infection
   Promit Moitra and Sudeshna Sinha
   (Manuscript in preparation)

Contents

Chapter 1

Introduction

1.1 Dynamics: a historical perspective

πάντα ῥεῖ. Everything flows. This is a quote attributed to the Greek philosopher Heraclitus, from pre-Socratic times. It is probably one of the earliest descriptions of the core essence of the field of study known as "dynamics". This body of knowledge has of course come a long way since then. However, owing to the infinite richness and complexity of phenomena observable in nature, this field is as active an area of research as it has ever been, and perhaps will always remain so.

Dynamics, in very simple terms, is the study of change. Any quantity that changes with time can be considered as a dynamical variable. A very successful descriptive language to analyse dynamical phenomena has been defined by mathematics, namely the field of differential calculus. Systems evolving continuously in time are represented mathematically, in the most general case, as follows:

$$\dot{\boldsymbol{X}} = F(\boldsymbol{X}, t) \tag{1.1}$$

where $\boldsymbol{X}(t) = \{x_1(t), x_2(t).....x_N(t)\}$ is an N-dimensional vector of state variables, t is time and $F(\boldsymbol{X}, t) = \{f_1(\boldsymbol{X}, t), f_2(\boldsymbol{X}, t).....f_N(\boldsymbol{X}, t)\}$ are the functions that describe the dynamics of the system. If the systems are *autonomous*, the set of functions $F(\boldsymbol{X})$ does not explicitly depend on time.

In order to model phenomena with spatial extent, where the dynamical evolution of the state variable depends on both the location and time, partial differential equations

were developed, for instance, to model diffusive processes in space:

$$\frac{\partial \phi(\boldsymbol{x}, t)}{\partial t} = \nabla.[D(\boldsymbol{x}, t)\nabla\phi(\boldsymbol{x}, t)] \tag{1.2}$$

where $D(\boldsymbol{x}, t)$ is the diffusion coefficient for density ϕ at location $\boldsymbol{x}$.

The field of dynamical systems has historically been dominated by the use of such ordinary or partial differential equations. In fact, at it's peak, the use of differential calculus led to the notion of an infinitely deterministic "clockwork" universe, that was presumed to be entirely predictable from it's current state. This notion was embodied by the emerging philosophy of causal determinism, according to which, in it's strongest form, it was conjectured that *similar antecedents lead to similar consequences*. Such notions were, however, soon to be challenged.

It gradually became apparent that a large class of differential equations, while representing a system's behaviour accurately, eluded tractable analytical solvability. This realization, along with the exponential growth of computing power, led to the genesis of novel approaches to understand dynamical systems by numerical simulation and analysis. Discrete algorithms were developed to solve intractable nonlinear equations numerically. Eventually, in a seminal paper titled "Deterministic non-periodic flow" [1] by Edward N. Lorenz in 1962, a major breakthrough occurred in our understanding of a fundamental hallmark of chaotic nonlinear dynamical systems - that of *sensitive dependence on initial conditions*. Although the study was being conducted with the aim of predicting weather patterns, it was demonstrated that two distinct initial conditions, infinitesimally close to each other in the phase space, can nevertheless follow radically different trajectories of dynamical evolution. Therefore, making predictions was demonstrated to be impossible without infinite precision in the knowledge of the initial conditions. This is not to be misconstrued simply as a practical constraint on predictability due to finite observational resolution, because the long term behaviour of an initial condition that is specified with *any* uncertainty becomes unpredictable. Such a humbling realization sowed the seeds of a paradigmatic shift in the study of nonlinear dynamical systems, and led to the development of *chaos theory*.

One of the approaches developed consequently was the study of the geometric properties of the phase space representation of the dynamics of a system, also known as attractors. Specifically, chaotic attractors, such as the Lorenz "butterfly attractor" shown in Fig. 1.1 were found to have very interesting geometric properties. It was observed that they are bounded, and yet they were not smooth. They represented a multitude

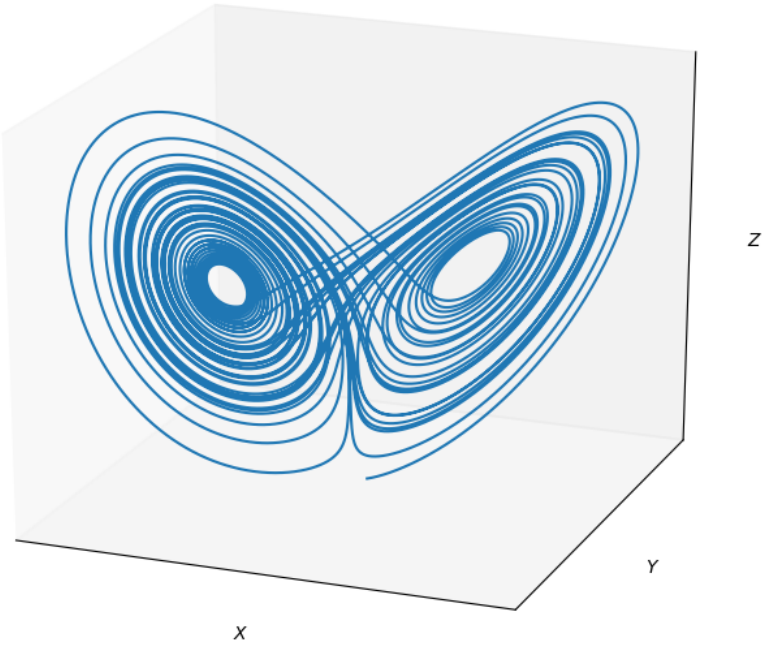

Figure 1.1: The "butterfly" attractor representing the chaotic dynamics of the Lorenz system

of possible trajectories diverging from infinitesimally close initial conditions. Such properties required the development of tools such as the analysis of fractional dimensions of geometric objects embedded in high dimensional spaces.

The stability properties of such attractors became another important aspect of investigation. Apart from the well established techniques of linear stability analysis, estimation of the Lyapunov spectrum of a system, has proven to be an effective and reliable method for the characterization of the chaotic properties of a dynamical system. Lyapunov exponents represent the rates of divergence of initially nearby trajectories in phase space. Presence of a positive Lyapunov exponent enables the characterization of the dynamics as chaotic. In recent years, estimating the size of, and characterizing the nature of, the basins of attraction of asymptotic attracting states, has emerged as a new and effective measure of the stability properties of the dynamics of complex systems [2].

Another major advancement in our understanding of the ubiquitous presence of chaotic dynamics occurred with the results published in a 1976 paper titled "Simple mathematical models with very complicated dynamics" [3], by Robert M. May. The model described in the study was a simple discrete-time difference equation in one variable, that modeled the dynamics of populations with non-overlapping generations, known as the logistic map:

$$x_{t+1} = F(x_t) = rx_t(1 - x_t) \tag{1.3}$$

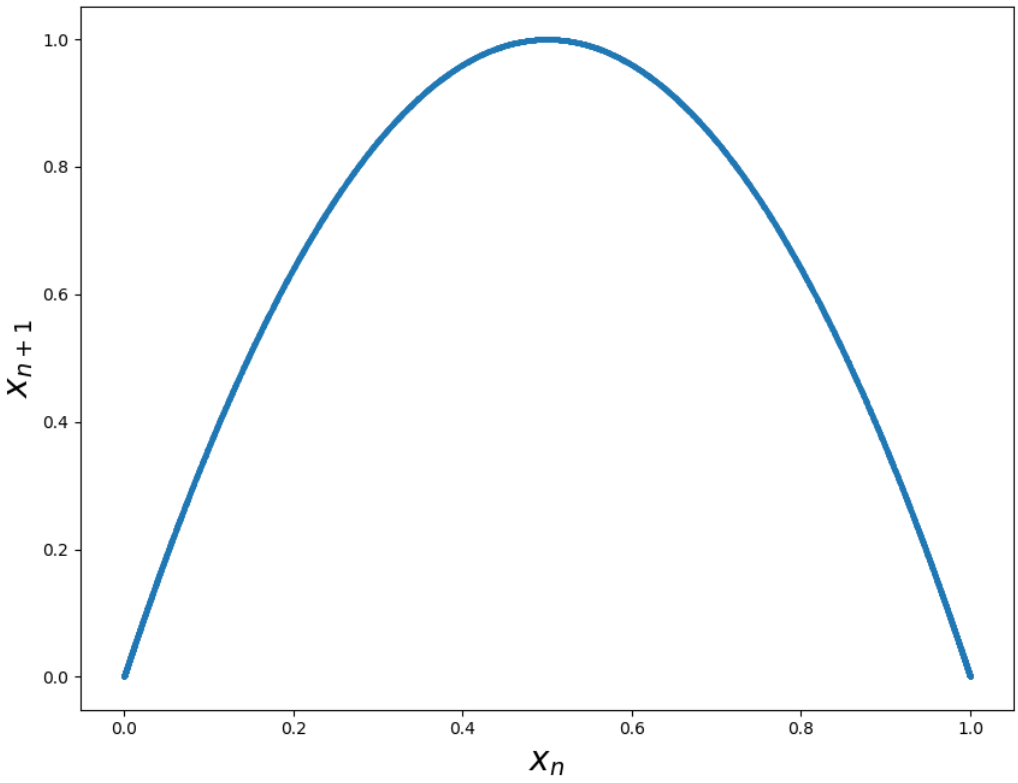

Figure 1.2: The return diagram (x_{n+1} vs. x_n) for the Logistic map, showing it's unimodal nature

Certain features of this map, represented by the return diagram, are shown in Fig. 1.2 It is evident that the map is unimodal, which means it is a continuous map from an interval to itself, with a unique turning point. One of the important observations from the dynamics of the logistic map was the dynamical route taken by the system, from stable solutions, through oscillatory orbits and finally approaching the fully chaotic state, as the system's parameter was gradually varied. This is represented by the bifurcation diagram

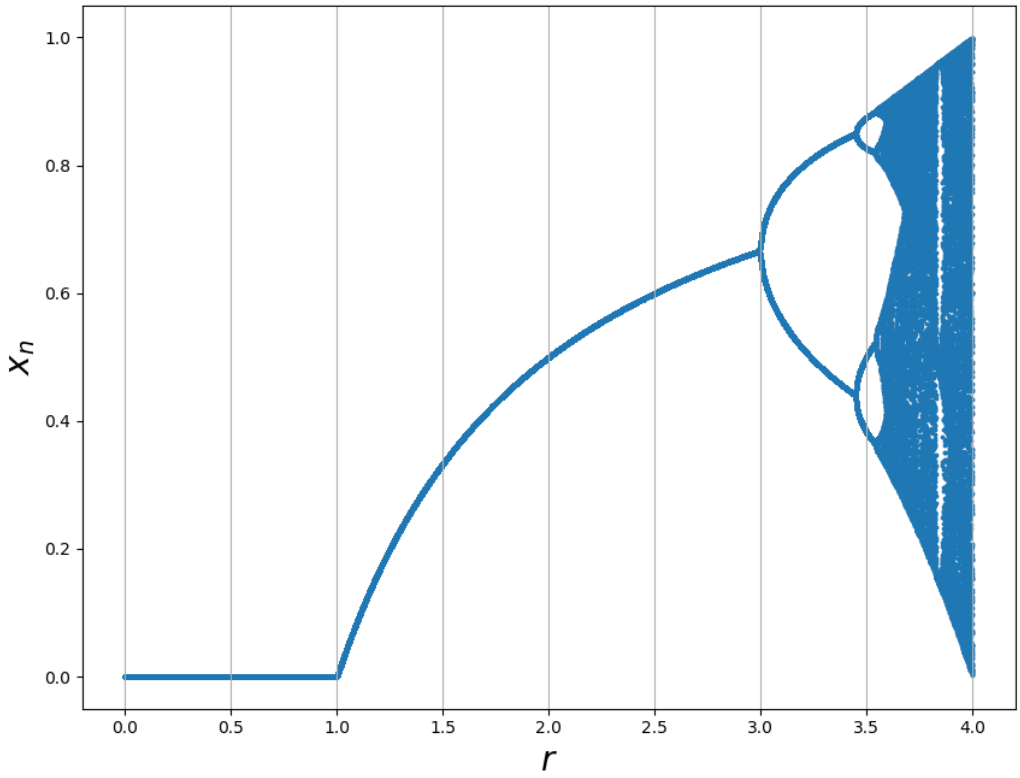

Figure 1.3: The bifurcation diagram (x_n vs. r) for the Logistic map, demonstrating the period doubling route to chaos

(Fig. 1.3), and is termed as a "period doubling cascade". The fact that such simple iterated maps could show sensitive dependence on initial conditions, behave chaotically in certain parameter regimes, demonstrating a rich diversity of dynamical behaviours along the way, led to a flurry of subsequent studies to develop tools (such as bifurcation analysis) to understand and characterise their dynamics.

1.2 Synchronization

Having made some progress in the understanding of the dynamics of a single system, explorations naturally extended towards systems of coupled dynamical elements. This led to the discovery of a plethora of regimes of collective behaviours. One of the most interesting and well explored phenomenon in this context was that of synchronization.

Synchronization broadly refers to the emergence of a functional dependence of the frequencies of an ensemble of coupled interacting dynamical systems. It is a phenomenon that had been observed in many physical and biological systems, often in contexts as simple as a crowd clapping, candle flames oscillating, or a swarm of fireflies flashing together. Although it might intuitively seem that for two oscillators to synchronize their frequencies, some conscious tuning (based on feedback from the neighbouring oscillators) is required, it was demonstrated that the phenomenon was prevalent in systems with a broad range of coupling forms and strengths.

Subsequently, studies on phase oscillators by Y. Kuramoto [4] revealed that coupled systems undergo a well defined phase transition from the unsynchronized to the synchronized state above a critical coupling strength. It has been characterized as a second order phase transition, owing to the property of reversibility of the transition. This generated a lot of interest in the phenomenon of synchronization, since such critical transitions have been observed in physical systems from seemingly unrelated contexts, such as the transition of magnetisation or spin, below a critical temperature.

Current avenues of investigation of the phenomenon of synchronization has broadened to include exploration of patterns of synchrony in complex systems. A seminal paper by D. Abrams and S. H. Strogatz [5] revealed the simultaneous existence of clusters of synchrony and asynchrony in a system of coupled oscillators, which they termed as a *chimera* state. Investigations in this direction continues relentlessly, with the aim of characterizing the conditions under which such phenomena occur.

In this thesis, the concept of synchronization has been utilized specifically to understand the underlying mechanism of the persistence of spatiotemporal oscillations in a spatially extended model of the dynamics of an infection spreading across a population.

1.3 Complex systems

As mentioned above, in recent years, a question of intense research activity has been the behaviour of interacting dynamical elements coupled with each other. Such systems are broadly classified as complex systems. Examples of such systems are present all around us, in natural and engineered systems - such as ecosystems, neural networks, power grids, social networks etc. These high dimensional problems have led to studies involving systems with multiple interacting dynamical units, such as populations of species coupled via their interactions as predators, preys or mutually cooperating species; or neurons

coupled via synapses, or profiles of individuals being connected on social networks, sharing data with each other. This has allowed an avenue for the natural extension of the analysis of these systems in spatial dimensions. The study of such dynamical systems can be classified in terms of the spatial and temporal characteristics of the system, as well as of the dynamical variables. Modelling and analysis of such complex dynamical systems requires one to ascribe either a discrete or continuous nature to the space that the system spans, the time with which the system evolves, and states attained by the system. In these terms, the approaches to study the dynamical behaviour of systems can be broadly (but non-exhaustively) classified as follows [6]:

Space	Time	State	Type
Continuous	Continuous	Continuous	Differential Equations (ODEs/PDEs)
Discrete	Continuous	Continuous	Coupled Oscillators (Coupled DEs)
Discrete	Discrete	Continuous	Coupled Maps
Discrete	Discrete	Discrete	Cellular Automata

Certain features of the dynamics of complex systems have generated a lot of research interest. One such feature is the emergence of collective dynamical behaviour across multiple scales. This is termed as emergent phenomena. It has been a very active field as it has proven to be exceptionally difficult and counter intuitive to predict such phenomena from the relatively simple and well understood behaviour of the individual dynamical elements. One of the most intensely discussed examples of emergent phenomena is known as self organized criticality. It was observed that while most systems, when allowed to evolve autonomously, approached stability (in conventional terms by minimizing their energy), certain systems of interacting dynamical elements, with very simple dynamics at the individual level, naturally organized themselves to a state that was minimally stable, and responded to even small perturbations by reorganization over large scales. A classic cellular automaton model, popularly known as the "sandpile" model, was demonstrated to approach a self organized critical state in the study conducted by Bak, Tang and Weisenfeld [7]. Certain patterns were observed in the statistics of such phenomena, such as the prevalence of power laws in the distributions of the extents of the reorganization events, and such phenomena remain active avenues of research.

1.3.1 Modeling spatial extent: lattices and networks

As mentioned above, lattices of interacting dynamical elements have been established as a very effective platform to model complex dynamics. Cellular automata were utilized to model systems extending over a discrete space, where each dynamical unit evolves over discrete time steps, attaining values from a discrete, finite state space. One of the modeling paradigms that built upon this concept, and emerged as an effective way to model interacting dynamical elements with continuous states, is termed as coupled map lattices, or CML, developed by K. Kaneko [8]. This modeling paradigm has led to the discovery of regimes of dynamic behaviour that had previously eluded *in silico* observation, such as spatiotemporal intermittency [9] (Fig. 1.4).

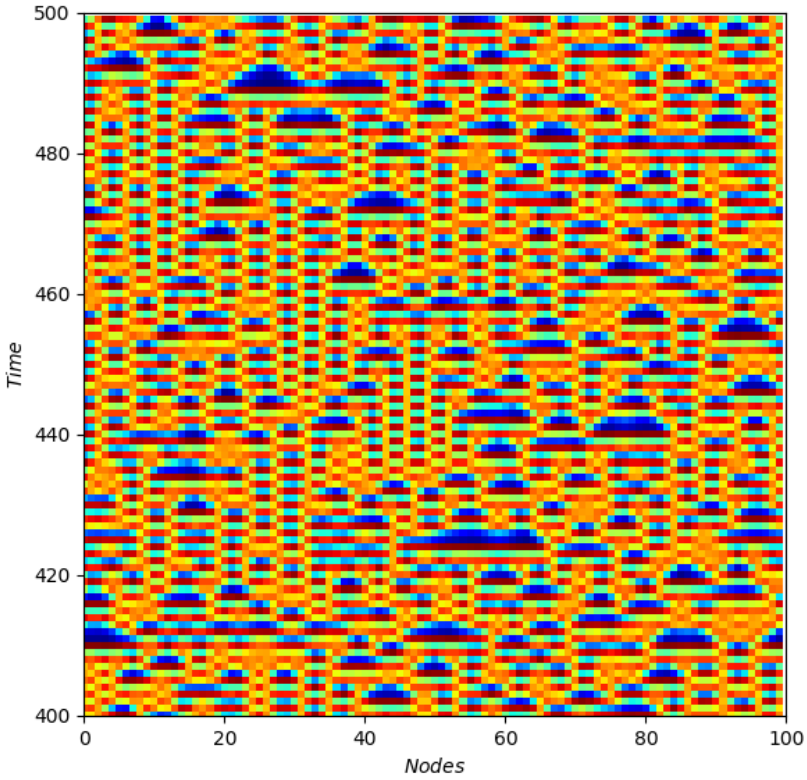

Figure 1.4: A lattice of coupled logistic maps, displaying spatiotemporal intermittency

However, lattices embodied an inherent constraint, in terms of the regularity of the underlying connectivity. While this is a natural feature of certain systems, and readily models spatial extent in an intuitive sense, examples of complex systems are abound where interactions are inherently non-local, such as long range interactions in social networks.

In very recent times, with ever increasing computational capacity, networks have become established as the natural choice of a platform to model complex systems. Each node in a networked system represents a dynamical unit, and the interactions between the nodes are implemented via connections, or edges, between such nodes. Structurally, a network is characterised by the topology of connections, which is represented by an adjacency matrix for the network. The network paradigm allows quite a bit of freedom in terms of modeling not only the non-locality of connections, but also directionality and strengths of interactions. Lattices emerge as a limiting case of network models, when the connections are only between nearest neighbours.

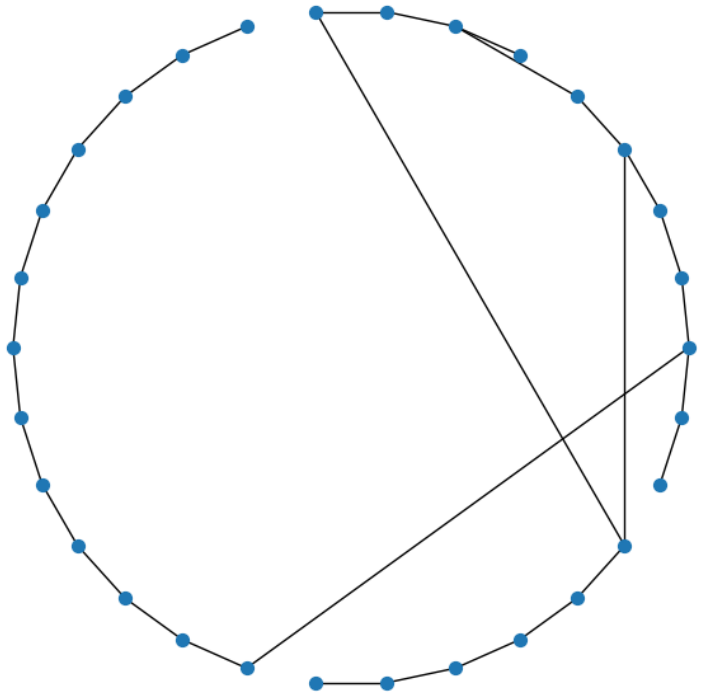

Figure 1.5: A typical small world network, with high clustering and short average path length

Apart from the flexibility proffered by the network paradigm, the reason for the adoption of networks as a fertile basis for modeling complex systems, has been the remarkable results presented in the study by D. Watts and S. H. Strogatz [10]. In the study, a method was developed to gradually tune the overall topology of a network (by proba-

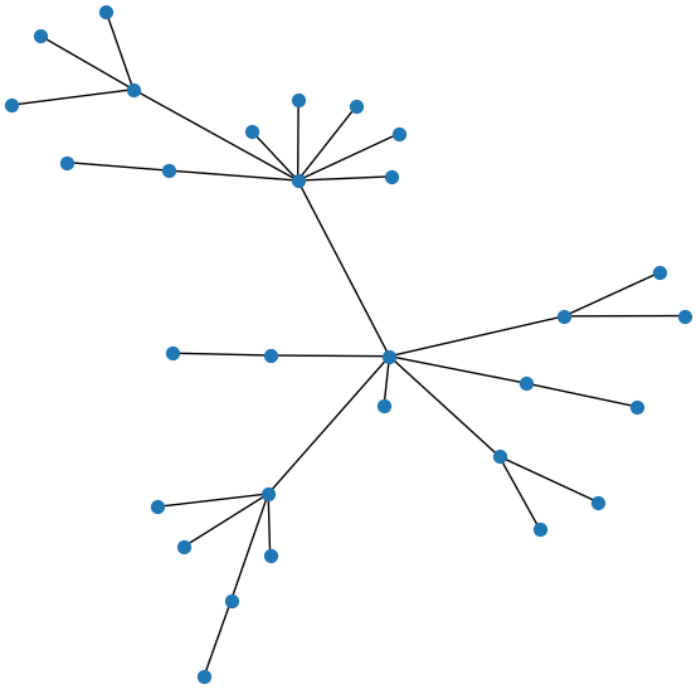

Figure 1.6: A typical random scale-free graph generated by the preferential attachment algorithm

bilistically rewiring the connections) from a regular lattice like structure, to a completely random topology. At an intermediate stage of this process (Fig. 1.5), the topology attained by the network was demonstrated to have structural properties that were similar to both a regular network (high clustering) as well as a random network (short average path lengths). Such structural properties have been accordingly observed in quite a few networked systems, such as power grids.

Another very interesting method to attain a network topology prevalent in observed scenarios was described by A. Barabasi [11] (Fig. 1.6). The study put forward a method to grow a network, node by node, based on the principle of preferential attachment. This protocol is naturally motivated by many systems which involve dynamical units gradually forming a network, such as the world wide web.

Such studies have demonstrated the immense latitude given by the network paradigm,

leading to many subsequent investigations into the interplay of individual dynamics and the topology of interactions, revealing a plethora of dynamical behaviours, and it continues to do so.

1.4 Outline of the thesis

The outline of the chapters in this thesis are as follows:

In Chapter 2, the dynamics of an infection spreading across a population is modeled, and the emergence of persistent infection in a closed region is explored. In this system, the disease progression of an individual is given by a discrete version of the SIRS model. The persistence of contagion is qualitatively and quantitatively investigated, under increasing heterogeneity in the partitioning of the population into different disease compartments, as well as increasing heterogeneity in the phases of the disease among individuals within a compartment.

It is observed that when the initial population is uniform, the infection does not persist in the population. However when the initial population consists of randomly distributed refractory and susceptible individuals, a single source of infection was found to cause sustained infection in the population. It is concluded that heterogeneity facilitates the de-synchronization of the phases in the disease cycle of the individuals, leading to steady state dynamics, or persistence, of the infection in the population. It is also observed that the average extent of the window of persistence of infection depends on the degree of heterogeneity in the initial composition of the population.

In Chapter 3, we focus on the *role of synchronization in the persistence of infection* in such a closed region. The following key result is observed: higher degree of synchronization in the individual states, both globally in the population and locally in the neighbourhoods, hinders persistence of infection. It is demonstrated that early short-time asynchrony appears to be a consistent precursor to future persistence of infection, and can potentially provide valuable early warnings for sustained contagion in a population patch. It is also found that *transient synchronization* can help anticipate the long-term persistence of infection. We also find that when the range of influence of an infected individual is wider, the infection persists for a smaller window of initially infected individuals. This counter-intuitive observation can also be understood through the relation between synchronization and infection burn-out.

In Chapter 4, we study the impact of segmenting a population patch into distinct communities, with different concentrations of infection. We find that a population structured into communities yields a persistently infected sub-population, in contradistinction to an equivalent population where the same initial fractions of susceptible, refractory and infected individuals are homogeneously distributed in space. It is observed that even after transience, the patterns of disease spreading in the two communities may be completely dissimilar, even though both communities settle down to the same average infected sub-population size. The time evolution of the total number of infected individuals in the two communities displays distinct periodic wave forms, with different amplitudes, but the same frequency.

In Chapter 5, we study a collection of populations modeled by the prototypical chaotic Ricker map. The feedback received by each population patch is modeled to be influenced by the local mean field of its neighbourhood. Specifically, we distinguish the terms of the dynamical map into two parts: the growth term and the regulation term. The growth term consists of a positive feedback, and the regulation term contains a negative feedback, from the variable that represents the population at each time step, leading to the characteristic unimodal shape of such population maps. In our study, instead of the commonly-used diffusive interactions among coupled populations, we consider networks of populations where the rate of population growth at a site is influenced by neighbouring populations. We find that such parametrically coupled networks of populations yield very interesting and non-intuitive collective behaviour.

The dynamics and distribution of the local populations, as well as the total biomass is examined in the system. We observe that when the range of coupling is sufficiently large, namely when enough neighbouring populations influence the growth rate of a population, the system yields remarkably large biomass values that are very far from the mean. These extreme events are found to be relatively rare and uncorrelated in time. It is also evident that at any point in time, exceedingly large population densities emerge in a few patches, analogous to an extreme event in space. These results indicate a *new mechanism in coupled chaotic systems that naturally yield extreme events in both time and space.*

In Chapter 6, we present a summary of the problems explored in this thesis, as well as the results and insights obtained from them, which potentially contribute to the understanding of emergent spatiotemporal collective behaviour in spatially extended complex systems, arising from the interplay of local dynamics and spatially distributed connections. We also present certain techniques and possible directions for further characterization and analysis of emergent behaviours of complex dynamical systems in general.

Chapter 2

Heterogeneity Facilitates Persistence of Infection

Adapted from the work published in :

Vidit Agrawal, Promit Moitra and Sudeshna Sinha,
Scientific Reports, **7**:41582, 2017.

2.1 Introduction

How a disease spreads in a population is a question of much interest and relevance, and consequently has been extensively investigated over the years [12, 13, 14]. Different classes of models mimicking infection spread are obtained by exploring different models of disease progression at the local/individual level. These may be simple disease cycles, that end in fatality or permanent immunity, or they may be diseases that have more complicated progression, including refractory periods where immunity is temporary. Further, experimental observations, such as of the spread of measles in Iceland, which being isolated provides a "natural laboratory" for the study of epidemics spreading, indicated that the spatial element is essential in constructing any theory for valid predictions [14]. So a variety of models have been propounded, taking into account different properties of the spatial domain in which the infection spreads.

A wide class of models focus principally on infection transmission, keeping the individual disease progression at the local level simple. For instance, there are models based on local transmission of infection, with the infection being ultimately fatal [15]. The probability of infection from the infected host (transmissibility) is found to be the crucial parameter in such host-pathogen models, and the pathogen must have a minimum transmissibility in order to propagate, with the host driven to extinction if it exceeds a certain transmissibility. Further simple models of disease transmission on small-world networks has been investigated [16], varying the probability of infection by a disease and/or the probability of its transmission. Such models display epidemic behavior when the infection or transmission probability is above a threshold, analogous to percolation thresholds. Similar studies on scale-free networks, with the disease cycle ending with permanent immunity shows that no long-term infection can be maintained as the number of susceptibles decline as the epidemic spreads [17]. Studies of disease models where the individuals become susceptible again, right after the infective period, shows that scale-free networks are more prone to spreading and persistance of infection, while exponential networks have an epidemic threshold above which the infection becomes persistent in time [18].

Another class of models investigates more complicated disease progression, such as diseases with temporary immunity. For instance in Ref. [19], for representative parameters the model exhibits expanding circular waves of infection, some of which are generated by unusual 'pacemaker centres'. When infected individuals recover, the interior of the growing wave boundary becomes a fresh pool of susceptible individuals. At the end of

the cycle, a distant infectee short cuts through the network to reinfect the wave's focal pacemaker, enabling it to perpetuate. The results from this study suggest that both the temporary immunity and the social structure have equal influence on the existence of periodicity in the disease outbursts, and small-world connectivity was seen to lead to persistent infection. A model with a similar disease progression has been studied, with infection rate being a control parameter [20]. By using deterministic (mean field) equations to describe the temporal evolution of the disease, it was found that the epidemics will be persistent when the control parameter is bounded in a certain range, and if the infection rate is sufficiently large, too many susceptibles get infected at the same time and therefore die simultaneously, leading to extinction.

Similar investigations of a generic model of excitable media with increasing density of random long-range connections [21], reported the existence of two qualitatively different regimes of self-sustained pattern formation. Starting from nearest neighbor coupling, as the random links were increased, dynamically different results were observed. Below a lower critical probability, the state of the system after an initial transient period was characterized by self-sustaining single or multiple spiral waves. Second, at the critcial probability, the spiral wave mode was suppressed and the system underwent a transition to periodic activity. Third, when the value of probability was increased above a system-size-dependent upper critical probability, the self-sustained activity ceased. This occurred due to the spiral waves being primarily created by shortcut-induced excitations. So a very large number of shortcut connections guaranteed almost simultaneous spread of excitation to nearly all cells, as a result of which the dynamics of the system tended to 'burn out' after a transient. Several other studies on small-world networks also showed the emergence of epidemic outbreaks for sufficiently large number of random connections [22, 23]. Further it was shown that time-varying networks yield epidemics more readily than static networks [24].

Lattice-based models for dealing with spatially-distributed host population, have also been explored. For instance, Ref. [25] yield results suggestive of self-organised criticality. By attaining a critical prevalence, the disease appears to reach a state where small fluctuations have the potential to induce cascades of infection on a wide range of time and length scales. This, in effect, maximises possibility of persistence by ensuring all spatial and temporal scales are accessed. In the context of persistence, another very interesting study [26] focuses on the local aspects of inhomogeneity in a spatially homogeneous environment. In this work, the excitable media is characterized by a globally stable equilibrium state, and also by a threshold mechanism which produces a large amplitude response to a sufficiently large stimulus. It was shown that spatial inhomogeneities in

such an excitable media tended to produce spatial patterns which oscillated periodically in time.

Lastly, a large class of models consider the disease progression in homogeneously well-mixed populations, where encounters are random, using an approach inspired by mass action kinetics, resulting in a sets of ordinary differential equations [27, 28, 29]. The advantage of these commonly used models based on differential equations (or difference equations [30]) is that they are most often analytically tractable, and can yield asymptotic stability regions for the equilibrium points. However, certain features are lost, as the homogeneity of a large population is the underlying assumption in these models.

In this work we will explore the following crucial question, that has not seen much focus yet: *what population compositions are conducive to the emergence of long-term persistence of infection in a population?* In order to address this question we will consider cellular-automata based descriptions of infection spreading, for a disease that has temporary immunity [22, 23]. We will consider initial populations with varying degrees of global heterogeneity, reflecting increasing non-uniformity in the condition of the individuals comprising the population. Our attempt will be to ascertain the influence of this heterogeneity on the persistence of infection. The model we will consider combines two distinct features. The first is the transition from the susceptible to the infected state, determined by the state of the immediate neighbourhood, which is *stochastic* in nature. The second feature is a *deterministic* disease cycle, which ensues upon infection. We give details below.

2.2 Model

Mathematically, epidemiological models have successfully captured the dynamics of infectious disease [31, 32]. One well known model for non-fatal communicable disease progression is the SIRS cycle. This model appropriately describes the progression of diseases with temporary immunity, such as small pox, tetanus, influenza, typhoid fever, cholera and tuberculosis [27, 28].

The SIRS cycle is described by the following disease compartments:

(i) Susceptible (denoted by symbol S) - An individual in this state remains susceptible until they contract the infection from another infected person in their neighbourhood. At the end of the refractory stage (namely the stage of temporary immunity) of the disease

cycle, the individuals return to this state.

(ii) Infected (denoted by I) - In this stage of the disease cycle, the individual is in an infected state, which signifies they can infect others around them.

(iii) Refractory (denoted by R) - At the end of the infectious stage, the individuals acquire temporary immunity to the disease. In this stage they neither get infected by infectious neighbors, nor do they infect anyone in their surroundings. Typically, this stage lasts longer than the infected stage, and at the end of this stage the individual loses the temporarily acquired immunity and becomes susceptible to the infection once again.

Specifically, in this work we consider a cellular automata model of the SIRS cycle described above [22, 23, 24]. In this model of disease progression, time t evolves in discrete steps, with each individual, indexed by (i, j) on a 2 dimensional lattice, characterized by a counter

$$\tau_{i,j}(t) = 0, 1, \ldots, \tau_I + \tau_R \tag{2.1}$$

describing its *phase* in the cycle of the disease [22]. Here $\tau_I + \tau_R = \tau_0$, where τ_0 signifies the total length of the disease cycle. At any instant of time t, if phase $\tau_{i,j}(\mathrm{t}) = 0$, then the individual at site (i, j) is susceptible; if $1 \leq \tau_{i,j}(t) \leq \tau_I$, then it is infected; if phase $\tau_{i,j}(t) > \tau_I$, it is in the refractory stage. For, phase $\tau_{i,j}(t) \neq 0$ the dynamics is given by the counter updating by 1 every time step, and at the end of the refractory period the individual becomes susceptible again, which implies if $\tau_{i,j}(t) = \tau_0$ then, $\tau_{i,j}(t+1) = 0$. Namely,

$$\begin{aligned} \tau_{i,j}(t+1) &= \tau_{i,j}(t) + 1 \qquad \text{if } 1 \leq \tau_{i,j}(t) < \tau_0 & (2.2) \\ &= 0 \qquad\qquad\quad \text{if } \tau_{i,j}(t) = \tau_0 & (2.3) \end{aligned}$$

Hence the disease progression is a *cycle* (see Fig.2.1). We consider the typical condition where the refractory period is longer than the infective stage, i.e. $\tau_R > \tau_I$.

We now investigate the spread of infection in a group of spatially distributed individuals, where at the individual level the disease progresses in accordance with the SIRS cycle. In particular, we consider a population of individuals on a 2-dimensional lattice

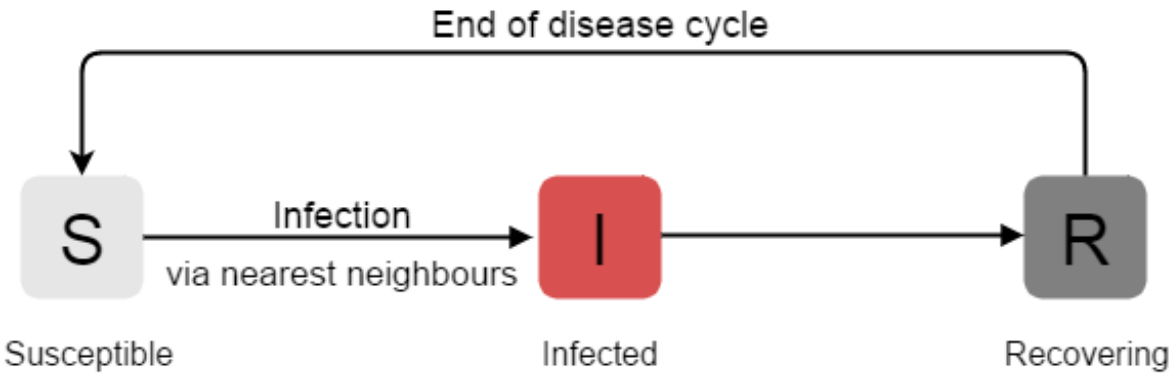

Figure 2.1: Schematic Representation of the SIRS cycle. The color scheme in all figures is as follows: black represents the refractory state (R); white represents the susceptible state (S); red represents the infected state (I).

where every node, representing the individual, has 4 neighbors [25]. Unlike many studies with periodic boundary conditions, here the boundaries are fixed with no interactions outside the boundaries. So our model mimics a patch of population, such as an island or an isolated habitat [14], and investigates the persistence of infection in such a closed region.

Condition for infection: Here we consider the condition that a susceptible individual (S) will become infected (I) *if one or more of its nearest neighbours are infected*. That is, if $\tau_{i,j}(t) = 0$, (namely, the individual is susceptible), then $\tau_{i,j}(t+1) = 1$, if any $1 \leq \tau_{x,y}(t) \leq \tau_I$ where $x, y \in \{(i-1, j); (i+1, j); (i, j-1); (i, j+1)\}$.

Notice that there are two distinct features determining the local state of the individuals. The first is the transition from the susceptible to the infected state determined by the state of the immediate neighbourhood, which is *stochastic* in nature and dependent on the distribution of initial states of the individuals in the population. The second feature is the *deterministic* disease cycle: I $\rightarrow$ R $\rightarrow$ S. This interplay of a probabilistic feature and a deterministic cycle shapes the dynamics of disease in the population.

In this work we focus on an unexplored aspect of such systems, namely we attempt to ascertain the dependence of the persistence of infection on the *composition of the population*. So the specific question of relevance here will be the connection between sustained long-time persistence of infection in a region from an infective seed(s) and the heterogeneity of the states of the individuals in the region.

Heterogeneity, namely non-uniformity in the states of the individuals, may be characterized in different ways. Consider a generic initial population patch comprised of a

random admixture of susceptibles, infected and refractory individuals, given by initial fractions S_0, I_0 and R_0. So, if either S_0, I_0 or R_0 tends to one, we have a homogeneous situation where almost all individuals are in the same state, namely almost all susceptible ($S_0 \to 1$), or almost all infected ($I_0 \to 1$), or almost all recovered ($R_0 \to 1$). Increasing deviations from this, reflects increasing heterogeneity in the population, as it implies an increasing spread among different disease compartments.

Another source of heterogeneity arises from non-uniform stages of disease within a disease compartment. In our study, we first consider the scenario where the sub-population of refractory individuals (given by R_0) are in the same stage of the disease cycle, namely the heterogeneity is entirely reflected by the variation of S_0, I_0 and R_0. We will then go on to study the effect of non-uniformity in the stages of recovery of the refractory individuals, bringing in yet another type of heterogeneity in the population, reflecting the spread in the states of individuals qualitatively in the same disease compartment. In the sections below, we now present our simulation results, focussing on the persistence of infection, obtained by sampling a large range of initial states, reflecting varying degrees of heterogeneity, both in the partitioning of the population into disease compartments, as well as non-uniformity in the disease phases within a compartment.

2.3 Spatio-temporal patterns of infection spreading

We first focus on the infection spreading patterns in the population. The principal question we ask is the following: when is infection persistent in a patch, and how this depends on the constitution of the initial population. In order to examine this, we study the spread of infection from a seed of infection (namely one or two infected individuals) across a patch of population composed of individuals at different stages in the disease cycle, and with varying degrees of heterogeneity in the population.

With no loss of generality we consider $\tau_I = 4$; $\tau_R = 9$; $\tau_0 = 13$ and a lattice of size 100×100. In our figures we represent the state of an individual in the disease cycle (namely S, I or R) by a color, with white denoting a susceptible individual, black denoting a refractory individual and red denoting an infected individual. The fraction of susceptible individuals in the population at time t is denoted by S_t, the fraction of infected individuals by I_t and the fraction of refractory individuals by R_t. In the sections below we will focus on the possibility of the prolonged existence of infection arising in different classes of initial populations, characterized by different S_0, R_0 and I_0.

2.3.1 Non-persistent Infection in a Homogeneous Susceptible Population

First we investigate the effect of an infected individual on a population patch where *all individuals are entirely susceptible to infection.* Namely, we consider the case where at the outset there is one infected individual and the rest of the population is in the susceptible state, with $\tau_{ij} = 0$.

Fig. 2.2 displays the spreading patterns obtained in such a scenario. It is evident that as time progresses the infection starts from the infected individual ("seed") and spreads symmetrically. This symmetric spreading pattern is readily understood from the condition for infection, which turns susceptible individuals to infected if any one of their neighbors is infected. So the infected seed infects its four neighbors, and these newly infected individuals in turn infect their nearest four neighbours, and so on. This process leads to an isotropic wave of infection which stops at the boundaries. In contradistinction, periodic boundary conditions [20], or the presence of non-local "short-cuts" in space [19, 21], would place the infecteds in the proximity of suscpetibles again, thereby perpetuating the infection.

We confirmed the generality of these observations for different relative lengths of the infectious and refractory periods, namely varying τ_I and τ_R (with $\tau_I < \tau_R$). We further ascertained that the choice of the location of the infected individual did not affect these qualitative trends.

The key factor in infection spreading is the contact of susceptible individuals with infected ones. It is clear that such an interaction takes place only at the outer edge of the wave of infection, while the inner boundary of the infected zone is contiguous only to refractory individuals. So the infection only spreads outwards, and does not move back into the interior of the lattice again.

Importantly, the infection is removed after a while from the closed region, and all the individuals comes to the end of the disease cycle and become susceptible again. So there is no infective site left in the population to perpetuate the infection and initiate another wave of disease spreading. Thus a *fully susceptible population does not allow infection to persist.*

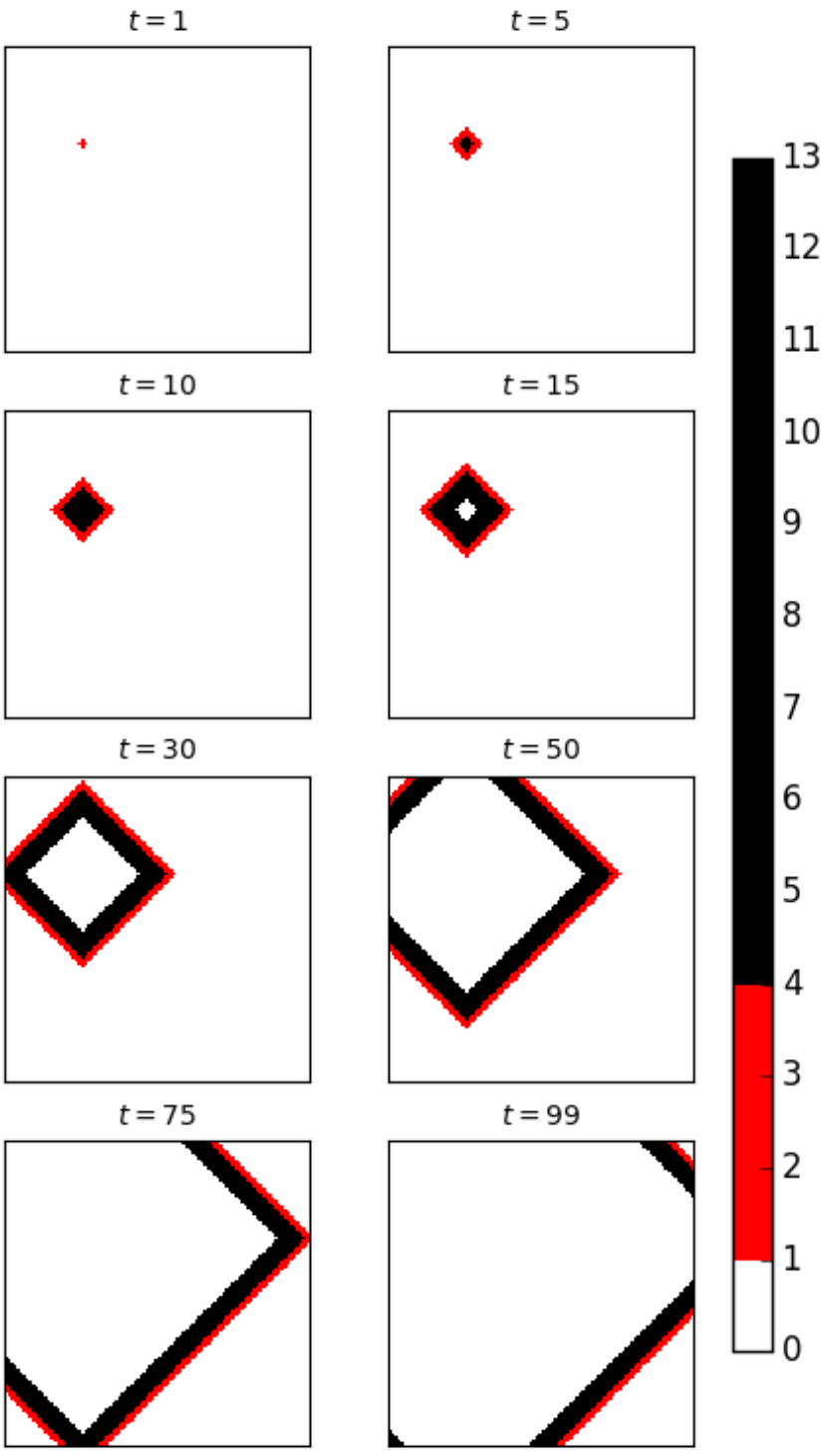

Figure 2.2: Snapshots at specific times, showing the spread of infection from one infected individual at $t = 0$, in a homogeneous initial population comprising entirely of susceptible individuals (i.e. $S_0 \sim 1$, $R_0 = 0$, $I_0 \sim 0$). The long bar shows the relative lengths of the susceptible (S), infected (I) and refractory (R) stages in the disease cycle, where $\tau_I = 4$, $\tau_R = 9$ and the total disease cycle τ_0 is 13 (see text).

2.3.2 Persistent infection in Heterogeneous Populations

Next we investigate the infection spread in the more realistic scenario where both refractory ($\tau_{i,j} > \tau_I$) and susceptible individuals ($\tau_{i,j} = 0$) are present in the initial population, and are randomly distributed spatially. We first consider the case where the refractory individuals have phases $\tau_{i,j} = \tau_I + 1$, namely, they are at the start of the refractory stage of the disease cycle. We investigate the persistence of infection in heterogeneous populations, with the initial state having (a) a single seed of infection and (b) varying initial fractions of infected individuals (I_0). In both scenarios, we analyze the effect of varying S_0 and R_0 on the persistence of infection.

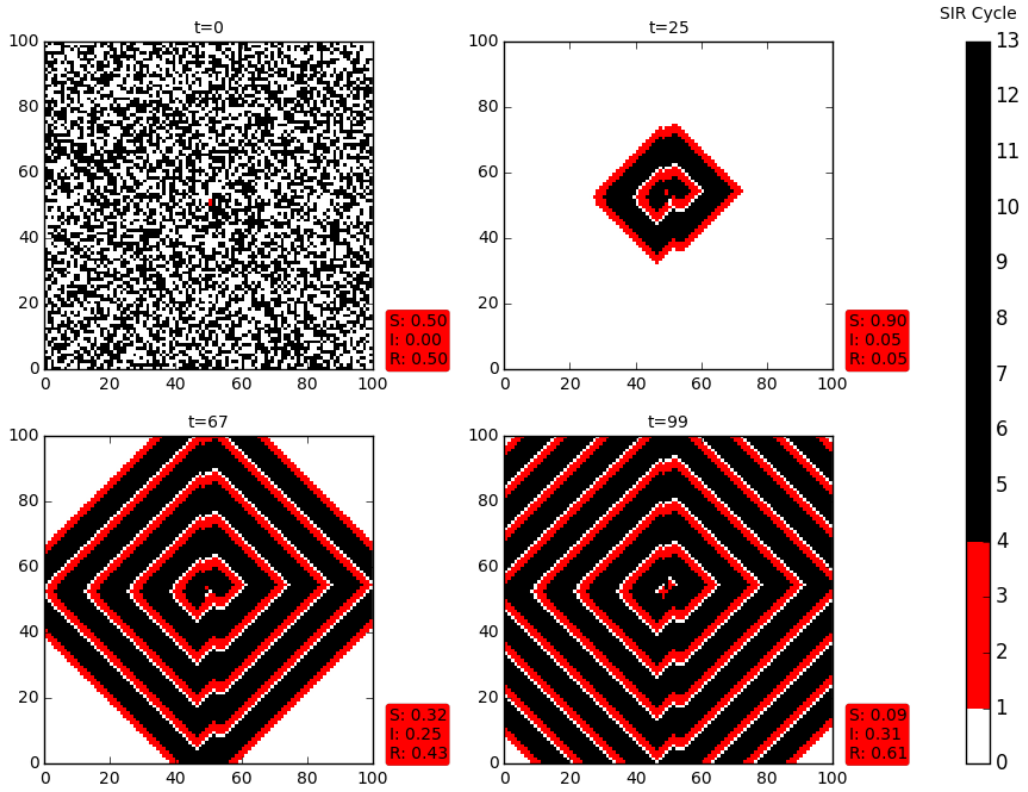

Figure 2.3: Snapshots of the infection spreading pattern in a heterogeneous population comprising initially of a random mixture of equal numbers of susceptible and refractory individuals ($S_0 \sim 0.5$, $R_0 \sim 0.5$ and $I_0 \sim 0$), with one infected individual at $t = 0$. Here the refractory individuals have phases $\tau_{i,j} = \tau_I + 1$ (namely, they are at the start of the refractory stage of the disease cycle). Again, the long bar shows the relative lengths of the susceptible (S), infected (I) and refractory (R) stages in the disease cycle, where $\tau_I = 4$, $\tau_R = 9$ and the total disease cycle τ_0 is 13 (see text). The red box shows the fraction of S, I and R individuals in the population at that instant of time. Interestingly, the spatially random population evolves into a more regular pattern after a short transient time.

To begin with, in Fig. 2.3, we illustrate the effect of a single infected individual on an initial population with equal numbers of susceptible and refractory individuals, namely $S_0 = R_0$. It is evident from these representative results that in a well mixed population, consisting of a random collection of both susceptible and refractory individuals, introduction of a single infected individual can lead to *persistent infection in the population.* Also notice that some of these spreading patterns are reminiscent of coalescing and interacting spiral waves initiated by local inhomogeneity in an uniform background [26].

This can be rationalized as follows: the mixed presence of susceptible and refractory individuals, implies that the disease cycles of the individuals in the population are *not synchronized* [29]. So there are always some individuals in the infective stage of the disease cycle in the population, and these act as seeds for continued infection propagation, leading to persistent infection. *Counter-intuitively then, the presence of individuals who are (temporarily) immune to the disease amongst susceptible ones leads to sustained infection, while in a completely susceptible population the infection dies out.*

Next we focus on the time evolution of an initial population consisting of a random mixture of S, I and R states. In particular we investigate the nature of the persistent infection in the population under varying initial fractions of infected individuals I_0. A typical random initial condition is shown in Fig. 2.4, with the initial fraction of infected sites I_0 being one-tenth and the initial fraction of susceptibile and refractory individuals being equal (i.e. $S_0 = R_0$). Here too we find that infection is sustained.

Further, interestingly, it is clear that there is an *approximate recurrence of the complex patterns of infected individuals in the population.* Fig. 2.5 shows the time evolution of the fraction of infected, refractory and susceptible individuals in the population, namely I_t, R_t and S_t, in the case displayed in Fig. 2.4. It can be clearly seen that after transience, I_t, R_t and S_t exhibit steady oscillatory dynamics, with period of oscillation close to the disease cycle length τ_0. This is consistent with the observed recurrence of the spatio-temporal patterns when persistent infection emerges.

A quantitative measure of the recurrence of patterns can also be obtained by calculating the difference of the state of the population from the initial state, as reflected by the Hamming distance:

$$H = \frac{1}{N} \sum_{i,j} |\tau_{i,j}(t) - \tau_{i,j}(0)| \tag{2.4}$$

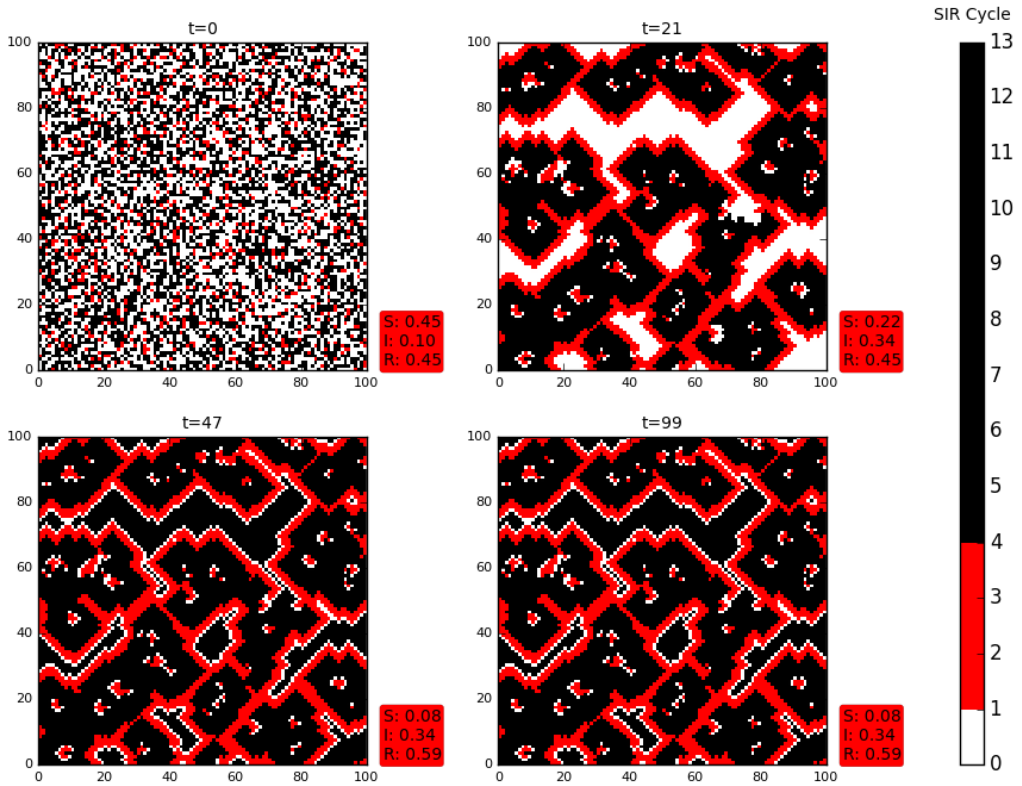

Figure 2.4: Snapshots of the infection spreading pattern in a heterogeneous population comprising initially of a random mixture of individuals, with $S_0 = R_0$ and $I_0 = 0.1$. Here the refractory individuals have phases $\tau_{i,j} = \tau_I + 1$ (namely, they are at the start of the refractory stage of the disease cycle). Again, the long bar shows the relative lengths of the susceptible (S), infected (I) and refractory (R) stages in the disease cycle, where $\tau_I = 4$, $\tau_R = 9$ and the total disease cycle τ_0 is 13 (see text). The red box shows the fraction of S, I and R individuals in the population at that instant of time.

where the sum is over all N sites in the lattice. The time dependence of the Hamming distance given above is shown in Fig. 2.6, and it clearly shows steady oscillations. This indicates that the fraction of the susceptible, infected and refractory individuals in the population, and more remarkably their *locations*, repeat almost periodically over time. It should be noted that the frequency of oscillation again approximately corresponds to the disease cycle length.

Another pertinent observation here is the dependence of this dynamics on disease cycle. As the length of the infectious stage (i.e. τ_I) increases, keeping the total disease cycle length invariant, the fraction of infected individuals I_t increases. The average I_t is proportional to the fraction of the disease cycle occupied by the infectious stage, i.e

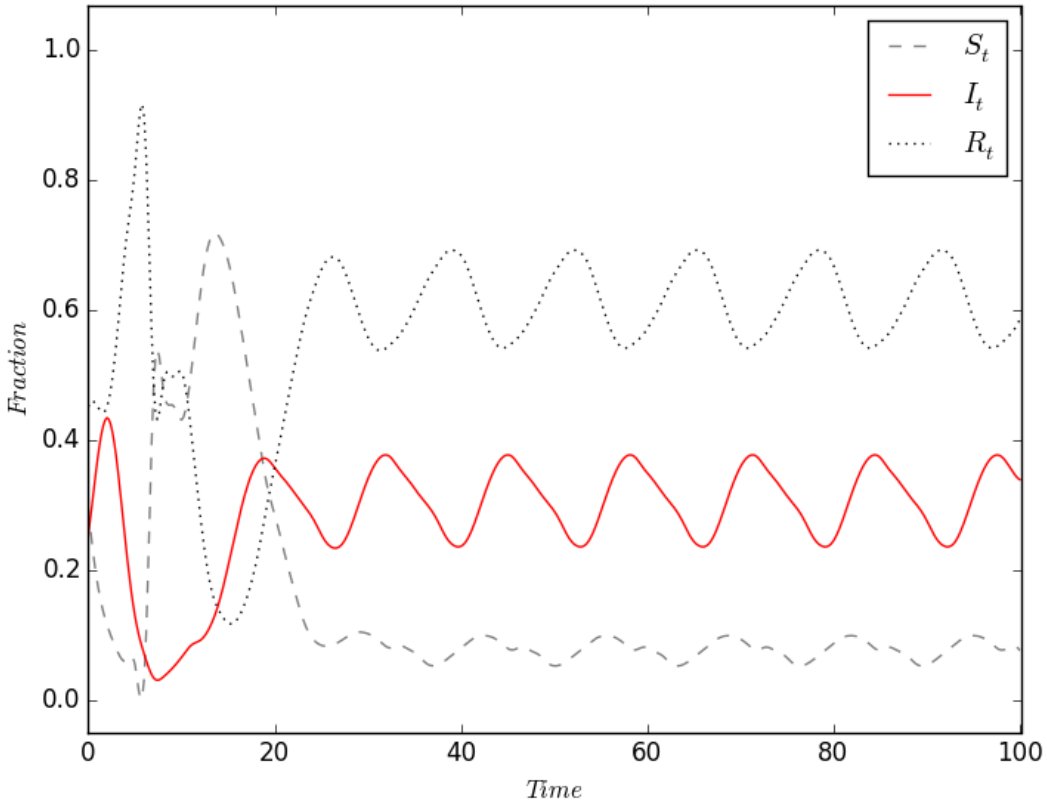

Figure 2.5: Time evolution of I_t, S_t, R_t, in a heterogeneous population comprising initially of a random mixture of individuals, with $S_0 = R_0$ and $I_0 = 0.1$.

the ratio τ_I/τ_0. So the size of the infected population strongly depends on the nature of disease as reflected in the length of the infectious stage of the disease.

2.4 Influence of the initial composition of the population on the persistence of infection

We now attempt to gauge the statistically significant trends in I_t, by averaging the fraction of infected individuals at asymptotic time t, arising from a wide range of random initial configurations at time $t = 0$. We denote this by $\langle I_t \rangle$. Such a global measure provides a quantitative estimate of the size of the basin of attraction of the persistent state.

In terms of this quantity, persistent infection is indicated by a non-zero value. However, after sufficient transient time-steps, if $\langle I_t \rangle$ is zero, it indicates that the infection has

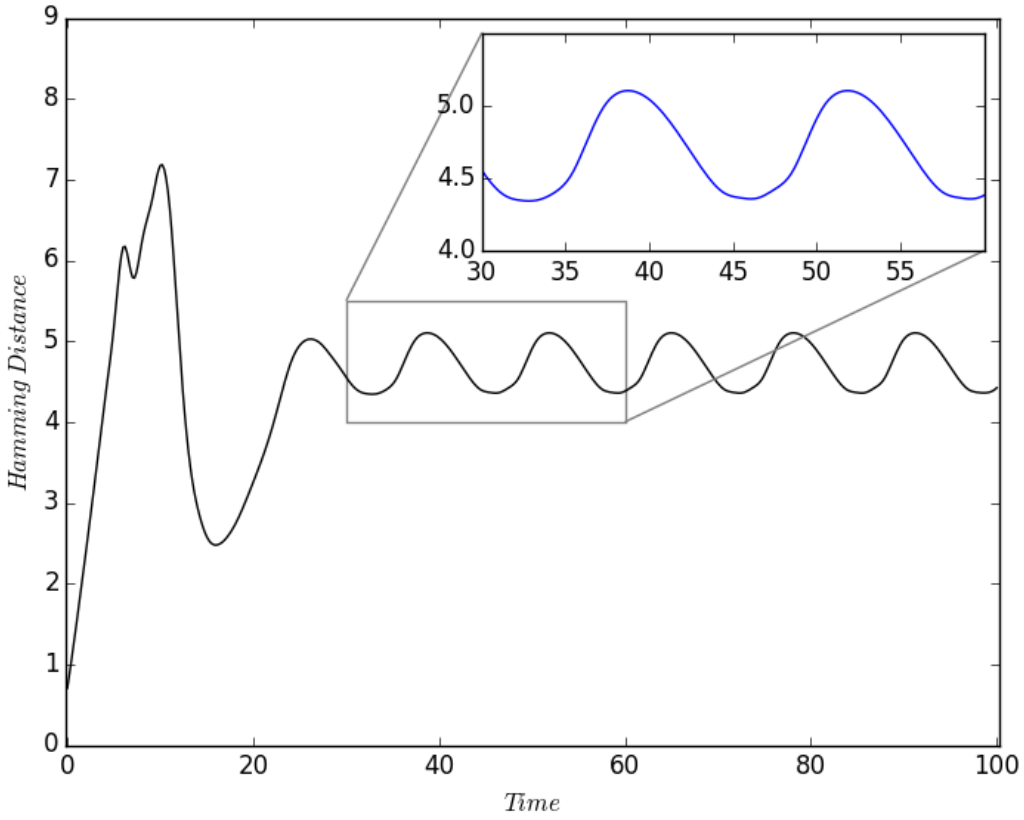

Figure 2.6: Hamming distance given by Eqn. 2.4 as a function of time, in a heterogeneous population comprising initially of a random mixture of individuals, with $S_0 = R_0$ and $I_0 = 0.1$. The inset clearly shows that the frequency of spatial oscillations are very close to the length of the disease cycle

died out. So $\langle I_t \rangle$ can serve as an order parameter for the transition to sustained infection in a population.

2.4.1 Dependence of persistence of infection on the initial fraction of susceptibles

For fixed τ_I and τ_0 we have calculated $\langle I_t \rangle$, for different initial fractions of susceptible individuals S_0. We explore the full possible range of $S_0 \in [0, 1]$, where $S_0 = 0$ signifies a population comprised entirely of refractory individuals who are immune to infection initially, and $S_0 = 1$ implies an initial population comprised entirely of individuals susceptible to infection. While the phase of the susceptible (S) sub-population is $\tau_{i,j} = 0$ of course, the refractory individuals (R) can be present in different stages in the refractory

period with $\tau_I < \tau_{i,j} < \tau_0$. We explore two different scenarios of the initial state of the refractory individuals in the population.

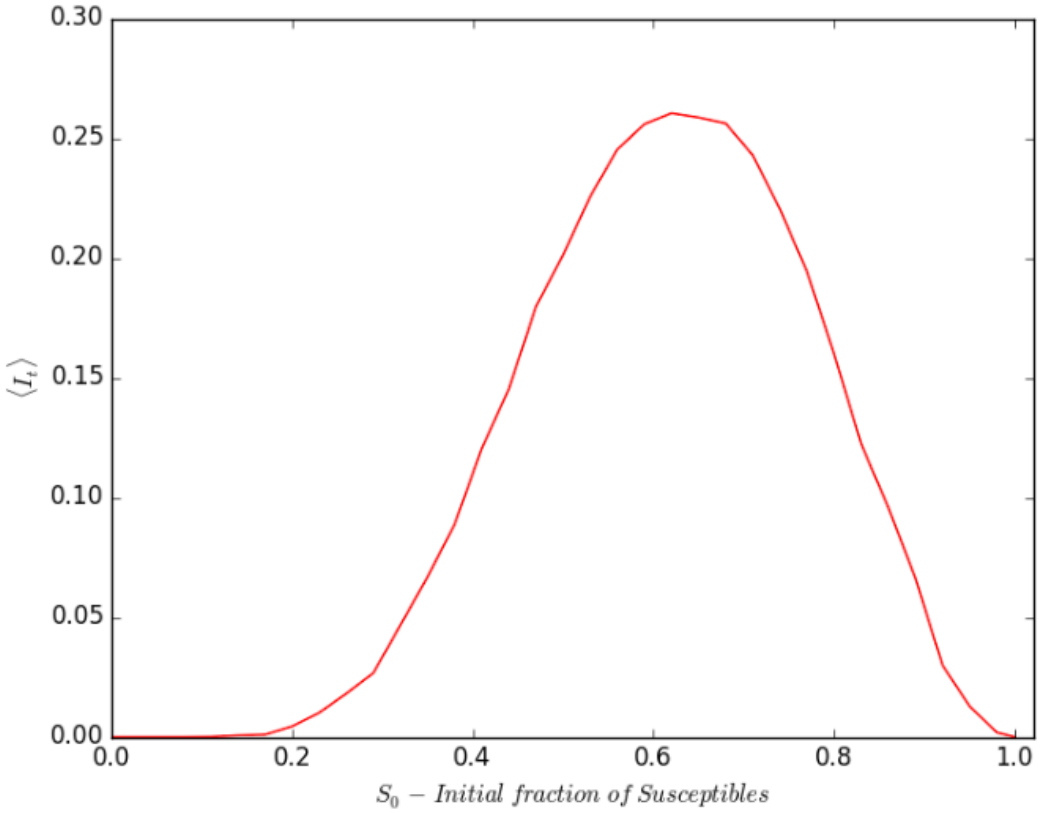

Figure 2.7: Variation of $\langle I_t \rangle$ (after transience) with respect to the fraction of susceptible individuals in the initial population S_0, arising from the presence of a single infected individual at time $t = 0$. Here the refractory individuals have the same phase, the disease cycle has $\tau_I = 4$; $\tau_0 = 13$, and I_t is averaged over 10^3 realizations of the initial population on the lattice. The specific case of a 100×100 lattice is displayed. However note that different lattice sizes yield the same result.

First we present the case where all the refractory individuals are at the start of the refractory stage of the disease cycle, i.e. all $\tau_{i,j} = \tau_I + 1$. So there is uniformity in the stage of disease progression in the refractory sub-population, though the individuals are randomly distributed spatially. We focus on the asymptotic state of infection in such a population, arising from a single infected individual at the outset. The results obtained from a large sample of initial states is shown in Fig. 2.7, and it is evident from there that $\langle I_t \rangle$ is *very low for both high and low* S_0, peaking around $S_0 \sim 0.65 - 0.75$. Namely, homogeneous initial populations where all individuals are immune ($S_0 = 0$), or all are susceptible to disease ($S_0 = 1$), do not yield persistent infection. Rather, mixed populations lead to most sustained infection, with persistently high numbers of infected individuals.

We can rationalize our observations as follows: If an infected individual is completely surrounded by refractory individuals with $\tau = \tau_I + 1$, it will complete the infectious stage without transferring the infection at all, as $\tau_I < \tau_R$. So the infection can spread only if the infected seed is contiguous to at least one susceptible individual. Now the probability of contact with a susceptible individual in the initial stages of infection spreading depends on the initial fraction of susceptibles S_0. This suggests that when S_0 is low, the chance of the infected individual being in contact with a susceptible one is low. As a result, as S_0 tends to zero, on an average, the infection eventually gets removed from the population, with the seed of infection crossing over to the refractory phase without infecting any other individual.

When there are more susceptible individuals in the initial population, there is a higher chance that the infected seed will encounter a susceptible neighbour. So as expected, increasing S_0 leads to a larger infected set on an average. However the surprising trend is the *decrease* in the infected set as the initial susceptible sub-population becomes too high, with the number of infected individuals tending to zero as the entire population becomes susceptible. This feels counter-intuitive, but can be understood as follows: Consider the limiting case where initially almost all the individuals are susceptible to the infection. Now the infection will spread immediately in isotropic waves, but will eventually stop at the boundaries. In analogy to the spread of forest fire, the boundary of refractory individuals is like scorched earth preventing spread across them. Now after the wave of infection passes, the individuals are in the refractory stage, leading eventually to the entire set being synchronized in the susceptible regime. There is no infected individual left then to act as a seed for a further wave of infection spreading. So the infection does not persist. The susceptible stage is like an "absorbing state", and in the absence of "infectious perturbation" the system remains fixed in that state.

In order to prevent the above scenario, one needs enough refractory individuals in the population. When R_0 is below 1/4 (i.e. $S_0 > 3/4$), typically the infected seed may not have a refractory individual among its four neighbours. So one expects that the persisting infection will have lower probability of occurrence as S_0 increases beyond 3/4. This is in accordance with the trends observed in the simulations.

We then see that for the *infection to persist* in a population, a *well mixed heterogeneous population is required*, with reasonable number of both susceptible and refractory individuals. *Randomly mixed populations prevent synchronization of the disease*, and this is the key to always having some source of infection left in the population.

2.4.2 Dependence of persistence of infection on the initial fraction of infecteds

We now vary the initial fraction of infected individuals I_0 in the population, over the entire range $[0, 1]$. For the remaining population, the initial fraction of susceptible and refractory individuals is set at different ratios. We consider an ensemble of initial conditions, with specific I_0, S_0 and R_0 and find the time averaged I_t, after long transience for each realization. The ensemble average of this quantity is displayed in Fig. 2.8. Notably, we find that there is a definite *window of persistence* over the range of I_0, where the infection never dies down and the fraction of infected individuals in the population is reasonably high on an average.

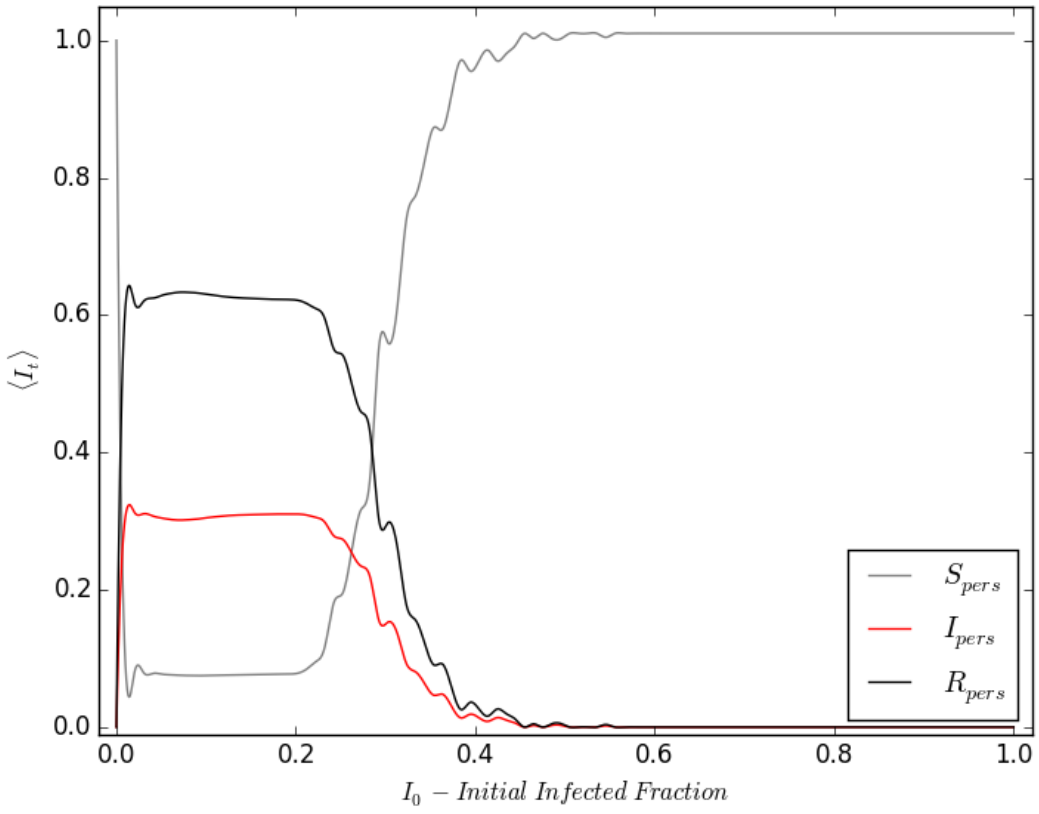

Figure 2.8: Variation of $\langle I_t \rangle$ (after transience) with respect to the initial fraction of infected individuals I_0 in the population, and $S_0 = R_0$. The refractory sub-population consists of individuals with phase equal to $\tau_I + 1$. Here the disease cycle has $\tau_I = 4$; $\tau_0 = 13$, and I_t is averaged over 10^3 initial realizations. The specific case of a 100×100 lattice is displayed. However note that different lattices sizes yield the same result.

In the state where infection is persistent, the individuals are unsynchronized and

spread over the different stages of the disease cycle. So on an average the fraction of infected individuals is $\sim \tau_I/\tau_0$, namely the fraction of the total disease cycle occupied by the infected stage. For instance, in the example shown in Fig. 4.1 with $\tau_I = 4$ and $\tau_0 = 13$, at the plateau of persistence, the infected fraction is approximately one-third of the population. The transition to persistent infection is sharp and occurs at $I_0 \to 0$. This implies that *the infection can spread and persist even when there is only a single infected individual in the initial population.* This is consistent with the results we presented earlier (cf. Fig. 2.7) on infection spreading from a single infected individual.

Interestingly, the infection ceases to persist for higher values of I_0, and the fall in persistence is rapid. That is, if the initial population has too many infected individuals, infection will not persist. This can be rationalized by noting that one needs a mix of susceptibles and refractory individuals in the population for persistent infection. For instance, considering the limiting case of all infected individuals in the initial state, it is clear that all individuals will go through the disease cycle in synchrony. So all individuals will become susceptible again together, but there will be no infective seed left in the population to perpetuate the infection.

2.5 Effect of varying degrees of non-uniformity in the refractory sub-population on the persistence of infection

Now we will explore the effect of non-uniformity within the refractory sub-population on the emergence of persistent infections. Namely, we will consider the refractory individuals in the initial population to be in different stages of disease progression. We will consider two distinct ways of interpolating between the completely heterogeneous and completely uniform limiting cases, in order to gauge the effect of heterogeneity on sustaining infection.

First we consider the initial refractory sub-population to be an admixture of subsets of individuals with uniform phase and with randomly distributed phases. Specifically, we explore initial refractory sub-populations comprised of some fraction f_{rand} with phases randomly distributed over the range $\tau_I + 1$ to τ_0, and the rest $1 - f_{rand}$ with fixed phase $\tau_R = \tau_I + 1$. We examine the spread and persistence of infection in such a scenario, under variation of the initial composition of the population.

Fig 2.9 exhibits the persistence of infection, with respect to varying S_0, arising in

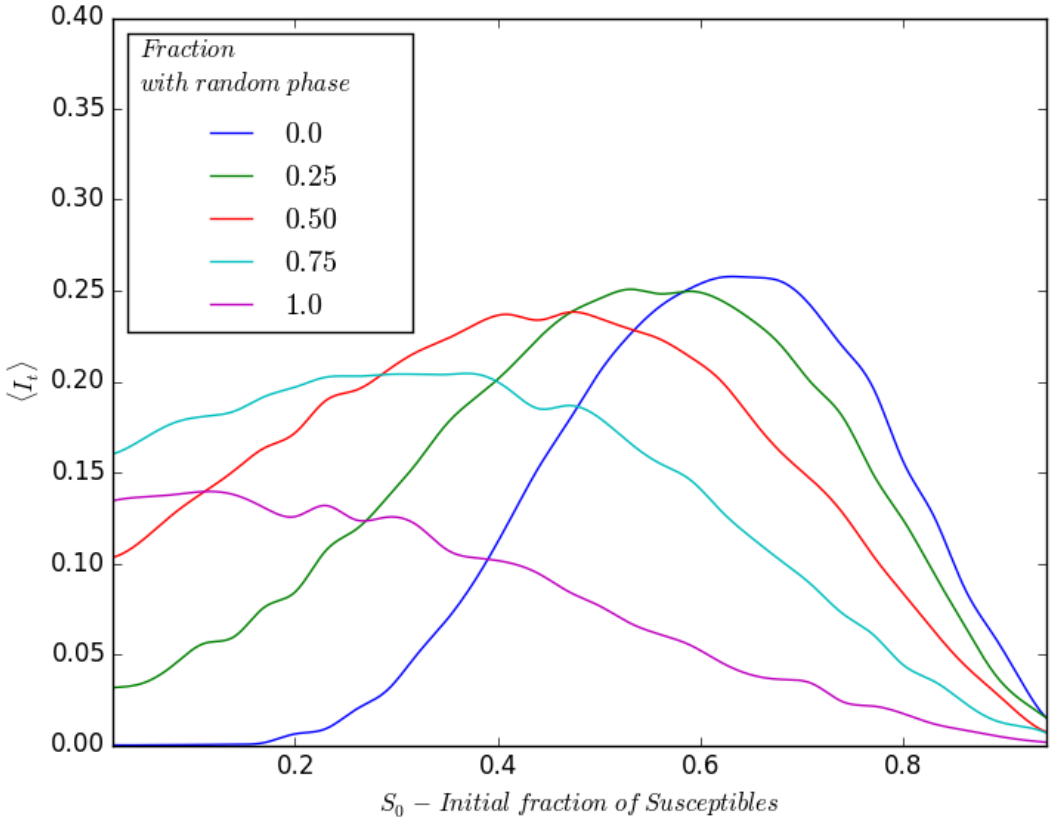

Figure 2.9: Variation of $\langle I_t \rangle$ (after transience) with respect to initial fraction of susceptible individuals S_0, for different fractions f_{rand} of the initial refractory sub-population having randomly distributed phases (see key). Here the disease cycle has $\tau_I = 4$; $\tau_0 = 13$, and I_t is averaged over 10^3 initial realizations and lattice size is 100×100.

a population that had a single infected individual initially. Different fractions of the initial refractory sub-population with randomized phases were explored, ranging from $f_{rand} = 0$ (i.e. completely uniform), to $f_{rand} = 1$ (i.e. completely heterogeneous). The trends clearly indicate a continuous cross-over from the condition where all refractory individuals are in the same phase, to the scenario where all are in random phases.

Further, we explore the effect of varying the initial fraction of infected individuals I_0, over the range $[0, 1]$. Fig. 2.10 exhibits the change in the window of persistence with respect to f_{rand}. It is evident that increasing f_{rand}, namely increasing the initial number of refractory individuals with *de-synchronized phases*, leads to a definite increase in the window of persistence. This implies that *for populations with a more heterogeneous refractory sub-population, the disease persists over a larger range of infected fractions* I_0 *of the initial population.*

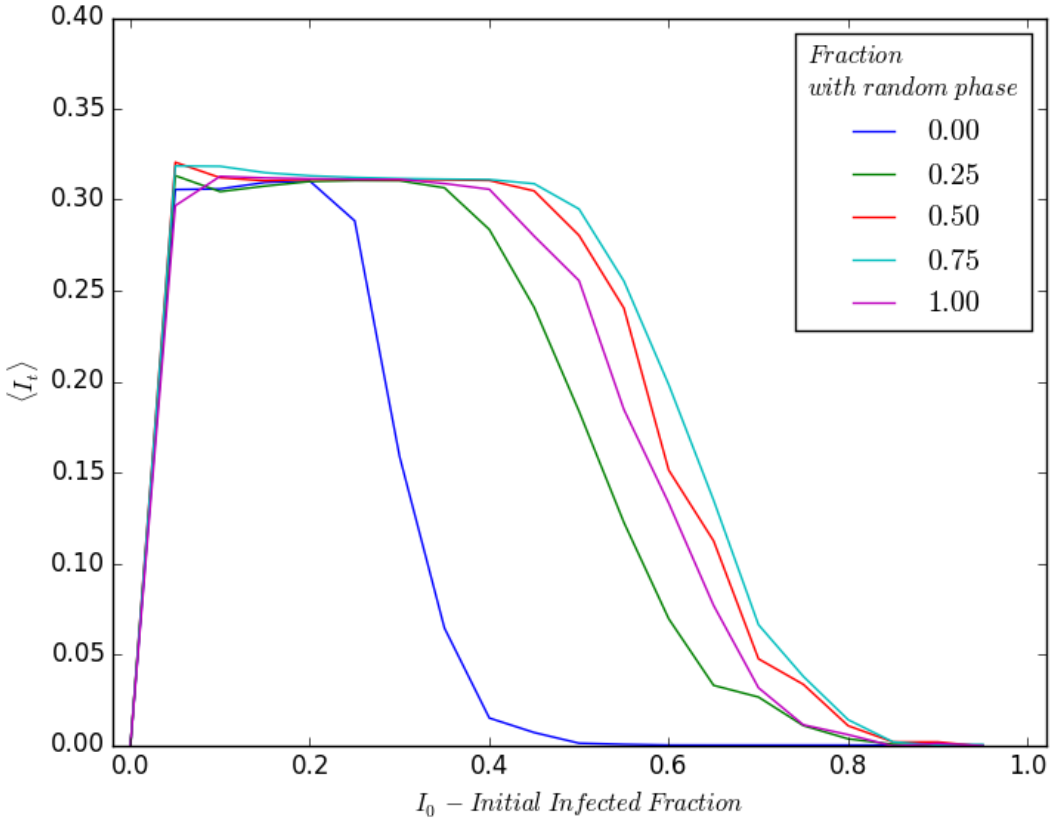

Figure 2.10: Variation of $\langle I_t \rangle$ (after transience) with respect to the initial fraction of infected individuals I_0 in the population, and $S_0 = R_0$. The initial refractory sub-population consists of different fractions f_{rand} with randomly distributed phases (see key). Here the disease cycle has $\tau_I = 4$; $\tau_0 = 13$, and I_t is averaged over 10^3 initial realizations. While the specific case of a 100×100 lattice is displayed, different lattices sizes yield the same result.

Note however, that there is also an apparent reduction in the window of persistence at very high f_{rand}. This can be rationalized by noting that when the entire initial refractory sub-population R_0 has uniformly distributed phases, there are a significant number of individuals who are closer to the end of their disease cycle (for instance, stage 12 or 13). These individuals become susceptible within a few time steps, and therefore bring the population closer to an overall state of homogeneity again, as all susceptibles are in the same phase (stage 0) and remain in that phase unless infected. We have observed qualitatively and quantitatively earlier, that a more homogeneous population leads to a reduced window of persistence. Hence, *presence of a significant number of individuals closer to the end of their disease cycle acts as a homogenizing factor for the population and is detrimental to persistence.*

Lastly, we study the effect of varying ranges of spread in the initial phases of the refractory individuals. Specifically we consider that the phase of the refractory individuals in the initial population to be randomly distributed over different ranges R_{rand}. In particular we examine the persistence of infection for R_{rand} ranging from $[\tau_I + 1, \tau_I + 1]$, (where all refractory individuals have the same phase) to $[\tau_I + 1,\ \tau_I + \tau_R]$ (where heterogeneity is large as the phases of the refractory individuals are distributed over the entire refractory range).

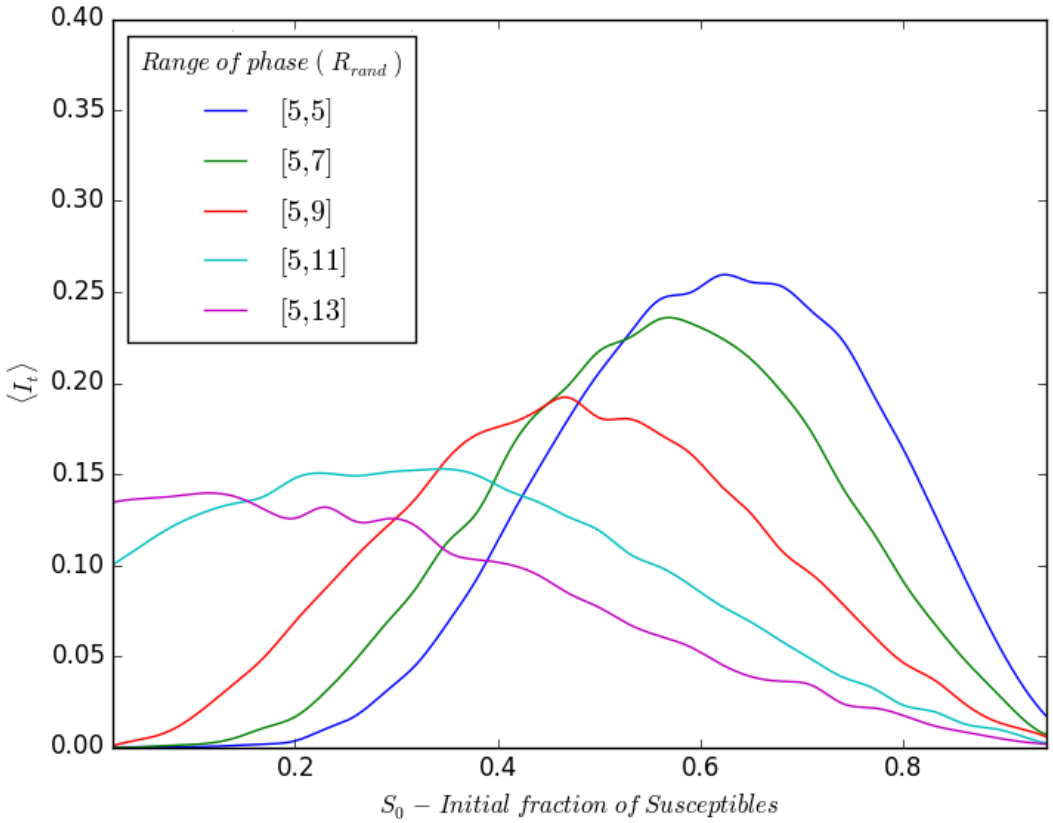

Figure 2.11: Variation of $\langle I_t \rangle$ (after transience) with respect to initial fraction of susceptible individuals S_0, for the case where there is a *single* infected individual in the population at the outset, and the refractory individuals in the population have phases τ randomly distributed over different ranges R_{rand} in the refractory stage : [5,5]; [5,7]; [5,9]; [5,11]; [5,13]. Here I_t is averaged over 10^3 realizations, lattice size is 100×100, and the disease cycle parameters $\tau_I = 4$, $\tau_0 = 13$.

Figs. 2.11-2.12 exhibit representative results of $\langle I_t \rangle$ as a function of the initial fraction of susceptibles S_0 and infecteds I_0. It can be clearly seen that a smooth cross-over takes place from the extremal case of all refractory individuals in the same phase, to the limit where the stages of the refractory individuals are spread randomly over the entire refractory period. The key observation here is that as the spread in phases increases, the

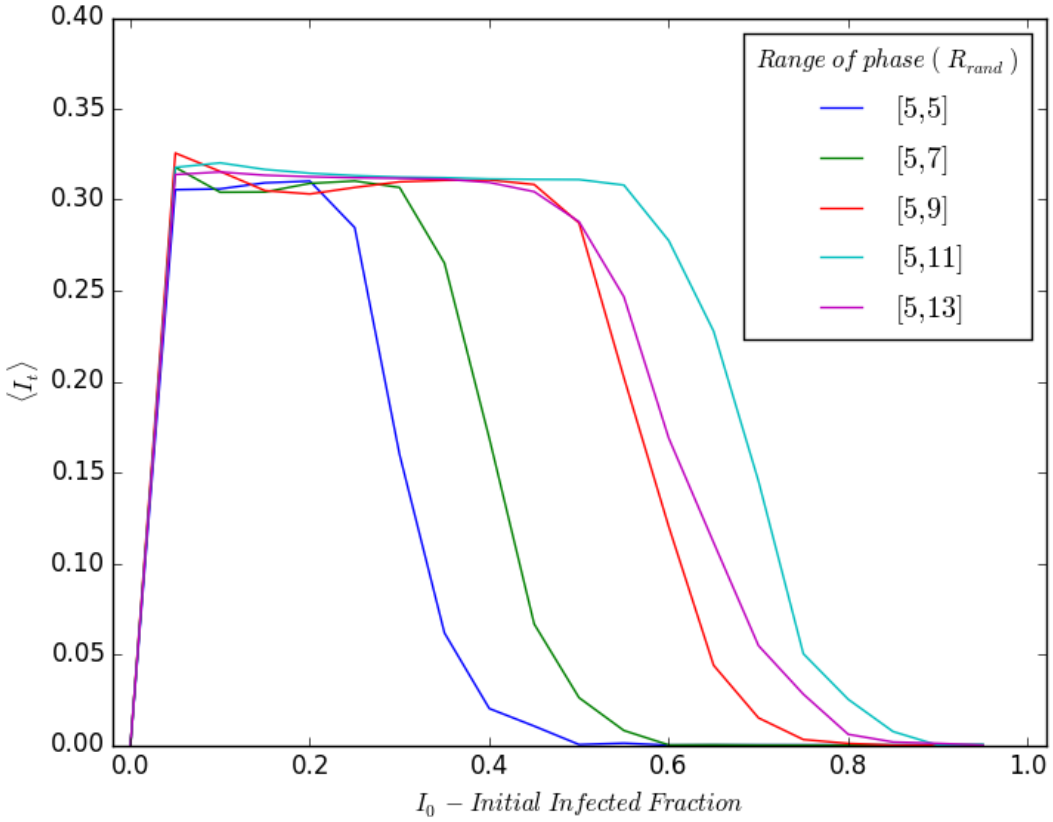

Figure 2.12: Variation of $\langle I_t \rangle$ (after transience) with respect to initial fraction of infected individuals I_0, for the refractory individuals having phases τ randomly distributed over different ranges R_{rand} in the refractory stage : [5,5]; [5,7]; [5,9]; [5,11]; [5,13]. Here I_t is averaged over 10^3 realizations, lattice size is 100×100, and the disease cycle parameters $\tau_I = 4$, $\tau_0 = 13$.

range of persistent infection becomes larger. Namely, when there is a large initial spread in the stages of disease among the individuals, at subsequent times there are always some individuals who can "pick up the baton of infection", leading to persistent infection.

So we see that in the completely heterogeneous case, low susceptible and high refractory initial subpopulations favour persistent infection. But in a completely uniform population, a higher fraction of susceptibles leads to persistent infection. This has the following important implication: when refractory individuals are not synchronized at the same phase of disease progression, even if there are few susceptible individuals in the population initially, the infection grows substantially and the average size of the infected sub-population is large. So we have demonstrated that even when the entire population is susceptible to infection, the infection eventually dies out, while even a few susceptibles among an heterogeneous refractory population gives rise to a large persistent infected

sub-population.

We can rationalize this counter-intuitive trend that persistent infection is more likely when the number of susceptible individuals in the initial population is low, as follows: When S_0 is low, there are many refractory individuals in the population surrounding the infected individual. These individuals are in various stages in the refractory period, and some become susceptible again while the seed is still infectious. If $S_0 \to 0$ and the refractory individuals are uniformly distributed over the refractory range τ_R, the probability of the seed encountering a susceptible individual while still infectious is proportional to τ_I/τ_R. Since at least one neighbour in contact with the seed needs to be susceptible, this probability should be greater than $\frac{1}{4}$ for the infection to spread, on an average. So when the infective stage τ_I is sufficiently long (as in our example of $\tau_I = 4$, in a disease cycle of length 13), extremely low initial S_0 can also lead to persistent infection.

Lastly, note that certain systems in the broad class considered here, have found persistent infection arising due to the presence of "short-cuts" or non-local connections in space. Such long-range links allow a distant infectee to jump through to re-infect and enable perpetuatuation [19, 21]. However, in our case there are no such "short-cuts" aiding persistence. Rather persistence of infection arises from the initial heterogeneity of the population, and this suggests yet another origin of self-sustained infection in a population.

2.6 Conclusion

In summary, we have explored infection spreading qualitatively and quantitatively in a patch of population, where the disease progression of the individuals was given by the SIRS model and an individual became infected on contact with another infected individual. Such an island or isolated patch or habitat, can provide a "natural laboratory" to study spread of epidemics [14]. Here we have focussed on the emergence of persistent infection in the patch, under varying degrees of heterogeneity in the initial population.

Specifically, we considered two scenarios of non-uniformity in the population. In one we consider varying fractions of the initial population in different disease compartments, and in another we examine varying spread in the phases of disease progression among the individuals. Our central result is the following: we find that an infectious seed does not give rise to persistent infection in a homogeneous population consisting of individuals at the same stage of disease progression. Rather, when the population consists of randomly

distributed individuals at various stages of the disease, infection becomes persistent in the population patch.

Now the initial state of the patch of population can occur in different ways. First, a random set of individuals may have colonized the patch, and so the initial state is typically a random mix of individuals. Alternately, we can think of a population comprised of individuals susceptible to a disease being invaded by individuals that may be infected or recovering (refractory), namely a small set of infective or recovered individuals, enter an island/patch of population comprised of individuals susceptible to the disease. The question then is, will this entry lead to persistent infection in the patch? The interesting indication of our study is that if only infecteds enter a population that is entirely made of susceptibles, the infection will die out. However, if a few infecteds (even one) enters along with some refractory individuals the infection will persist. Alternately, if susceptible and refractory individuals are quarantined in a patch, a single infected can lead to sustained infection. Further, if individuals who have recovered from the disease at different points in time are in an isolated group, the entry of even a single infected individual can lead to persistent infection in the group, while the entry of an infected in a group of entirely susceptible individuals or individuals at the exact same stage of recovery, will only lead to transient waves of infection, which will soon die out.

In order to broadly gauge the underlying mechanism that leads to the persistence of infection, one must actually focus on the scenarios where infection burns out. Infections die out eventually when there is too much synchrony in the population, as this can lead to most of the patch entering the refractory stage, and subsequently the susceptible stage, simultaneously. This leaves no infective seed in the population, and no new wave of infection can be initiated. For persistence of infection one then needs a *balance* between sufficiently large number of susceptibles (so that the disease can spread), as well as enough refractory individuals (so that there is no synchronization).

The key to persistent infection therefore, is the random admixture of an infected allows spread of disease, without the entire neighbourhood entering the infective stage synchronously. The counter-intuitive consequence of this is that infection eventually dies out when an infective seed enters a population that is entirely susceptible, while its entry in a population comprised of individuals in different stages of recovery (some of whom will become susceptible within the infective period of the infected individual) gives rise to persistent infection. So our observations suggest that initial heterogeneity leads to greater propensity for sustaining an infected sub-population, thereby facilitating persistent infection refractory and susceptible individuals, leading to de-synchronization

of the phases in the disease cycle of the individuals. So we have demonstrated that when the entire population is susceptible to infection, the infection eventually dies out, while even a few susceptibles among an heterogeneous refractory population gives rise to a large persistent infected sub-population.

Chapter 3

Synchronization Inhibits Persistence of Infection

Adapted from the work published in :

Promit Moitra, Kanishk Jain and Sudeshna Sinha,
Europhysics Letters, **121**:6, 2018.

3.1 Introduction

One of the outstanding problems in the area of infectious epidemics spreading across a population has been obtaining reliable early warning signals for persistence of infection in a region. This is a problem of obvious significance, as it can potentially influence strategies of long-term control of disease. Mathematically this is a challenging problem, as one has to consider large interactive complex systems that are strongly nonlinear and typically not well mixed. In this work we attempt to uncover what dynamical features at early times are strongly correlated to long-term characteristics, such as the continued presence of infection in a population patch. Such features, if found to exist, can potentially provide important *early warning signals* for persistent infections.

The mathematical epidemiological model used in this study is the discrete spatially extended SIRS model, as in the previous problem. The individual dynamics are shown in the schematic Fig 3.1

The total length of the disease cycle, denoted by τ_D, is equal to $\tau_I + \tau_R + 1$, including the state $\tau = 0$ the individual returns to at the end of the refractory period. In this work we consider the typical condition where the refractory stage is longer than the infective stage, i.e. $\tau_R > \tau_I$.

3.2 Spatiotemporal evolution of infection

We now investigate the spread of disease in a spatially distributed group of individuals, where at the individual level the disease progresses in accordance with the SIRS cycle described by the Cellular Automaton model above. In particular, we consider a population of individuals on a 2-dimensional square lattice of linear dimension L, where every node represents an individual [25]. Unlike many earlier studies, we are interested in a *closed* patch of individuals. So instead of the commonly used periodic boundary conditions, the boundaries of our system are fixed, with no individuals outside the boundaries. We will focus on the emergence of persistent infection in such an isolated patch.

We consider a following condition for spread of infection: if one or more of its nearest neighbours of a susceptible individual is infected, then the susceptible individual will become infected. That is, if $\tau_{i,j}(t) = 0$, (namely, the individual is susceptible), then $\tau_{i,j}(t+1) = 1$, if any $1 \leq \tau_{x,y}(t) \leq \tau_I$ where x, y belong to a neigh-

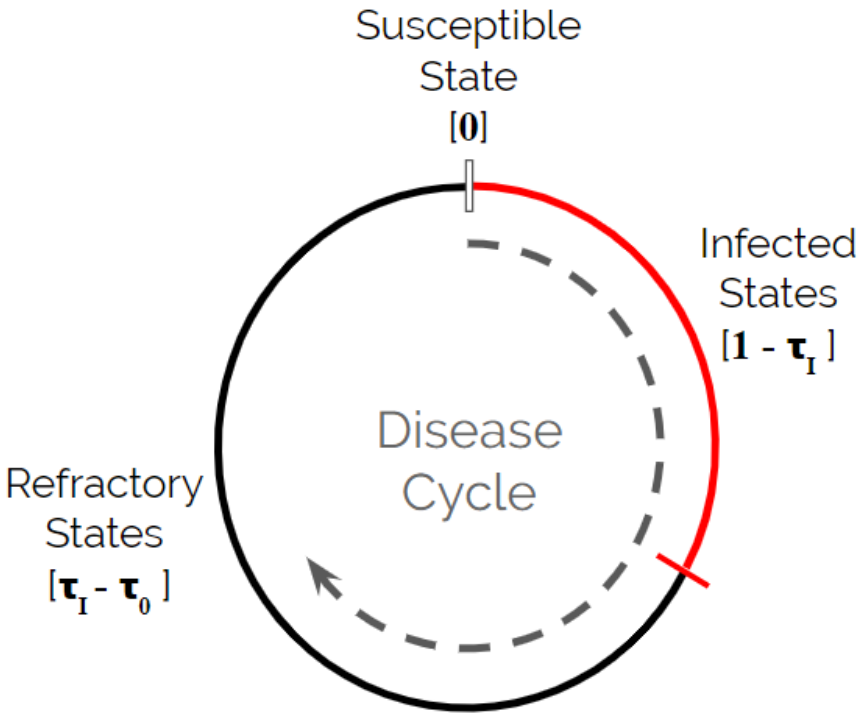

Figure 3.1: The individual oscillatory dynamics of the disease model, represented schematically. The susceptible state S, where $\tau = 0$, is an absorbing state. Once infected, the dynamics is deterministic for an individual, and progresses as shown. The interaction between individuals occurs in the infected phase I, with $\tau \in [1, \tau_I]$. The refractory phase R ($\tau \in [\tau_I, \tau_0]$) confers individuals with temporary immunity, preventing the spread of infection, till they become susceptible again.

bourhood consisting of 4 individuals, namely the von Neumann neighborhood, given by: $x, y \in \{(i-1, j), (i, j+1), (i+1, j), (i, j+1)\}$. Further, we will also consider a neighbourhood comprising of 8 individuals, namely the Moore neighbourhood, given by: $x, y \in \{(i-1, j), (i, j+1), (i+1, j), (i, j+1), (i-1, j-1), (i+1, j+1), (i-1, j+1), (i+1, j-1)\}$ We denote the number of neighbours by K, with the von Neumann neighbourhood having $K = 4$, while the Moore neighbourhood has $K = 8$. Larger K implies that an infected individual can affect individuals in a larger zone around it, namely the infected individual has a larger range of influence. So the dynamics of this extended system combines deterministic, as well as probabilistic elements. The disease progression of an infected individual is deterministic, with the infected period of length τ_I, followed by the refractory period of length τ_R. However, the process of contracting the infection is probabilistic, arising from the interplay of the localized nature of the interactions and the random initial states of the individuals.

Now the infection in this closed patch can either die out, or it can persist. So it is of considerable significance to find the conditions that lead to sustained infection, as well as to uncover the salient features that characterize the persistent state. The relevant quantity here is the asymptotic fraction of infected individuals in the population. To obtain an appropriate measure of this we first find the fraction of infecteds at time t, denoted by $I(t)$. In order to gauge asymptotic trends, we consider this fraction of infected individuals, after long transient time, averaged over several disease cycles, denoted by $\langle I \rangle$. This quantity serves as an order parameter for persistent infection, with non-zero $\langle I \rangle$ indicating persistent infection, while $\langle I \rangle = 0$ indicates that infection has died out in the patch. Further we consider the ensemble averaged $\langle I \rangle$, denoted by $\langle\langle I \rangle\rangle$. This quantity reflects the the size of the basin of attraction of the persistent state, and indicates the probability of persistent infection arising from a generic random initial condition of the population. So $\langle\langle I \rangle\rangle$ is non-zero when persistent infection arises from typical initial states and zero otherwise.

By studying the dependence of $\langle\langle I \rangle\rangle$ on the initial fraction of infecteds I_0, susceptibles S_0 and refractory individuals R_0 in the population, it was found in Ref. [33] that for sustained contagion in a population, the initial population needed to be a well mixed heterogeneous collection of individuals, with sufficiently large number of both susceptible and refractory individuals. Further, it was found that in a population composed of an admixture of susceptible and refractory individuals, persistent infection emerged in a window of reasonably low I_0, with $I_0 \to 0$ at the lower end of this persistence window. Similar phenomena have been observed in diseases modeled by SEIR where spatial heterogeneity was seen to play an important role in the persistence of disease [34]. Further, in more general terms, these results are reminiscent of the observation of noise-sustained oscillations of excitable media [35], with noise playing the role of heterogeneity.

In this work we will focus on the *correlation between synchronization and persistent infection*. We ask two complementary questions: First, does lack of synchronization characterize the state of the population where infection is sustained. Secondly, and more significantly, does the lack of synchronization in the *early stages of disease spreading* lead to persistent infection at later times. We will explore this question by *introducing local and global measures of synchronization*. Lastly, we will demonstrate that when the range of infection transmission of an infected individual is wider, one obtains lower persistent infection. We will account for this counter-intuitive observation through the relation between synchronization and infection burn-out.

3.2.1 Synchronization characterizes populations with sustained infection

We first explore the degree of global synchronization in the system, by calculating the quantity:

$$\sigma(t) = |\frac{1}{N}\Sigma^N \exp^{i\phi_{m,n}(t)}| \tag{3.1}$$

where $\phi_{m,n} = 2\pi\tau_{m,n}/\tau_D$ is a geometrical phase corresponding to the disease stage $\tau_{m,n}$ of the individual at site (m, n). Here the indices m and n run from 1 to L, namely over all $N = L \times L$ individuals in the population patch. We use Eqn. 3.1 to obtain the asymptotic time averaged synchronization order parameter, denoted by $\langle\sigma\rangle$, by averaging $\sigma(t)$ over time, of the order of several disease cycles, after transience. This reflects the synchronization in the emergent system, namely the asymptotic degree of synchronization in the population arising from a specific initial state. So when the phases of disease of the individuals are uncorrelated, that is the disease cycles of the individuals in the population are not synchronized, $\langle\sigma\rangle$ is close to 0. On the other hand when the individual disease cycles are quite synchronized, $\langle\sigma\rangle$ tends to 1. We will then go on to calculate the ensemble averaged asymptotic synchronization order parameter denoted by $\langle\langle\sigma\rangle\rangle$, obtained by further averaging the time-averaged asymptotic synchronization order parameter $\langle\sigma\rangle$ over a large number of initial states characterized by a specific (I_0, S_0, R_0). This order parameter indicates the probability of synchronization arising from a generic random initial condition of the population. We will use this measure, alongside the ensemble averaged persistence order parameter $\langle\langle I\rangle\rangle$, to help us gauge the broad correlation between synchronization in the emergent population (or lack thereof) with persistent infection.

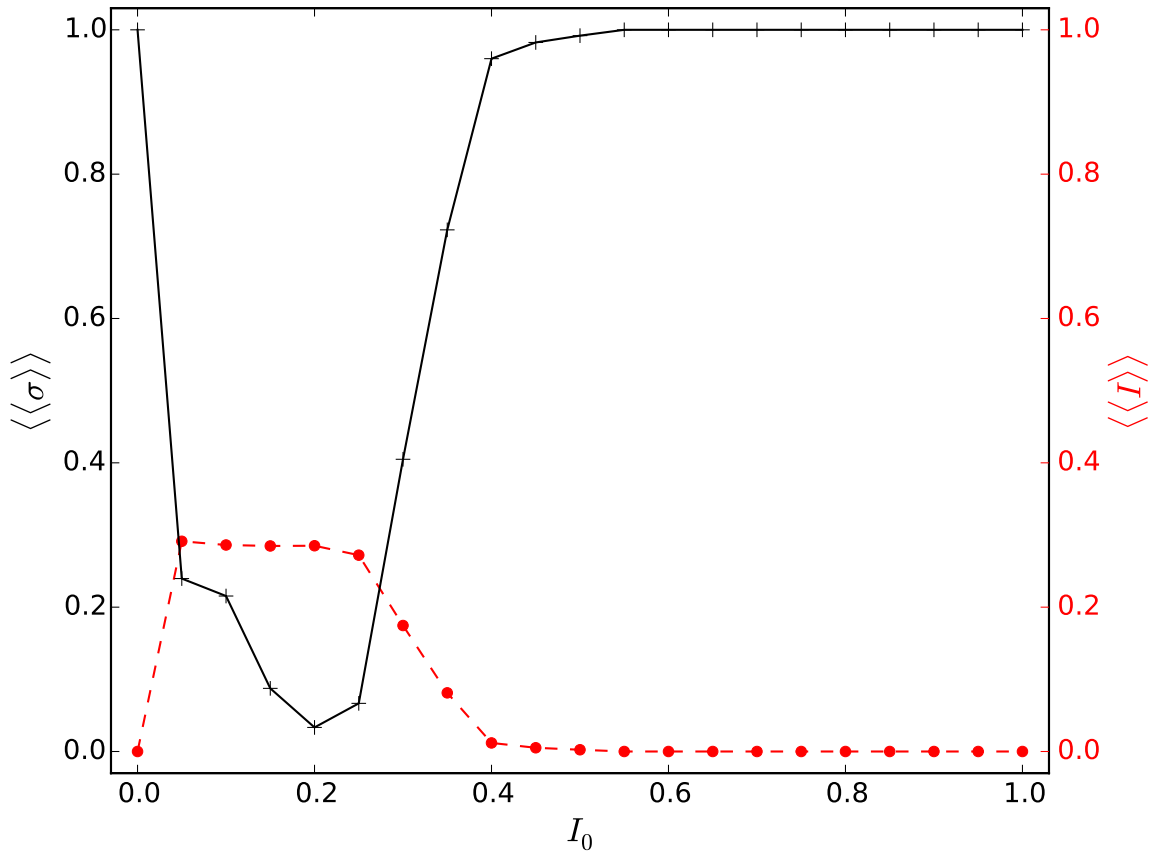

Figure 3.2: Dependence of the ensemble averaged asymptotic synchronization order parameter $\langle\langle\sigma\rangle\rangle$ (black solid line) on the initial fraction of infecteds in the population I_0 (with equal initial fractions of susceptible and refractory individuals: $S_0 = R_0$). where $\langle\langle I\rangle\rangle$ is obtained by averaging over 30 time steps (after the system has evolved through 100 transient time steps) and for 100 random initial conditions. Here system size is 100×100 and $K = 4$. The figure also shows the variation of $\langle\langle I\rangle\rangle$ (red dashed line) with respect to I_0, where $\langle\langle I\rangle\rangle$ is an ensemble averaged order parameter reflecting the degree of persistence of infection in the population.

Fig. 3.2 shows $\langle\langle I\rangle\rangle$ and $\langle\langle\sigma\rangle\rangle$, for different initial fraction of infecteds I_0 in the population. As mentioned before, one observes persistent infection (i.e. $\langle\langle I\rangle\rangle \neq 0$), in a window of I_0 [33]. Further, it is now clearly evident that in this same window of persistent infection, the global asymptotic synchronization order parameter is the lowest. So *higher persistence of infection is consistently correlated with lower degree of synchronization*, distinctly implying that a population where infection is persistent is generally characterized by low synchronization among the individuals. Specifically, for instance for the case of persistent infection with $\langle\langle I\rangle\rangle \sim \frac{1}{3}$, we find $0 < \langle\langle\sigma\rangle\rangle < \frac{1}{3}$. On the other hand, for cases where the infection eventually dies out, i.e. $\langle\langle I\rangle\rangle \sim 0$, we have $\langle\langle\sigma\rangle\rangle \sim 1$. So it is evident that there is clear inverse dependence of infection persistence as reflected by

$\langle\langle I\rangle\rangle$ and degree of synchronization of the disease cycles of the individuals in the emergent population as reflected by $\langle\langle\sigma\rangle\rangle$. *So one can infer that a population where persistent infection emerges, is quite unsynchronized.*

3.2.2 Transient synchronization results in weaker persistence of infection

We have shown above that lack of synchronization is a key feature of populations with sustained infection, and the asymptotic synchronization order parameter $\langle\sigma\rangle$ successfully characterizes populations with different degrees of persistence of infection. This motivates us to explore the second question: is synchronization in the initial (transient) stage, which we will call *transient synchronization* here, an indicator of future persistence of infection in the population?

First, we show in Fig. 3.3 and Fig. 3.4 illustrative examples in order to visually examine the state of the system at various instances of time within the first disease cycle, arising from two distinct initial conditions. The first example is a population with initial fraction of infecteds $I_0 = 0.1$ for which the infection persists, and the second example has $I_0 = 0.5$ for which the infection burns out (cf. Fig. 3.2). Clearly the case with long-term persistence of infection is marked by a lack of synchrony. On the other hand, the case where the infection dies out shows pronounced synchrony within the *first few time steps*. We would now like to investigate if this qualitative observation holds consistently, quantitatively, over a large range of initial states.

3.3 Quantifying finite-time transient synchronization

In order to quantify the early time synchronization in the system, we introduce a finite time average of the synchronization order parameter $\sigma(t)$, from the initial time ($t = 0$) up to a specific time $t = T$ denoted by $\langle\sigma_T\rangle$. Such a measure reflects the degree of synchronization over short time-scales, at early times. We further consider the ensemble average of this quantity, where the average is over a large set of initial states with a specific initial partitioning (I_0, S_0, R_0). This quantity reflects the degree of synchronization typically arising up to time T in the population, from a generic initial state, for a specific (I_0, S_0, R_0), and is denoted by $\langle\langle\sigma_T\rangle\rangle$. When $T \sim \tau_0$ (of the order of a single disease

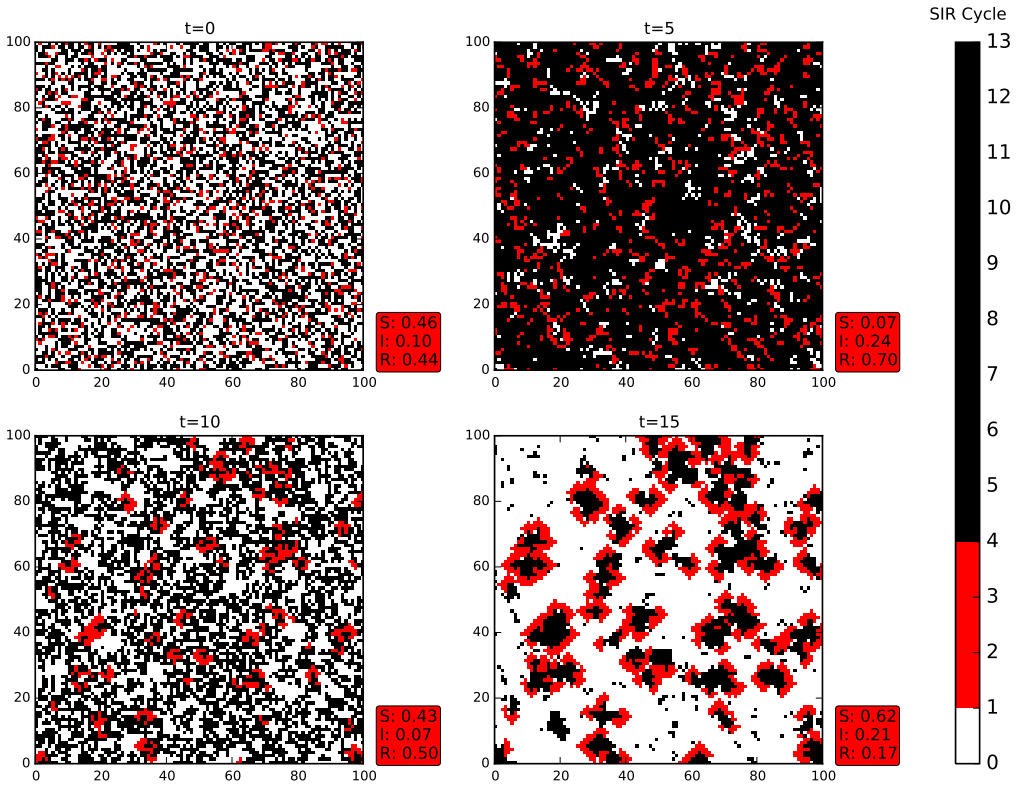

Figure 3.3: Snapshots of the infection spreading pattern at very early times $t = 0, 5, 10, 15$, in an initial population comprising of a random admixture of individuals, with $S_0 = R_0$ and $I_0 = 0.1$ and (b) $I_0 = 0.5$. The colour bar shows the relative lengths of the susceptible (S), infected (I) and refractory (R) stages in the disease cycle, where $\tau_I = 4$, $\tau_R = 9$ and the total disease cycle τ_D is 14. The red box shows the fraction of S, I and R individuals in the population at that instant of time. Notice that the population appears to lack of synchrony in the individual states, and has a non-uniform distribution. The infection persists in this case.

cycle), this quantity reflects the transient synchronization or early-time synchronization, namely synchronization of the population within the first cycle of disease. In this work we will aim to *explore if this quantity can offer a consistent early warning signal for persistence of infection in the patch of population.*

Specifically we will now investigate $\langle\langle\sigma_{15}\rangle\rangle$, namely the case where $T = \tau_D + 1$, where τ_D is the length of the disease cycle. So this quantity reflects the synchronization of the individual disease cycles in the population at early times, and can serve as an useful *order parameter for transient synchronization*. When $\langle\langle\sigma_{15}\rangle\rangle \to 1$, complete synchronization of the individual disease cycles in the population is obtained soon after one disease cycle.

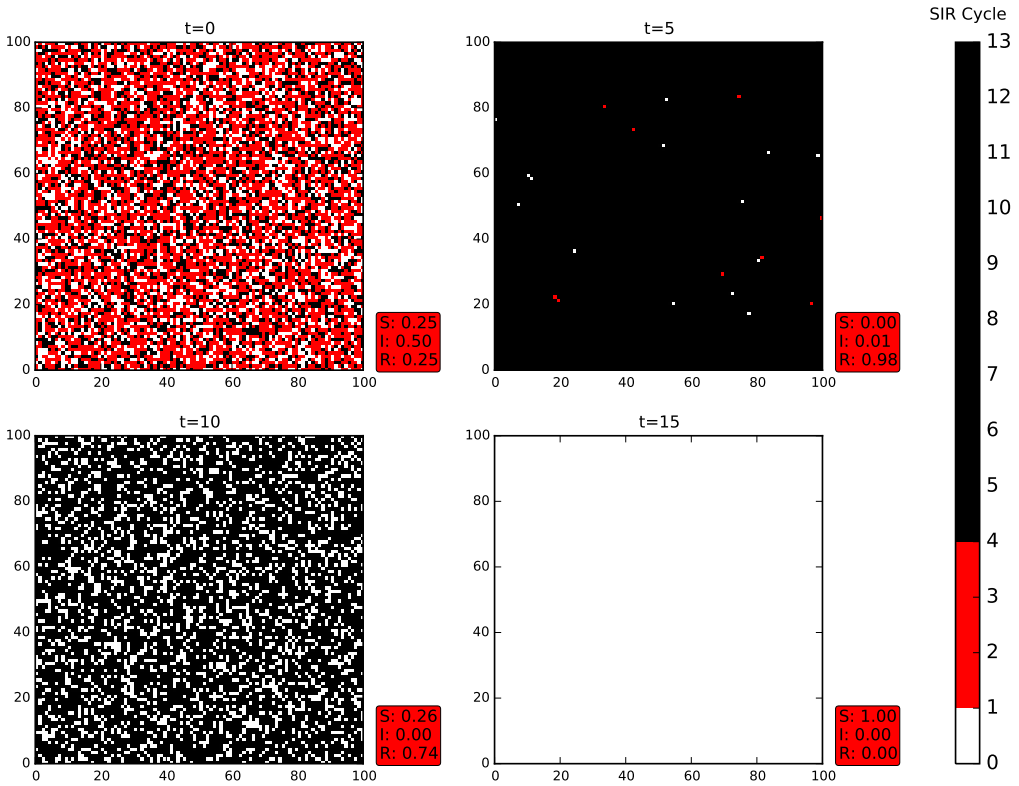

Figure 3.4: Snapshots of the infection spreading pattern at very early times $t = 0, 5, 10, 15$, in an initial population comprising of a random admixture of individuals, with $S_0 = R_0$ and $I_0 = 0.5$. The colour bar shows the relative lengths of the susceptible (S), infected (I) and refractory (R) stages in the disease cycle, where $\tau_I = 4$, $\tau_R = 9$ and the total disease cycle τ_D is 14. The red box shows the fraction of S, I and R individuals in the population at that instant of time. Notice that the population appears to be in synchrony in the individual states, and has a more uniform distribution. The infection dies out in this case.

Fig. 3.5 shows the dependence of the degree of transient synchronization $\langle\langle\sigma_{15}\rangle\rangle$, namely the degree of synchronization right after completion of the first cycle of disease, on the fraction of infecteds I_0 in the initial population. It is evident that the onset of the persistence window is clearly indicated by minimum $\langle\langle\sigma_{15}\rangle\rangle$, i.e. the transient synchronization is the lowest when persist infection begins to emerge in the population. So, the *early synchronization properties of the system allows one to gauge the future persistence of contagion*. A valuable consequence of this observation is that early-time synchronization can serve as an early warning signal for sustained infection at a much later time.

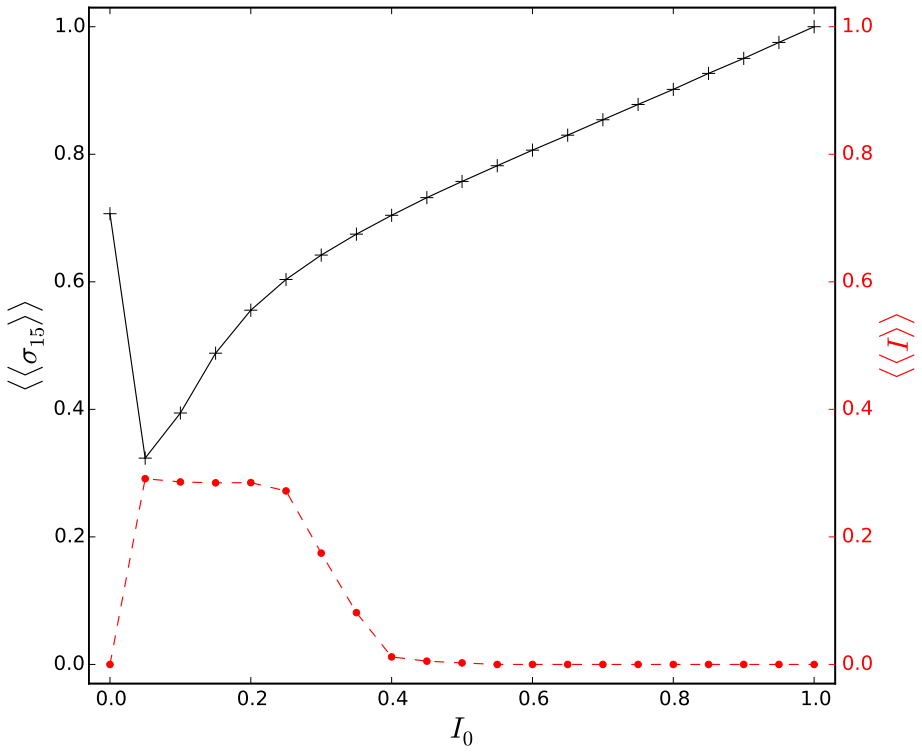

Figure 3.5: Dependence of the transient synchronization order parameter $\langle\langle\sigma_{15}\rangle\rangle$ on the initial fraction of infecteds $I_0 \in [0, 1]$ (with $S_0 = R_0$ and system size 100×100). Here the synchronization order parameter at each I_0 is obtained by averaging over 100 random initial conditions. The quantities are obtained by averaging over $I_0 \in [0, 1]$, with $S_0 = R_0$. Here $K = 4$.

Now we examine the explicit correlation between $\langle\langle\sigma_{15}\rangle\rangle$ and the asymptotic fraction of infecteds in the population $\langle\langle I\rangle\rangle$. This is shown in Fig. 3.6, from where one can clearly see a well-defined transition to long-term persistent infection as the transient states get more synchronized. So the asymptotic fraction of infecteds decreases sharply at short-time synchronization order parameter values close to 2/3. Namely, there exists a critical transient synchronization order parameter $\sigma_T^\star$, beyond which persistent infection does not occur (i.e. $\langle\langle I\rangle\rangle \sim 0$). Note that this critical $\sigma_T^\star$ reflects early-time properties, while offering a clear correlation with an asymptotic phenomena. It quantitatively confirms our intuition that when the system is more synchronous at early times, there is greater propensity of the infection dying out.

So we conclude that greater degree of synchronization at early times hinders the sustenance of infection. Thus *early short-time asynchrony appears to be a consistent precursor to future persistence of infection, and can perhaps provide valuable early warning signals*

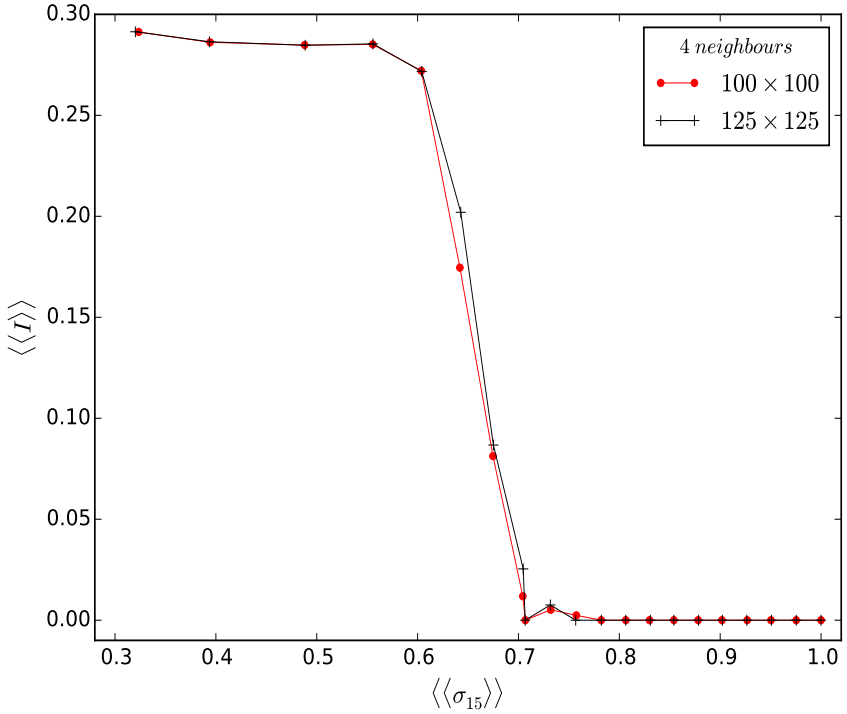

Figure 3.6: Correlation between the asymptotic persistence parameter $\langle\langle I\rangle\rangle$ and the ensemble averaged transient synchronization order parameter $\langle\langle\sigma_{15}\rangle\rangle$. The quantities are obtained by averaging over $I_0 \in [0, 1]$, with $S_0 = R_0$. Here $K = 4$.

for anticipating sustained contagion in a population patch.

3.3.1 Transient Local synchronization

Now we explore the correlation of transient *local synchronization*, namely synchronization in a local neighbourhood of an individual. This is important, as infection spread is a local contact process and so the composition of its local neighbourhood is most crucial for an individual. In order to capture finite-time local synchrony, we introduce the following synchronization parameter:

$$\sigma_K^{(i,j)}(t) = |\frac{1}{K+1}\Sigma_{m,n}\exp^{i\phi_{m,n}(t)}| \tag{3.2}$$

where $\phi_{m,n}$ is a geometrical phase corresponding to the disease stage $\tau_{m,n}$ of the individual at site (m, n). Here the indices m and n run over the site index and all K sites

contained within the neighbourhood of (i, j). The average of $\sigma_K^{(i,j)}(t)$ over all sites (i, j) in the system is denoted by $\sigma_K(t)$.

The focus of our investigation is the finite time average of $\sigma_K(t)$ from initial time $(t = 0)$ to time T, where T is of the order of one disease cycle length. We denote this measure of finite-time local synchronization as $\langle \sigma_{K,T} \rangle$. The ensemble averaged $\langle \sigma_{K,T} \rangle$ is denoted by $\langle\langle \sigma_{K,T} \rangle\rangle$, and this quantity reflects the typical transient local synchronization present in the system.

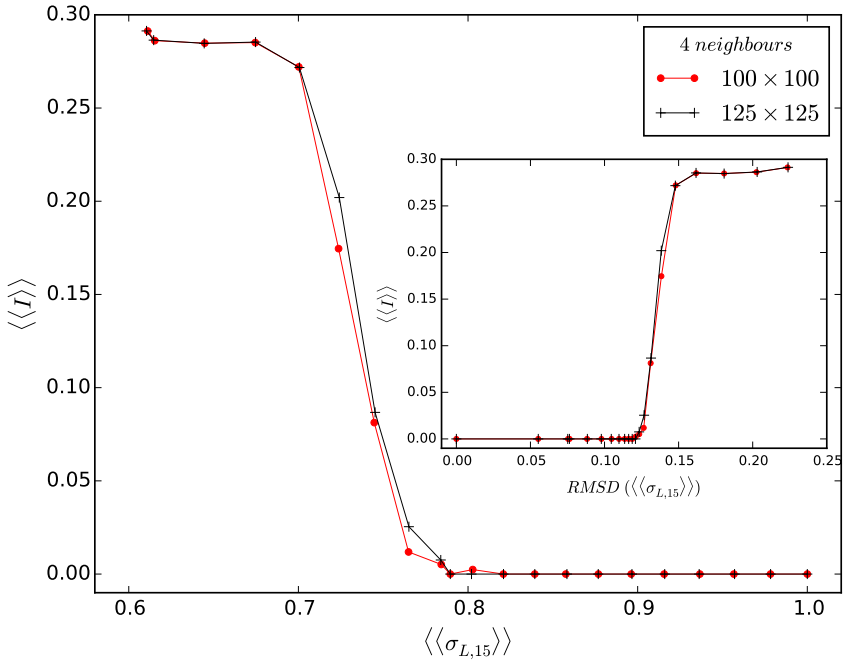

Figure 3.7: Dependence of the asymptotic persistence parameter $\langle\langle I \rangle\rangle$ on the ensemble averaged transient local synchronization order parameter $\langle\langle \sigma_{K,15} \rangle\rangle$. The quantities are obtained by averaging over $I_0 \in [0, 1]$, with $S_0 = R_0$ and $K = 4$. Inset shows the dependence of $\langle\langle I \rangle\rangle$ on the root mean square deviation (RMSD) of $\sigma_{K,15}$.

We show the explicit correlation between the transient local synchronization order parameter $\langle\langle \sigma_{K,15} \rangle\rangle$ and the asymptotic fraction of infecteds in the population $\langle\langle I \rangle\rangle$ in Fig. 3.7. It is clearly evident that there exists a sharp transition to infection burn-out as transient local synchronization goes beyond a critical value $\sigma^\star_{K,T} \sim 3/4$. Broadly speaking then, on an average, local neighbourhoods need at least one neighbour whose state in not in sync with the other neighbours, to allow the sustenance of infection in the population. That is, when *local neighbourhoods are synchronized beyond a critical degree during early stage of disease spreading, persistent infection does not occur.* So, though critical $\sigma^\star_{K,T}$ depends on early-time spatially local information, it offers a clear indication

of asymptotic phenomena.

Further notice that the spread in transient local synchronization across initial states, as reflected by the root mean square deviation (RMSD) of $\langle \sigma_{K,T} \rangle$ in the inset of Fig. 3.7, also exhibits a sharp transition from the case of non-persistent infection (i.e. $\langle\langle I \rangle\rangle = 0$) to persistent infection (where $\langle\langle I \rangle\rangle \sim 1/3$). This suggests that when the early-time local synchronization has deviations larger than a critical RMSD, infection persists over a long time in the population patch.

3.4 Dependence of persistence of infection on the range of infection transmission

Lastly, we explore the influence of the range of infection transmission on the persistence of infection. Specifically we investigate the case of $K = 8$, namely the case where infected individuals can affect eight neighbours. So now the range of influence of the infected individual is double that presented earlier, where K was 4. Fig. 3.8 shows the dependence of the persistence order parameter $\langle\langle I \rangle\rangle$ on the fraction of infected individuals I_0 in the initial population, with $S_0 = R_0$. It is clearly evident from the figure that persistent infection is lower when the infected individual influences a larger number of neighbouring individuals. That is, surprisingly, a *larger range of infection transmission hinders long-term persistence of the disease.*

However, this counter-intuitive result is completely in accordance with our earlier observation, namely higher synchronization implies lower persistence of infection. This is clearly bourne out by the asymptotic synchronization order parameter, which is also displayed in Fig. 3.8 alongside the persistence order parameter $\langle\langle I \rangle\rangle$. From the figure it can be seen that for $K = 8$ the synchronization is enhanced, and so $\langle\langle \sigma \rangle\rangle$ is low only in a very small range of I_0. It is this precise range that supports persistent infection. Since the range of low synchronization is significantly smaller for $K = 8$ vis-a-vis $K = 4$, we correspondingly have a significantly smaller range of persistent infection when the range of infection transmission is larger.

Further, we again examine the explicit correlation between the transient synchronization, as reflected by $\langle\langle \sigma_{15} \rangle\rangle$, as well as the local transient synchronization, as reflected by $\langle\langle \sigma_{K,15} \rangle\rangle$, and the asymptotic fraction of infecteds in the population $\langle\langle I \rangle\rangle$. These are shown in Fig. 3.9 and Fig. 3.10, from where one can again clearly see a well-defined

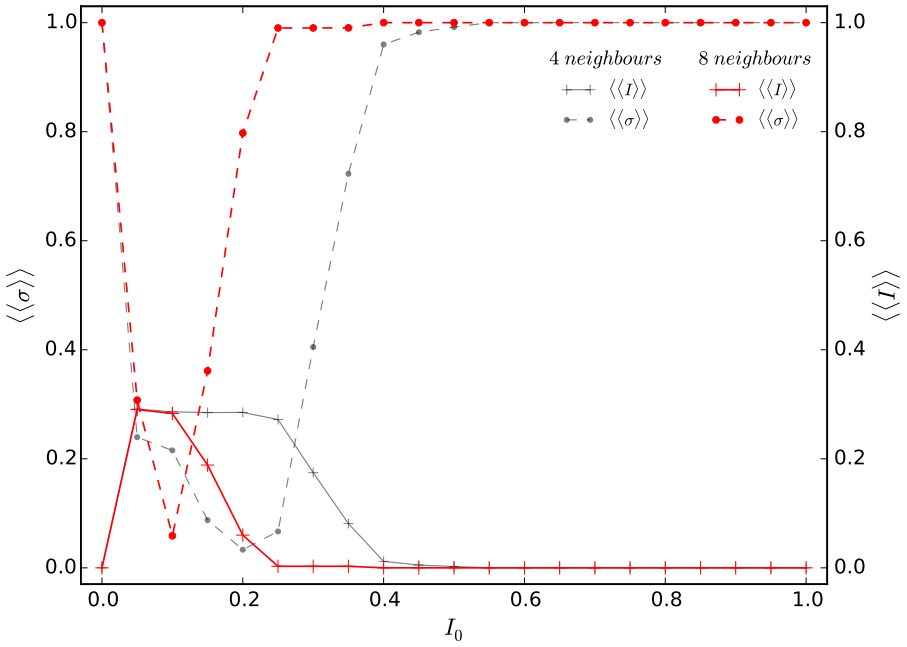

Figure 3.8: Dependence of $\langle\langle I\rangle\rangle$ on the initial fraction of infected individuals I_0 in the population, for the case of $K = 8$ (solid red line) and the case of $K = 4$ (red dashed line) for reference. Here system size is 100×100. Alongside we show the dependence of the ensemble averaged asymptotic synchronization order parameter $\langle\langle\sigma\rangle\rangle$ on I_0, for the case of $K = 8$ (solid black line) and the case of $K = 4$ (black dashed line) for reference.

transition to long-term persistent infection as the transient states get more synchronized both locally and globally. So again, quantitatively it can be seen that early-time local and global properties offer a clear indication of asymptotic persistence properties. This lends further credence to our central observation, and demonstrates the robustness and generality of the phenomenon with increasing range of infection transmission.

Also interestingly, as in the case of $K = 4$, the asymptotic fraction of infecteds again decreases sharply at transient synchronization order parameter values close to $2/3$ and local transient synchronization order parameter values around $3/4$. However we observe that the precise value of the critical transient synchronization order parameters, $\sigma_T^\star$ and $\sigma_{K,T}^\star$, beyond which persistent infection does not occur (i.e. $\langle\langle I\rangle\rangle \sim 0$), is lower for the system with a wider range of infection transmission. This implies that larger desynchronization of the phase of the individual disease cycles is necessary in order to obtain persistent infection, when the range of infection transmission is larger. This is consistent with the counter-intuitive observation that persist infection arises over smaller parameter ranges for larger K, as evident in Fig. 3.8.

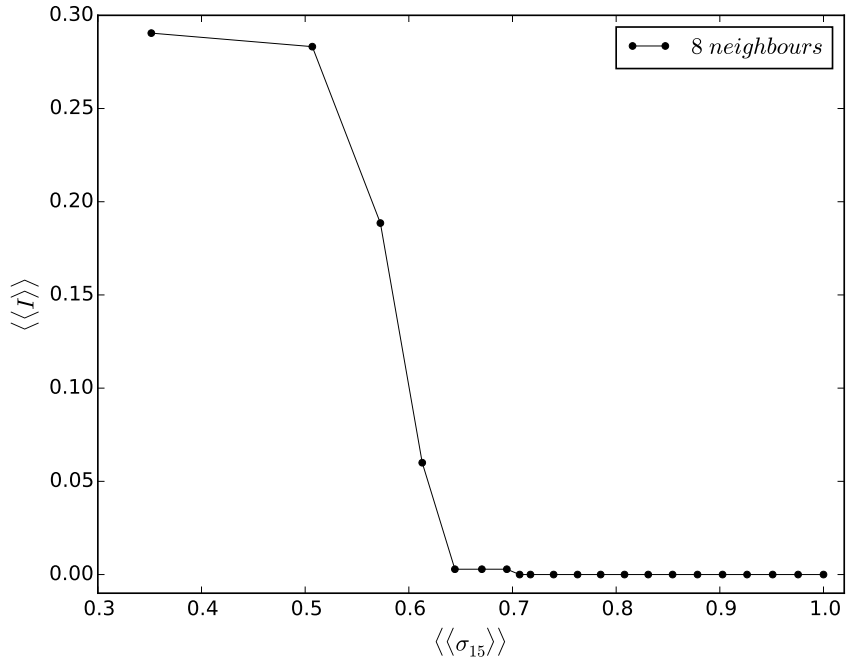

Figure 3.9: Dependence of the asymptotic persistence parameter $\langle\langle I\rangle\rangle$ on the ensemble averaged transient synchronization order parameter $\langle\langle \sigma_{15}\rangle\rangle$. The quantities are obtained by averaging over $I_0 \in [0, 1]$, with $S_0 = R_0$. Here system size is 100×100 and $K = 8$.

3.5 Discussion

In summary, we have explored the emergence of persistent infection in a closed region where the disease progression of the individuals is given by the SIRS model, with an individual becoming infected on contact with another infected individual within a given range. We focussed on the role of synchronization in the persistence of contagion. Our key result is that higher degree of synchronization, both globally in the population and locally in the neighborhoods, hinders persistence of infection. Importantly, we found that *early local asynchrony appears to be a consistent precursor to future persistence of infection*, and can potentially provide valuable early warnings for sustained contagion in a population patch. Thus transient local synchronization can help anticipate the long-term persistence of infection. Further we demonstrated that when the range of influence of an infected individual is wider, one obtains lower persistent infection. This counter-intuitive observation can also be understood through the relation of synchronization to infection burn-out.

Lastly, our results also have broad relevance in the context of large interactive excitable systems. For instance, the system we study here is reminiscent of models of reaction-

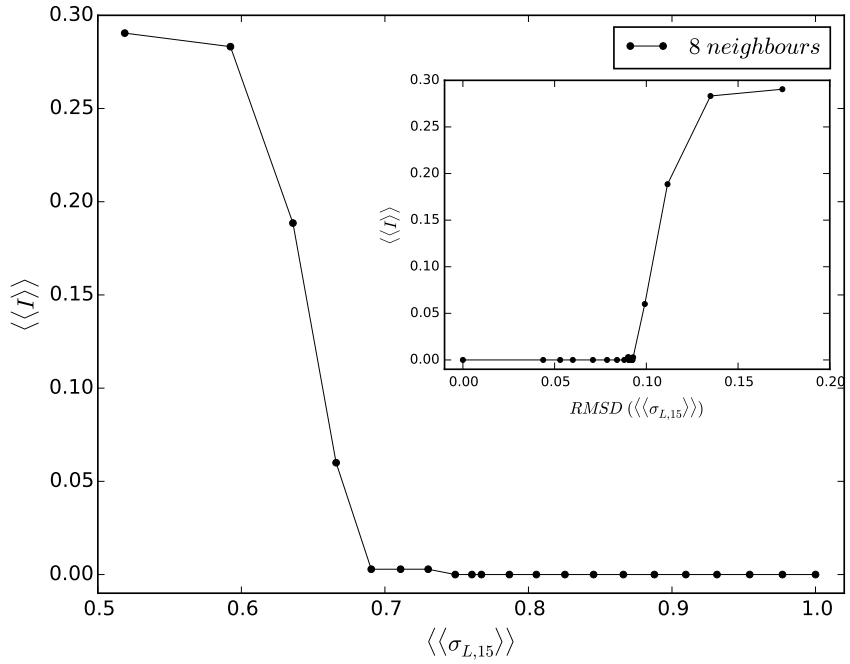

Figure 3.10: Dependence of the asymptotic persistence parameter $\langle\langle I\rangle\rangle$ on the ensemble averaged transient local synchronization order parameter $\langle\langle\sigma_{K,15}\rangle\rangle$. The quantities are obtained by averaging over $I_0 \in [0, 1]$, with $S_0 = R_0$. Inset shows the dependence of $\langle\langle I\rangle\rangle$ on the root mean square deviation (RMSD) of $\sigma_{K,15}$. Here system size is 100×100 and $K = 8$.

diffusion systems [36], heterogeneous cardiac tissue [37, 38] and coupled neurons [39]. The self-sustained excitations in these systems are analogous to the state of persistent infection we have focused on in this work. Specifically, persistent chaotic activity in a patch of tissue is characteristic of atrial fibrillation, and so our observations may have potential relevance to such phenomena arising in cardiac tissue. In the context of brain functions, neuronal circuits are able to sustain persistent activity after transient inputs, and studies have suggested that the asynchronous phase of synaptic transmission plays a vital role in the this persistent activity which is of considerable importance to motor planning and memory. Further, in the context of metapopulations [40], there exists research which argues that enhanced coherence would decrease the probability of species persistence [41]. So our demonstration of the potential of *early short-time local and global synchronization* as an early warning signal for anticipating persistent activity, has relevance to such phenomena as well.

Chapter 4

Effect of Community Structure on the Persistence of Infection

4.1 Introduction

We now investigate the spread of infection in a group of spatially distributed individuals, where at the individual level the disease progresses in accordance with the SIRS cycle, as modeled by the cellular automaton described in the previous chapters. In this work we focus on an unexplored aspect of such systems, namely we attempt to ascertain the *dependence of the persistence of infection on the structure of the population.* So the specific question of relevance here will be the correlation between sustained long-time persistence of disease in the two communities and the difference in the initial states of the two communities. That is, we will investigate the dependence of infection persistence (if any) on the initial differences between the communities constituting the population.

In particular, we consider a population of individuals in two distinct communities. Each community is a 2-dimensional $N \times N$ lattice where every node, representing an individual, has 4 immediate neighbors. Within each patch, the phases of the disease cycle are randomly distributed among individuals such that the distributions of infecteds, susceptibles and refractory individuals are spatially uniform over the lattice constituting each community. The boundaries of the communities are fixed, with no interactions outside the patch. So each community mimics a closed population patch, such as an island or an isolated habitat.

Now we consider two such communities to be connected through a small number of links. The connections between the two communities may be spatially adjacent or randomly located. The fraction of inter-community links along the adjoining edges of the communities is denoted by f_{ic}. This quantity is analogous to a connection density between the communities, and reflects the probability that individuals from a community can interact, through migration or transport across the boundary, with a set of individuals in the other community. In this work we will consider a wide range of connection densities, from one or two connections, to links along the entire boundary edge between the communities. The central results of our work here, based on order parameters obtained by averaging over space and time, do not depend on the location of the links.

4.2 Spatiotemporal Patterns of Disease Spreading among the Communities

We first study the spatiotemporal patterns of the spread of infection among the two communities connected via a few links along an adjoining edge. With no loss of generality, we display results for two communities of size 100×100.

In order to explore the effect of heterogeneous communities on persistence of disease, which is the principal focus of our investigation, we consider the communities to have varying initial fractions of susceptibles $S_0^{(i)}$, infecteds $I_0^{(i)}$ and refractory individuals $R_0^{(i)}$, where $i = 1, 2$ is the index of the community. So the communities are comprised of random admixtures of infected, susceptible and refractory individuals, which may differ on an average, in varying degrees.

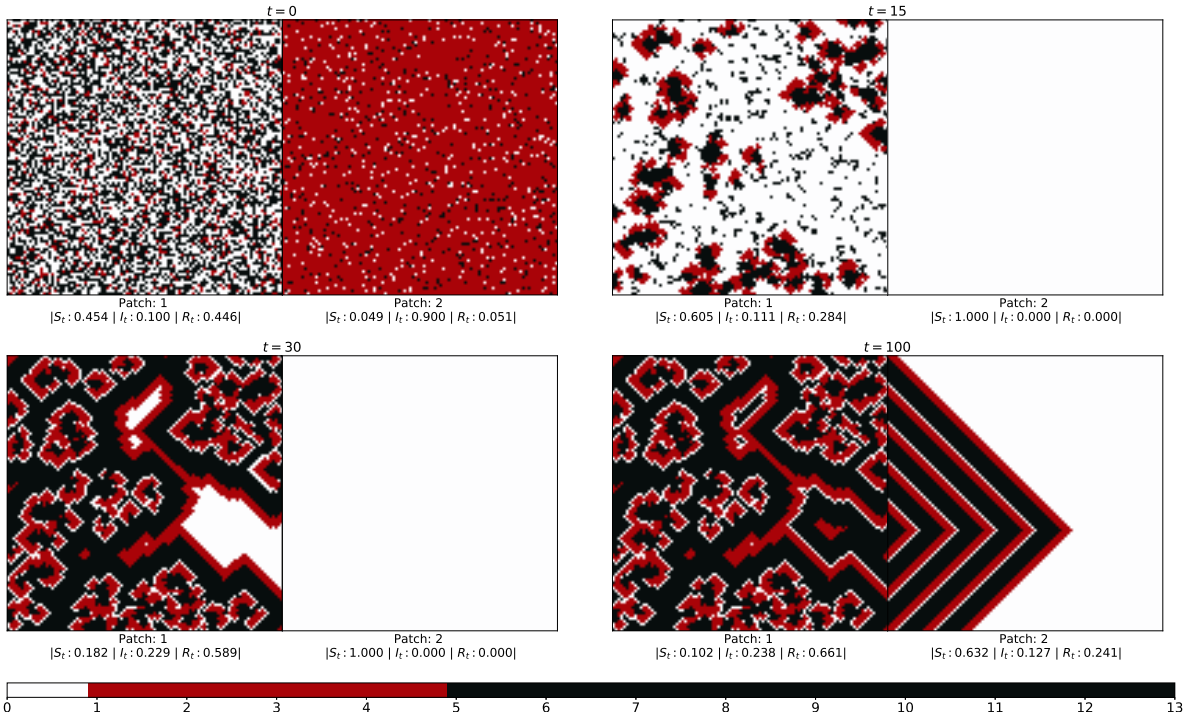

Figure 4.1: Infection spreading patterns for two communities, where the initial fraction of infecteds is $I_0^{(1)} = 0.1$ in patch 1 and $I_0^{(2)} = 0.9$ in patch 2, with the initial fraction of susceptible and refractory individuals being equal in both communities (i.e. $S_0^{(i)} = R_0^{(i)}$ for $i = 1, 2$). Here the fraction of boundary sites that have inter-community connections is $f_{ic} = 0.1$, i.e. 10 sites on an average interact with the other community.

We explore the number of infecteds in the emergent state of the entire population, under varying differences in the initial states of the communities. That is, we investigate the long-term presence of infection in both communities under progressively increasing

difference in the initial states of the patches. Representative results are displayed in Figs. 4.1-4.2. Fig. 4.1 shows the infection spreading patterns for two communities, where the initial fraction of infecteds is $I_0^{(1)} = 0.1$ in one patch and $I_0^{(2)} = 0.9$ in the other. As a reference Fig. 4.2 shows the infection spreading patterns for two communities, where the initial composition is identical. Note that the *average* initial fractions of infected, susceptibles and refractory individuals is the same in both systems, i.e $I_0^{(1)} (= I_0^{(2)})$ in Fig. 4.2 is equal to $\frac{(I_0^{(1)}+I_0^{(2)})}{2}$ in Fig. 4.1. So the populations in the two figures do not differ on an average. However, the populations are very different in terms of the heterogeneity in the distribution of the infecteds. In Fig. 4.1 the communities are significantly different in initial composition and so the system as a whole is strongly non-uniform, while in Fig. 4.2 the disease phases are uniformly distributed across the population and there is no difference in the distributions of the two communities. It is clearly evident then from Fig. 4.1 via-a-vis Fig. 4.2, that *populations partitioned into distinct communities yield long-term persistence of disease, while a population with uniformly distributed individuals in different stages of disease, results in the extinction of the infection from the entire population.*

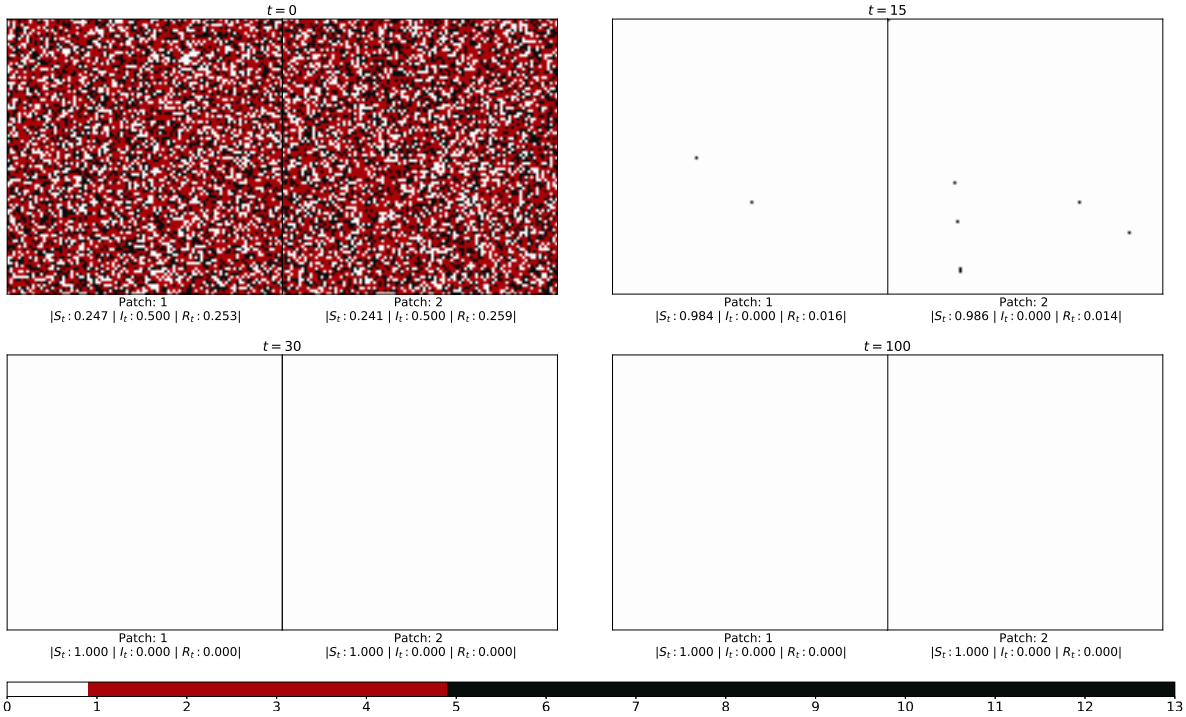

Figure 4.2: Infection spreading patterns for two communities, where the initial fraction of infecteds is $I_0^{(1)} = I_0^{(2)} = 0.5$ in both patches, and $S_0^{(1)} = S_0^{(2)} = R_0^{(1)} = R_0^{(2)}$. Here all sites along adjoining edge of the two communities have inter-community connections (i.e. $f_{ic} = 1.0$).

Figs. 4.3-4.4 shows the time evolution of the fraction of infected individuals in the

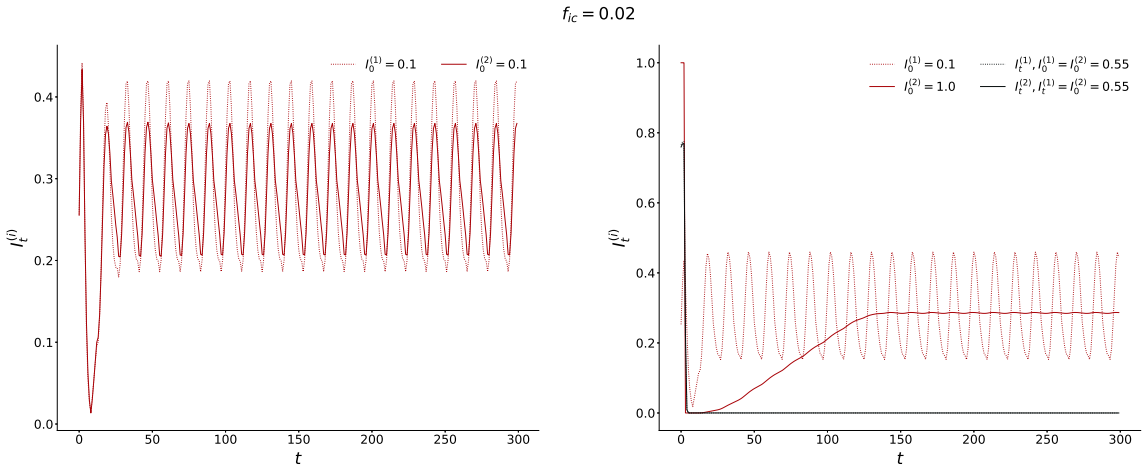

Figure 4.3: Time evolution of the fraction of infected individuals $I_t^{(i)}$ in the two communities, of size $N = 100 \times 100$, where the initial fraction of infecteds is (a) $I_0^{(1)} = I_0^{(2)} = 0.1$ and (b) $I_0^{(1)} = 0.1$ and $I_0^{(2)} = 1.0$ (with $S_0^{(i)} = R_0^{(i)}$ for $i = 1, 2$). On an average two boundary sites have inter-community connections (i.e. $f_{ic} = 0.02$). In (b), as a reference the evolution of two identically distributed communities with the same average number of infecteds as the average of the two communities (i.e. $\frac{(I_0^{(1)} + I_0^{(2)})}{2} = 0.55$) spread uniformly across the communities, is shown by the black/grey lines. Clearly, the infected fraction rapidly goes to zero when the phases of disease are uniformly distributed among the communities, namely there is no persistence of infection for spatially homogeneous populations.

two communities for the case of communities with identical average initial states, and for communities with very different initial states. It is clear from the time series that when the initial state of the patches are close, the wave forms are similar in both amplitude and frequency. However, when the initial states of the communities are markedly different, the time evolution of the infected sub-set has very different amplitude, though same frequency. Interestingly, the *average* fraction of infected is the *same* in both communities, though the pattern of evolution is significantly different. The patch which had a much higher initial fraction of infecteds evolves to an oscillatory pattern with very low amplitude around the average value of approximately 1/3, while the fraction of infecteds in the patch with low initial fraction of infecteds oscillates with large amplitude around the same mean value (~ 0.3). So after transience, two communities with very different initial average composition settle down to identical average behaviour. Nevertheless, the local evolution of infection bears a discernible mark of the distinct initial states.

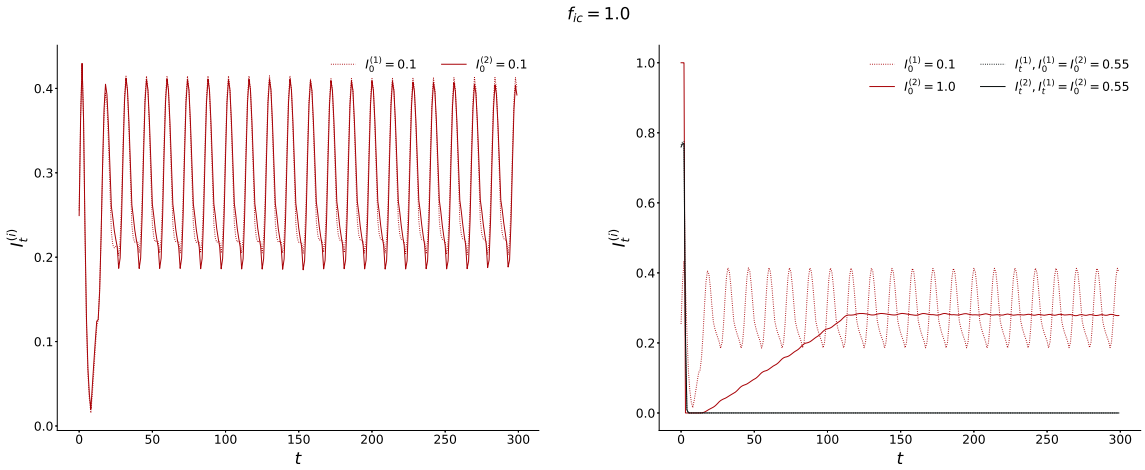

Figure 4.4: Time evolution of the fraction of infected individuals $I_t^{(i)}$ in the two communities, of size $N = 100 \times 100$, where the initial fraction of infecteds is (a) $I_0^{(1)} = I_0^{(2)} = 0.1$ and (b) $I_0^{(1)} = 0.1$ and $I_0^{(2)} = 1.0$ (with $S_0^{(i)} = R_0^{(i)}$ for $i = 1, 2$). Here all sites along the adjoining edge of the communities have connections across the boundary in the other community (i.e. $f_{ic} = 1$), with the inter-community links being spatially random. In (b), as a reference the evolution of two identically distributed communities with the same average number of infecteds as the average of the two communities (i.e. $\frac{(I_0^{(1)} + I_0^{(2)})}{2} = 0.55$) spread uniformly across the communities, is shown by the black/grey lines. Clearly, the infected fraction rapidly goes to zero when the phases of disease are uniformly distributed among the communities, namely there is no persistence of infection for spatially homogeneous populations.

4.3 Dependence of the Persistence Order Parameter on Heterogeneity

In order to quantify the long-term persistence of disease we define a persistence order parameter $\langle\langle I_t \rangle\rangle$, given as the fraction of infected individuals in the entire population (comprised of both communities), after transience, averaged over time of the order of several disease cycles, and further averaged over a large sample of random initial states. This persistence order parameter indicates the absence of infection in the long-term when equal to zero, and indicates the sustained presence of infection when non-zero.

Specifically, we first consider the initial infected fraction $I_0^{(1)}$ of one patch to be $I_0^* = 0.1$. This implies that initially, 10% of the population in the patch is infected. The fractions $S_0 = R_0$ for both communities, unless otherwise specified. Now, if this patch was considered independent of the second patch, this fraction of initial infecteds I_0^* would yield persistent infection [33].

The initial infected fraction of the second patch $I_0^{(2)}$ is varied as $I_0^* + \Delta$. So Δ serves as an useful parameter reflecting the difference between the initial fractions of infected individuals present in the communities, indicative of the heterogeneity of the system. In particular, in our representative examples, $\Delta \in [0.0, 1-I_0^*] = [0.0, 0.9]$. This provides us a parameter to control the spatial compartmentalization, or non-uniformity, of the disease phases within the system. Larger Δ indicates a more heterogeneous system, comprised of more diverse communities.

We explore the variation in this persistence order parameter $\langle\langle I_t \rangle\rangle$, under increasing differences between the initial states of the two patches Δ. We scan the full range of Δ between 0.0 to 0.9. When $\Delta = 0.0$, both communities have equal initial fractions of infected individuals ($I_0^{(1)} = I_0^{(2)} = I_0^* = 0.1$), and so the spatial distribution of disease phases of the entire population is uniform. When Δ is very large, for instance equal to 0.8, $I_0^{(2)} = I_0^* + \Delta = 0.1 + 0.8 = 0.9$. This implies that the second patch has a much higher density of infected individuals than the first one, thus yielding an exceedingly non-uniform spatial distribution of disease phases in the system. The question we focus on here is the correlation between this spatial heterogeneity and the long-term behaviour of the coupled communities, specifically in terms of the sustained presence of disease and the patterns of infection spreading.

It is important to note that as Δ is varied, the average fraction of initially infected individuals in the full system, comprised of both the communities, also changes. Specifically, as we vary Δ from 0.0 to 0.9, with $I_0^{(1)} = 0.1$, $I_0^{(2)}$ varies from 0.1 to 1.0. This implies that the collective average infected fraction of the two communities $\langle I_0 \rangle = \frac{I_0^{(1)} + I_0^{(2)}}{2}$, varies from $(0.1 + 0.1)/2 = 0.1$ to $(0.1 + 1.0)/2 = 0.55$.

In order to establish that the emergent patterns of infection in the two coupled communities, depend on the initial spatial non-uniformity of the individual disease phases, and not on the collective average infection initially present in the communities, it is illustrative to compare our observations in two contrasting conditions. As a reference for comparison (as we had done earlier in Figs. 4.1-4.2), we first find the asymptotic fraction of infecteds in the entire population, $\langle\langle I_t \rangle\rangle$, for a population comprised of two communities whose average initial state is identical (i.e. $I_0^{(1)} = I_0^{(2)}$), namely there is spatial uniformity (on an average) between the patches. We consider different average initial fraction of infecteds $\langle I_0 \rangle$ in this population, spanning the full range corresponding to different values of Δ, given as:

$$\langle I_0 \rangle = \frac{I_0^{(1)} + I_0^{(2)}}{2} = \frac{I_0^* + I_0^* + \Delta}{2} = I_0^* + \frac{\Delta}{2} \tag{4.1}$$

We find the persistent infected set for initial populations with increasing average infected fractions $\langle I_0 \rangle$, obtained by varying Δ as in Eqn. 4.1. The initial spatial homogeneity is maintained by initializing both communities with an equal fraction of infected individuals (i.e. $I_0^{(1)} = I_0^{(2)} = \langle I_0 \rangle = I_0^* + \frac{\Delta}{2} \in [0.1, 0.55]$). With this constraint, we vary their collective average infected fraction, and track the long-term presence of infecteds in the entire population.

In order to establish the impact of spatial non-uniformity on the long-term persistence of infection, we identify the distinct features that arise specifically in heterogeneous communities, by comparison to reference control systems that are spatially uniform. From Fig. 4.5, it can be ascertained that when the initial spatial distribution of infected individuals between the two communities is significantly different, the infection is persistently present in both the communities asymptotically, for all initial conditions. The red curve shows the response of the system if the two patches were not segmented, and behave as a single uniform patch, with the infected individuals initially distributed uniformly as in Fig. 4.2. When the average initial infection of this system increases, the *persistence of infection drops significantly*. However, when the two patches have distinct densities of initial infection as in Fig. 4.1, with the sum total of infecteds in the two communities being the same as in the reference system on average, *the infection sustains itself in both the communities*. Thus we can conclude that the presence of infection in the long run originates due to the non-uniform spatial distribution of the disease phases in the two communities, and not due to the variation in the overall average initial infection present in the system.

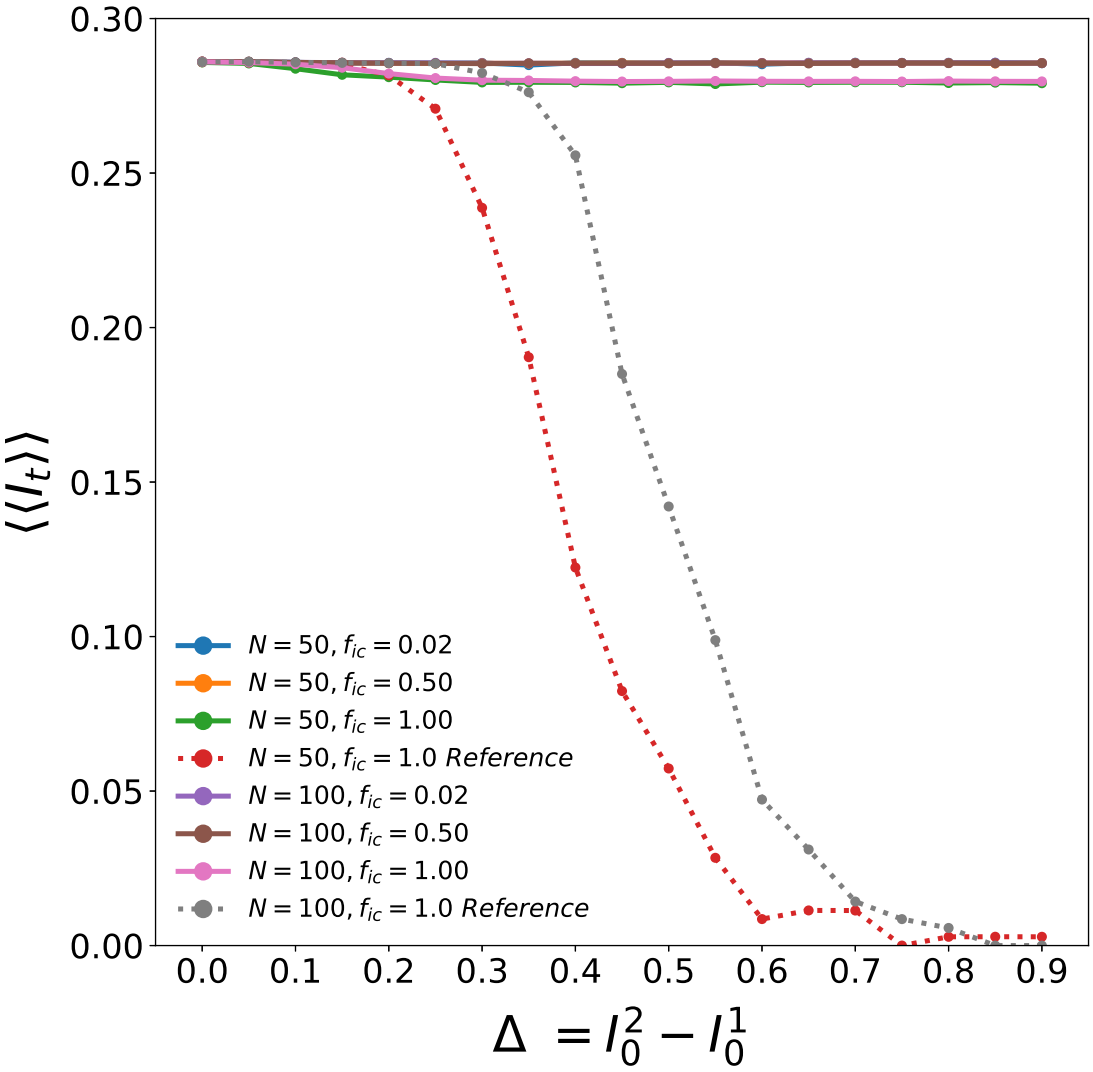

Figure 4.5: Dependence of the persistence order parameter $\langle\langle I_t \rangle\rangle$ of the community 2 (i.e. average asymptotic fraction of infected individuals in the second patch) on parameter Δ (which quantifies the difference in the initial composition of the communities). Here the initial infecteds $I_0^{(0)} = I_0^*$ and $I_0^{(2)} = I_0^* + \Delta$, community size is 50×50 and the fraction of boundary sites with inter-community connections is: $f_{ic} = 0.02$ (blue), 0.5 (yellow) and 1.0 (green). The red curve shows the variation of persistence order parameter $\langle\langle I_t \rangle\rangle$ for the reference case of $I_0^{(1)} = I_0^{(2)} = \langle I_0 \rangle = I_0^* + \frac{\Delta}{2}$.

Fig. 4.6 shows the dependence of the average difference in amplitudes of the emergent oscillations in the size of the infected sub-population in the two communities $\langle \Delta A \rangle$, on the difference in the initial composition of the communities, quantified by parameter Δ. As in Fig. 4.5, here the initial infecteds $I_0^{(0)} = I_0^*$ and $I_0^{(2)} = I_0^* + \Delta$. Different fractions f_{ic} of

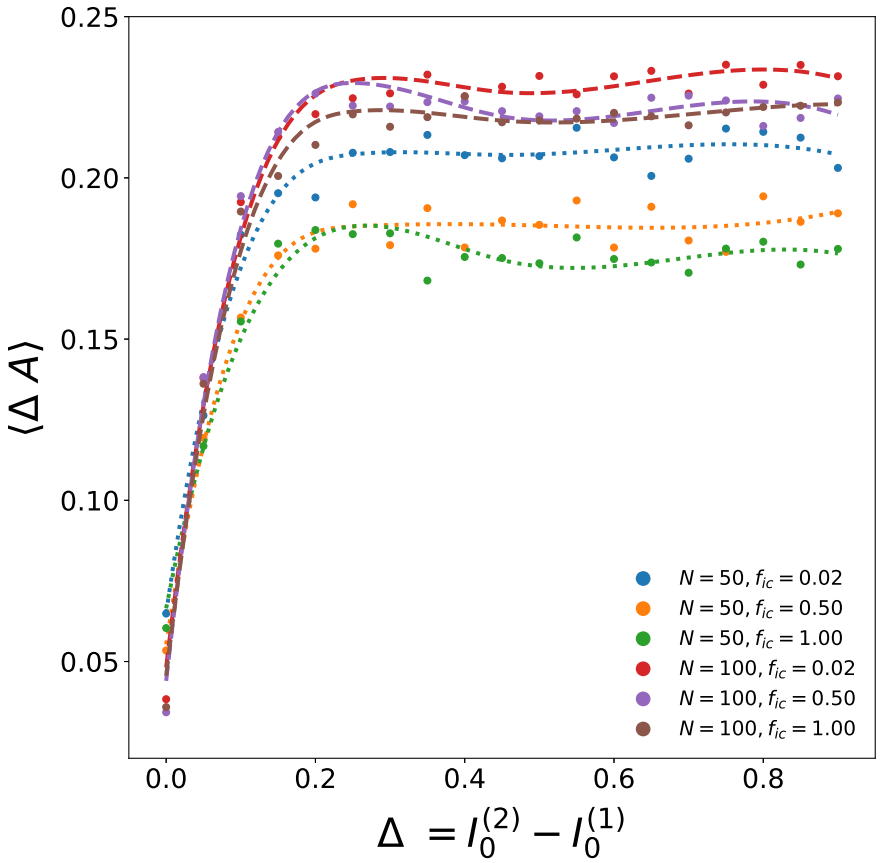

Figure 4.6: Dependence of the average difference in amplitudes of the emergent oscillations in the size of the infected sub-population in the two communities $\langle \Delta A \rangle$, on Δ (which quantifies the difference in the initial composition of the communities). Here the initial infecteds $I_0^{(0)} = I_0^*$ and $I_0^{(2)} = I_0^* + \Delta$, community size is 50×50 and the fraction of boundary sites with inter-community connections is: $f_{ic} = 0.02$ (blue), 0.5 (yellow) and 1.0 (green).

boundary sites with inter-community connections are investigated. It is clear that there is a sharp transition to a large amplitude difference in the oscillatory patterns of the two communities as $\Delta \to 0$. This suggests that the smallest non-uniformity in the constituent communities yields *distinct temporal patterns*, even though the *average* quantities (such as the average number of infecteds, susceptibles and refractory individuals) evolve to *same* values in the two communities after transience. So, as evident through the spatiotemporal spreading patterns in Fig. 4.1, the initial differences in the constitution of the communities is clearly discernible even at long-times, in spite of the homogenization of the average composition of the communities.

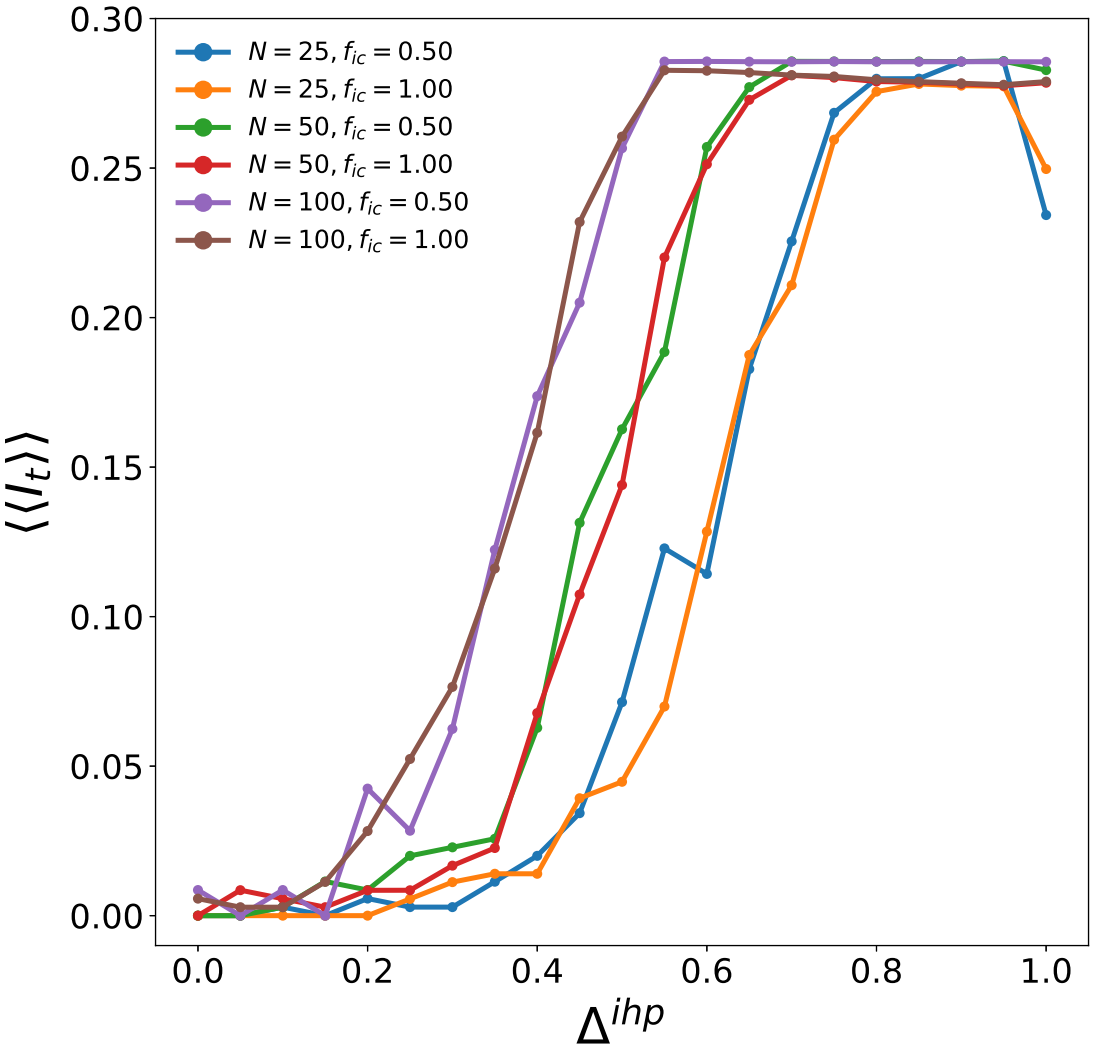

Figure 4.7: Dependence of the persistence order parameter $\langle\langle I_t\rangle\rangle$ of the community 2 (i.e. average asymptotic fraction of infected individuals in the second patch) on parameter Δ, which determines the initial infecteds of the two communities as follows: $I_0^{(1)} = I_0^* - \frac{\Delta}{2}$ and $I_0^{(2)} = I_0^* + \frac{\Delta}{2}$, with $I_0^* = 0.5$. Here the community size is 50×50 and 100×100 (i.e. $N = 50, 100$), and the fraction of boundary sites with inter-community connections is $f_{ic} = 0.02, 0.5, 1.0$. So Δ is a parameter that quantifies the difference in the initial composition of the communities, while maintaining the same average fractions of disease phases in the entire population, i.e. $I_0^{(2)} - I_0^{(1)} = \Delta$, with $\frac{(I_0^{(1)} + I_0^{(2)})}{2} = 0.5$ across all Δ.

Fig. 4.7 shows the dependence of the persistence order parameter $\langle\langle I_t\rangle\rangle$ of the community 2 (i.e. average asymptotic fraction of infected individuals in the second patch) on parameter Δ, where the initial infecteds of the two communities is given in terms of

Δ as follows: $I_0^{(1)} = I_0^* - \frac{\Delta}{2}$ and $I_0^{(2)} = I_0^* + \frac{\Delta}{2}$, with $I_0^* = 0.5$. So Δ is a parameter that quantifies the difference in the initial composition of the communities, while maintaining the same average fractions of disease phases in the entire population, i.e. $I_0^{(2)} - I_0^{(1)} = \Delta$, with $\frac{(I_0^{(1)}+I_0^{(2)})}{2} = 0.5$ across all Δ. Results from two different community sizes are shown, with the first case where the two communities are of sizes 50×50 each, and the second case where the communities are of sizes 100×100. Further, we consider different fractions f_{ic} of boundary sites with inter-community connections, 0.5 and 1.0. The first striking feature is that there is a *transition to persistent infection when the difference between the communities is sufficiently large*. It is also clearly evident that the persistence of infection does not depend in any significant way of the density of inter-community links. We also observe that larger communities yield persistent infection at smaller Δ, implying that one obtains persistent infection for fairly small differences in the constituent communities when the communities are large.

4.4 Conclusion

In summary, we have explored the long-term persistence of infection qualitatively and quantitatively in two communities, where the disease progression of the individuals was given by the SIRS model and an individual became infected on contact with another infected individual. Such weakly connected islands or patches of habitats can provide a test-bed to study the sustenance of disease in adjacent regions [14].

We demonstrate that when the population is compartmentalized into distinct communities, with very different compositions of diseased individuals in each, the entire system comprising of the connected communities is much more to prone to long-term persistent infection than a system which has an uniform admixture of infected, refractory and susceptible individuals in the same proportion.

Our central result is the following: if a population is structured into distinct communities, the infection will persist. This is in contrast to the situation where infected, susceptible and refractory individuals are uniformly distributed in a region, in which case there will be rapid transient waves of infection that will quickly die out.

So an important consequence of our results is the following: we have established that the persistence of infection is crucially dependent on the distribution of the disease phases in a population, and not merely determined by the average properties. This implies that descriptions of disease spreading that are relevant to well-mixed populations, such as

differential equation based models, may not be able to capture the long-term persistence of infection in a region. Specifically, we find that the more spatially non-uniform a population is, the greater is the probability of persistent disease in the population. That is, a population compartmentalized into distinct sections that differ significantly from each other would be more likely to sustain the disease cycle and yield a situation where the population has an infected set of individuals at all times. Thus the important feature of persistent infection is strongly correlated to the structure of the population and the heterogeneity of its initial composition, and cannot to fully understood from spatially averaged data.

Chapter 5

Extreme Events in Networks of Chaotic Population Maps

Adapted from the work published in :

Promit Moitra and Sudeshna Sinha,
Chaos, **29**:023131, 2019.

5.1 Introduction

Extreme events have generated a lot of research attention due to their large impact in phenomena ranging from weather to traffic flows [42]. An extreme event is one where the relevant state variable(s) of a natural or human engineered system exhibits periods of small scale deviations about a level, interrupted by abrupt large excursions to values that differ very significantly from its mean value, typically several standard deviations away from the mean. These recurrent unusually large (or small) values are very important, as they signal occurrences of catastrophic significance, such as extreme weather events [43], rogue waves in the ocean [44] or optical systems [45], large-scale blackouts in power supply networks [46] or market crashes [47]. Further, though relatively rare, the magnitude of these events is so large that their consequence, in terms of damage or cost to contain the event, is very large.

A question of vital importance is to find generic mechanisms that naturally yield such extreme events. Efforts to obtain extreme events typically involve stochastic models, such as the recent random walk model of transport on networks [48]. There have also been a few recent studies of excitable systems, such as diffusively coupled FitzHugh-Nagumo units, which generate extreme events [49].

The emergent behaviour of large interactive systems is often counter intuitive and interesting. The question being explored here is: *Can coupled chaotic systems yield a significant number of extreme events?*. Specifically it is demonstrated how networks of parametrically coupled chaotic systems are capable of generating extreme values, i.e. how such networks give rise to recurrent strong deviations from mean behaviour that occur aperiodically at random intervals. Unlike earlier models yielding extreme events, the model under study here has no stochastic environmental influences or sources of random fluctuations, in either the state variables or the parameters determining the dynamics of isolated sites. Nor are the dynamical constituents of the system excitable units, naturally capable of exhibiting "pulse-like" behaviour or "spikes". Rather, a new scenario is presented, namely the emergence of extreme events in a deterministic system of coupled chaotic maps, typically modelling population dynamics.

Another novel aspect of extreme events is demonstrated in this work. The events were observed to be *extreme in both space and time*, namely when a time snap-shot of the system is observed, a few sites/patches with very large populations were found. It is concluded that these coupled populations, with increasingly large coupling neighbourhoods, display extremely large and relatively rare explosive growth in progressively

isolated patches, akin to an "extreme event" in space, in addition to a marked propensity for extreme events in the variation of the total biomass in time.

5.2 Model

Populations modelled by the prototypical Ricker (Exponential) Map [50] are considered. Such a map is widely used to model population growth of species with non-overlapping generations, and is given by the functional form:

$$x_{t+1} = f(x_t) = x_t e^{r(1-x_t)} \tag{5.1}$$

where (dimensionless) x_t is the population scaled by the carrying capacity at generation t, taking values in the range $[0, \infty)$, i.e. the iterates of the map are non-negative, at all parameter values, as can be discerned from Fig 5.1. The solutions of this iterated function system follow a period doubling route to chaos, as the parameter r is varied from 0 to 4, as shown in Fig. 5.2. The term $e^{r(1-x_t)}$ models the effective growth rate, incorporating the feedback of the existing population on the next generation.

A collection of N such populations [51, 52] are considered, characterized by the variable x_t^i, at each node/site i ($i = 1, \ldots N$) at time instant t. In this system, the nodal populations are intrinsically chaotic oscillators whose dynamics is governed by the Ricker map (Eq. 5.1), with the parameter for each node fixed at the chaotic limit $r = 4$. Each node couples to a set of neighbours and the range of coupling, namely the size of the connected neighbourhood k, can vary from two nearest neighbours to global coupling. The presence of these populations in the neighbourhood provides feedback to the population and modifies it's growth rate [53]. Specifically the feedback is provided by the local mean field $\langle x \rangle$ as the argument in Eq. 5.1, rather than simply x, namely: $\exp[r(1 - \langle x \rangle)]$. So the *effective growth rate* of the populations is modified by the mean population of the neighbourhood, and not merely by the existing population in that particular patch. This is in contrast to the most commonly used diffusive coupling, where the population density of the node is modified [54], rather than the growth rate.

The complete dynamics is then governed by:

$$x_{t+1}^i = e^{r(1-\langle x_t^i \rangle)}\ x_t^i + D\eta_i(t) \tag{5.2}$$

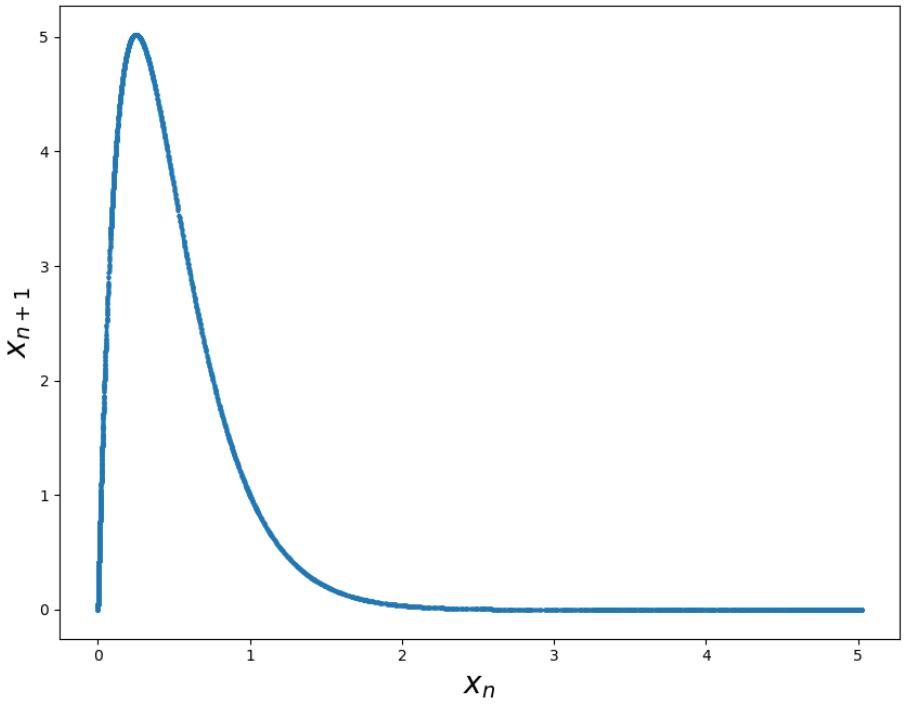

Figure 5.1: x_{n+1} vs. x_n for the Ricker map (Eq. 5.1), with $r = 4$, which is in the regime of fully developed chaos

where $\eta_i(t)$ is a delta-correlated uniform noise in the range $[0 : 1]$, characterized by $\langle \eta_j(t)\eta_j(t+t')\rangle = \delta_{ij}\delta(t')$, with noise strength $D = 10^{-10}$.

The parametric coupling is through the mean field of the coupling neighbourhood (including self), given as:

$$\langle x_t^i \rangle = \frac{1}{k}\sum_j x_t^j \tag{5.3}$$

where k is the total number of neighbours that influence a population patch, including self-feedback, i.e. the sum also includes site i and $k-1$ other distinct sites determined by the topology of the connections. Such a parametric form of coupling then provides a "tuning" of the effective growth rates of the populations at each node, at each time step, drawing feedback from the local mean population in the connected neighbourhood. This form of coupling where the *growth rates are influenced by the local mean field of its neighbourhood*, has not been adequately explored, compared to the usual diffusively coupled systems. The presence of a noise floor, though very small, provides a natural

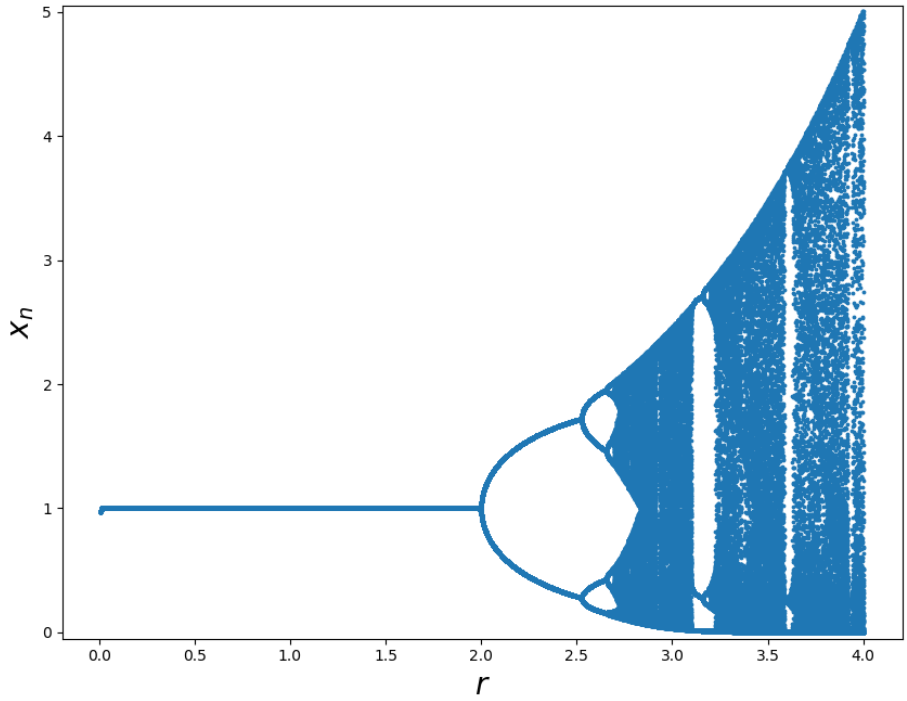

Figure 5.2: x_n vs. $r \in (0, 4]$ for for the Ricker map (Eq. 5.1)

robustness to the results.

In the present study, the small-world connection topology is considered, as it is widely applicable to a range of biological and engineered systems. The small-world topology, as described in [10], is obtained by a process of probabilistic rewiring, starting from a regular graph of degree k (i.e. each node has exactly k neighbours). Varying the probability of rewiring, p, enables one to tune the connection topology from the limiting case of an ordered lattice structure on one hand (at $p = 0$), to the limit of completely random connections on the other (at $p = 1$). The small-world topology attained by the network at intermediate p ($p \sim 0.1 - 0.2$), simultaneously shows certain characteristics of a lattice (a significant clustering coefficient) as well as a random network (short mean path lengths). These simultaneous contrasting properties of the small-world topology, have been observed to enhance collective dynamical properties such as signal propagation speeds and synchronizing ability. Considering the ubiquitous presence of this topology in networks which have naturally evolved in a distributed manner, such as cortical brain networks, social networks or power grids, there is a lot of research interest regarding the impact of this topology on collective dynamics. Specifically, the fraction of random short-cuts, quantified by the rewiring probability p, provides a framework to establish a

link between the structure of the network and the dynamic behaviour of the networked system.

The quantities of considerable interest in this network of populations is the *local population density* in the patches, and their variations in time. The primary focus of this study was the deviation of these local population densities from the average, and the probability of the occurrence of very large populations at a site. These quantities enable the exploration of the emergence of extreme events at spatial locations, signalling explosive growth at a site. Such events are of catastrophic significance, even if rare, as they may entail serious consequent damage.

Another relevant quantity of interest is the total biomass of the system, representing the *global dynamical state of the network*, at an instant of time t, defined as follows:

$$B(t) = \sum_{j=1}^{N} x_t^j \tag{5.4}$$

where N is the system size.

The presence of large excursions of the biomass from mean-values is investigated, over an observed window of time $T \sim 10^3$ (post transience), as such an event would signal the occurrence of *collective explosive growth* in time.

In this work, the changes in local population densities are explored, as well as the total biomass of the system. Namely spatially local quantities are tracked, as well as global indicators reflecting collective properties. The central questions are as follows: Does feedback from neighbouring populations yield extreme events in space or time? Does the spatial extent of coupling among the patches, i.e. the size of the "neighbourhood" of each site, affect the probability of obtaining spatial or temporal extreme events? In particular, the size of the coupling neighbourhood k is varied, as well as the relative size of the coupling neighbourhood k/N (i.e. k scaled by system size), and the impact of the neighbourhood on the emergence of extreme events is investigated.

5.3 Emergence of Extreme Events in the Network

Fig. 5.3 displays the spatial behaviour of the populations at each site i, i.e. x_t^i, $i = 1, \ldots N$, at different times, starting from an initial state that is randomly distributed over the range

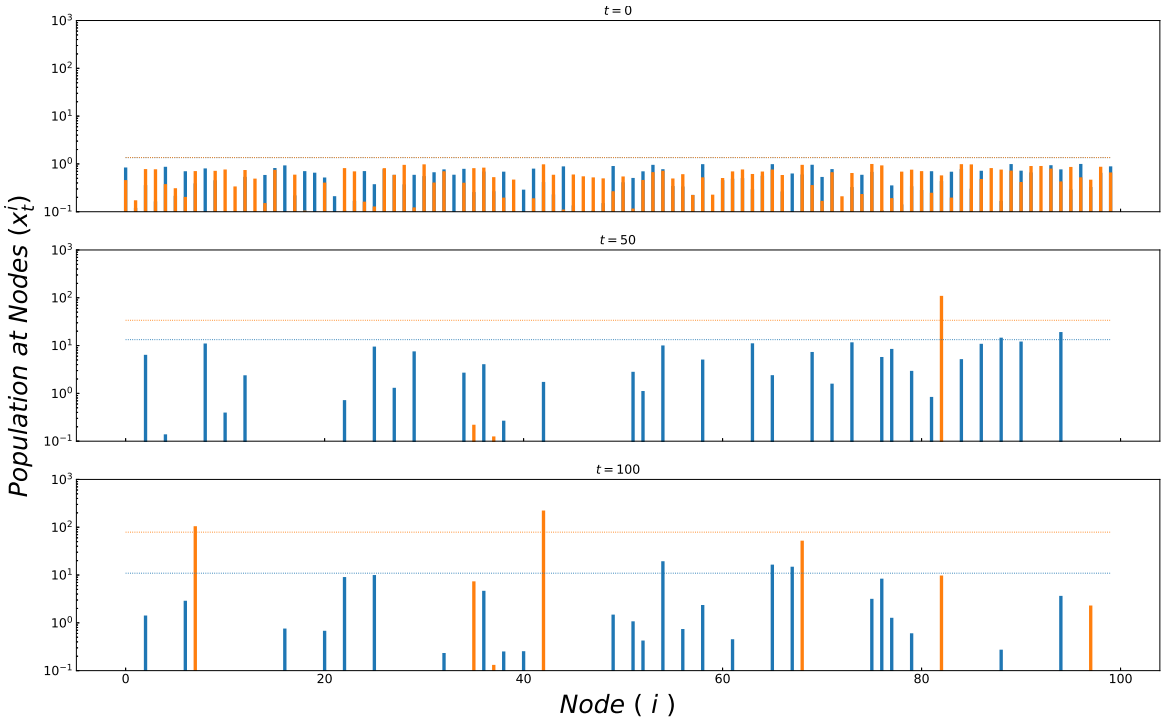

Figure 5.3: Population densities x_t^i, $i = 1, \ldots N$, where system size $N = 100$, at different times $t = 0, 50, 100$. The initial state x_0^i is randomly distributed over the range $(0 : 1]$. The dotted line marks the $3\sigma_t$, where σ_t is the standard deviation of the population densities at time t. Here we have a small world network of populations, with fraction of random links $p = 0.15$. The size of the coupling neighbourhood is $k = 2$ (denoted in blue) and $k = 50$ (denoted in yellow). Note that the population densities are shown on a *log-scale*. So it is evident that the maximum emergent population density is at least an order of magnitude larger than that in the initial state.

$(0 : 1]$. The figure also displays the value $3\sigma_t$. Population densities above this deviate significantly away from the mean, and thus can be considered an extreme event in space. It should be noted that the initial state has *no* site with an extreme value. However as the system evolves, extreme events in space emerge. The population densities are shown on a log-scale in the figure. So it is evident that the maximum emergent population density is *at least an order of magnitude larger than that in the initial state.*

Interestingly, it is observed that the system splits into two distinct groups: *active* sites characterised by dynamics that occasionally lead to extremely large populations, and *inactive* sites characterised by exceedingly low population densities. So it is clearly evident from the temporal patterns of the network that *extreme local growth in patches occurs at the expense of other patches which are driven to near-extinction.* This observation has ecological significance, as it indicates that in this population network, the coupling form allows a few populations patches to grow enormously at the cost of the large number of

remaining patches.

For small k, where each population patch is coupled to only a few neighbouring patches, most sites remain active. However, it is clearly evident that with increasing neighbourhood sizes, the activity of the system is confined to a few population patches in the system, with these active sites showing explosive growth. So as the coupling neighbourhood goes from local to near-global coupling, the system yields more *explosive localized growth patterns*, i.e. as the sites couple to a larger number of patches, a larger number of patches become near-extinct and some patches grow explosively yielding extreme spatial events. This phenomenon is distinct from the behaviour observed typically in diffusively coupled systems.

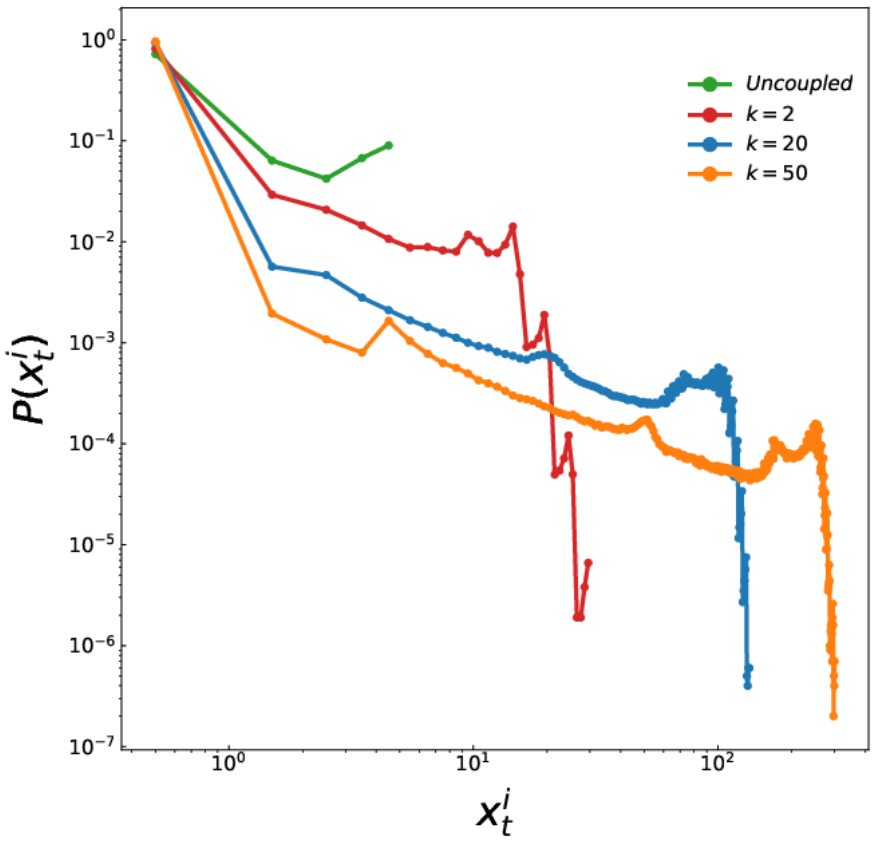

Figure 5.4: Probability distribution of population densities x_t^i, for the case of different coupling neighbourhood sizes k (cf. key), for $p = 0.15$ and network size $N = 100$. As a reference, the case of networks of uncoupled populations ($k = 0$) is also shown

The distribution of the population densities, sampled over long times post-transience, is displayed in Fig. 5.4. Clearly, as the size of the coupling neighbourhood increases,

the tail of the distribution stretches to larger values. In contrast, the distribution of population densities in a network of uncoupled chaotic maps is confined to values an order of magnitude smaller than those emerging in coupled networks and has no extended tail. Though the probability of obtaining these very high population densities in coupled networks is low, they are significant as they yield rare explosive growth at sites, namely, extreme events.

A quantitative estimate of the propensity of such extreme events in space is defined. In order to gauge the probability of encountering an extreme event in a network at any given point in time, the following measure is calculated: an "extreme event" in space is defined (with no significant loss of generality) to be one that is more than three standard deviations away from the mean value of the populations on the entire network at that point in time, i.e. $\langle \bar{x}_t \rangle \pm 3\sigma_t$. The number of sites exhibiting such explosive growth is noted, scaled by the system size N. Averaging this ratio over long times after transience and over a large set of random initial states, provides an estimate of the frequency of extreme events in space, and is denoted by $P_{\mathrm{S}}^{\mathrm{XE}}$. Specifically in this work this probability is estimated by sampling 10^3 time steps (post transience), evolved from 10^2 random initial states.

The results of $P_{\mathrm{S}}^{\mathrm{XE}}$ for representative values of p are displayed in Fig. 5.5. The top panel of the figure shows results for low k/N, clearly indicating a very sharp transition at k/N close to zero, i.e. there is a jump from $P_{\mathrm{S}}^{\mathrm{XE}} \sim 0$ at $k = 0$ (i.e. the case of uncoupled populations) to a significantly large value at the lowest sampled non-zero k. The maximum $P_{\mathrm{S}}^{\mathrm{XE}}$ is observed to occur around $k/N \sim 0.025$, after which the probability of extreme events in population patches decreases with increasing coupling neighbourhood, as a power law given by: $P_{\mathrm{S}}^{\mathrm{XE}} \sim (k/N)^{\nu}$, where ν is a function of p. In particular, $\nu = -0.4$ for $p = 0.05$, $\nu = -0.47$ for $p = 0.15$ and $\nu = -0.56$ for $p = 0.5$, suggesting that $\nu \sim p^{0.15}$. It is also clear that even as $P_{\mathrm{S}}^{\mathrm{XE}}$ falls with k for large k, it still remains significantly higher than the probability of an extreme occurrence in uncoupled populations. So the first important finding is the following: *parametric coupling induces the emergence of extreme population densities in localized patches.*

The *maximum population density* in the network is focused on next, $x_{max}(t)$, at an instant of time t. The mean value of this is estimated, denoted by $\langle x_{max} \rangle$, by averaging $x_{max}(t)$ over long times post transience, for a large sample of random initial states [55]. So $\langle x_{max} \rangle$ reflects the maximum population density that may be expected in the network at any point in time, and large values of $\langle x_{max} \rangle$ suggest the emergence of extreme population densities in space. Further, Fig. 5.6 displays the relation between $\langle x_{max} \rangle$ and the number

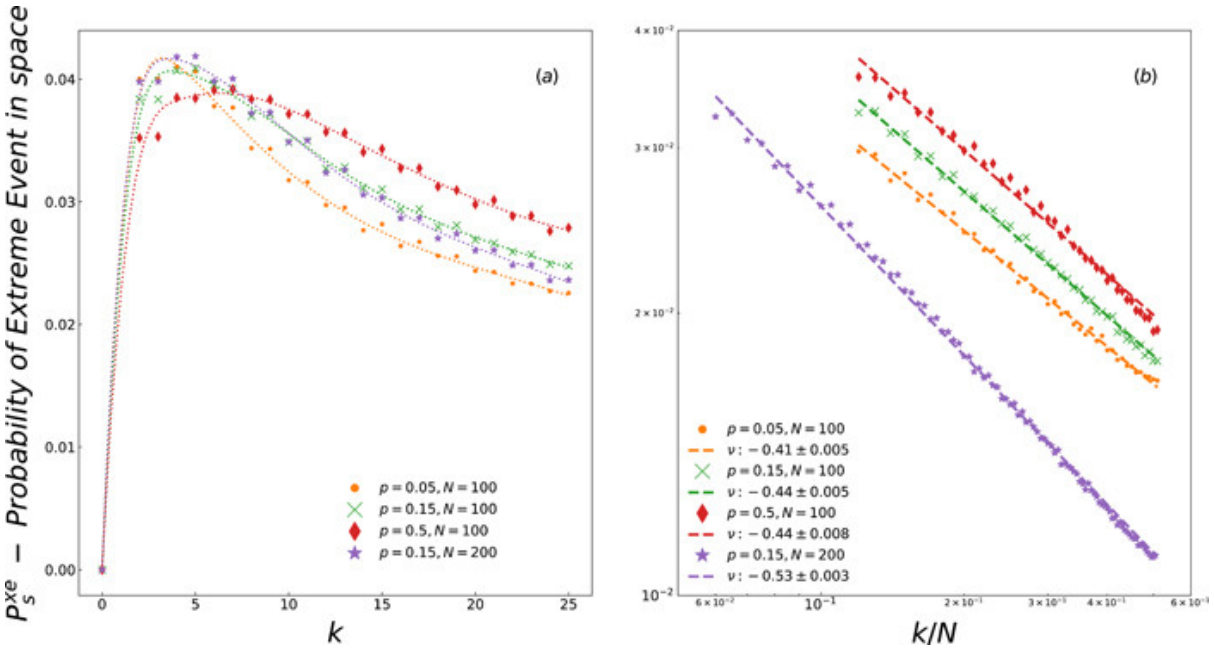

Figure 5.5: Dependence of the probability of extreme events in space $P_{\mathrm{S}}^{\mathrm{XE}}$ (see text for definition) on the relative neighbourhood size k/N. Here network size $N = 100$, with fraction of random links $p = 0.05$ (yellow), $p = 0.15$ (green) and $p = 0.5$ (red). (a) shows $P_{\mathrm{S}}^{\mathrm{XE}}$ for $k/N \leq 0.2$, clearly indicating a sharp transition at $k/N \to 0$. (b) shows $P_{\mathrm{S}}^{\mathrm{XE}}$ for $0 < k/N < 1$, indicating the power law dependence of $P_{\mathrm{S}}^{\mathrm{XE}}$ on k/N, for higher k/N (see fitted curves): $P_{\mathrm{S}}^{\mathrm{XE}} \sim (k/N)^{\nu}$.

of neighbours k, for $k \leq 20$. As can be observed, for small k, $\langle x_{max} \rangle \sim k$, i.e. the *maximum population density grows linearly with the number of neighbours influencing a patch.* A significant implication of this is that when the size of the coupling neighbourhood is small, the size of the network does not matter. So for small k, networks of different sizes yield the same maximum population density $\langle x_{max} \rangle$, when the coupling neighbourhoods are of the same size.

We now attempt to rationalize this result by analyzing the dynamics of a population patch in the network.

$$x_{t+1}^i = x_t^i e^{r(1-\langle x_t^i \rangle)} = x_t^i e^{r(1-\frac{1}{(k+1)}\sum_j x_t^j)}$$

Which can be separated out as

$$x_t^i e^{r(1-\frac{1}{(k+1)}x_t^i)} e^{-\frac{r}{(k+1)}\sum_{j\neq i} x_t^j}$$

Now, we observed that a node with very high population density is typically connected

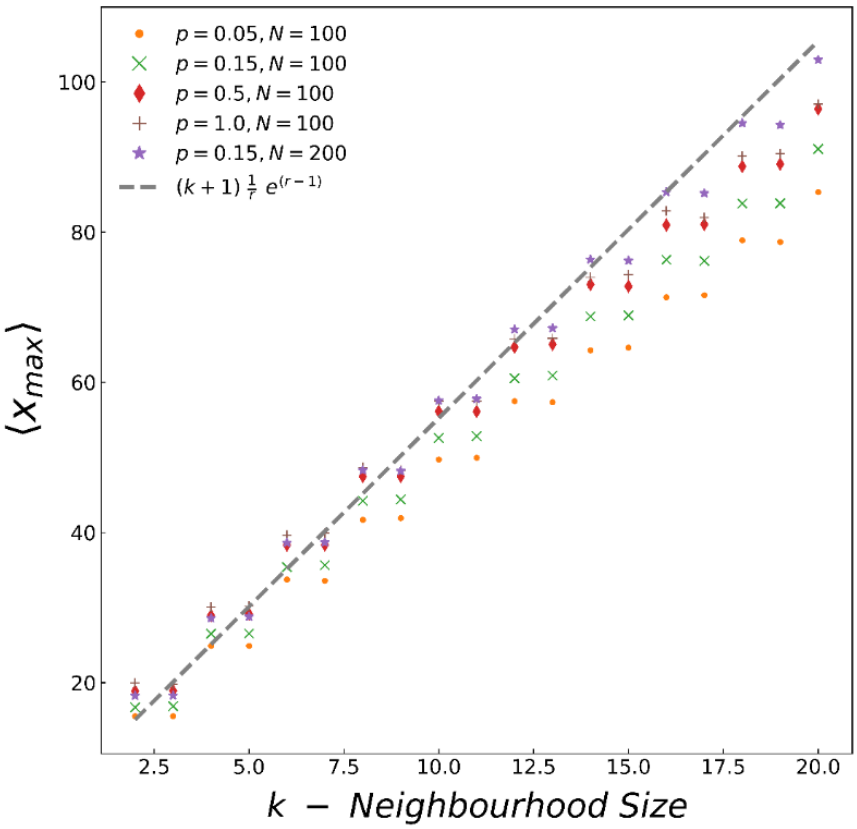

Figure 5.6: Dependence of the average maximum population density $\langle x_{max} \rangle$ on k/N for different fractions of random links p and systems sizes N, for small $k(< 20)$. A linear estimation, given by Eq. 5.5, is shown by the gray dashed line.

to nodes with very low population densities. Therefore, to a first approximation, the sum over x^j of all nodes $j(j \neq i)$ coupled to a node i is close to zero. So effectively, the dynamics at the nodes with very large population densities can be mimicked by the dynamical map

$$f(x) = xe^{r(1-\frac{1}{(k+1)}x)}$$

Calculating the extremum of the function above shows that the maxima of $f(x)$ will occur at $x = (k+1)/r$, namely,

$$x_{max} \sim (k+1)\frac{1}{r}e^{(r-1)} \tag{5.5}$$

This implies a linear dependence of x_{max} on k. The functional form in Eq. 5.5 is matched well by simulations of networks of varying sizes N and fractions of random links p, as is evident from Fig. 5.6, for small k. For larger the overall contribution from neighbours (excluding self) to the local feedback deviates more from zero, and this lowers the prefactor, yielding values of x_{max} that are lower than the linear prediction of Eq. 5.5.

Further, it is observed that the fraction of random links p in the network does not influence the extremal values $\langle x_{max} \rangle$. This is evident through the near identical results obtained for p ranging from 0.05 to 1 in Fig. 5.9.

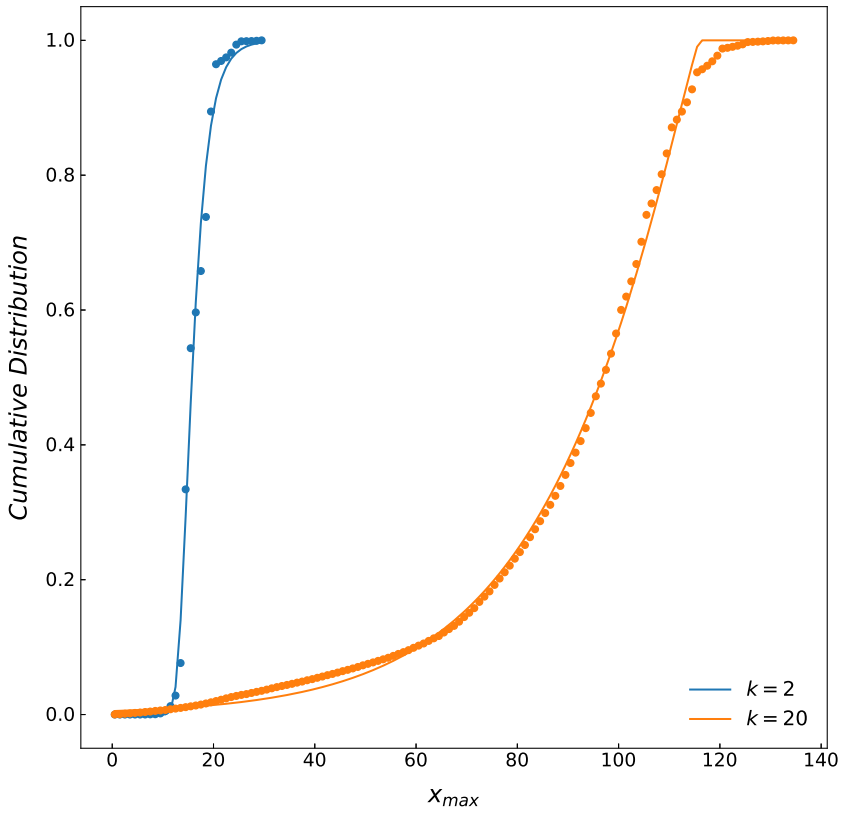

Figure 5.7: Cumulative distribution function $F(x_{max})$ of the maximum population density x_{max} for $k = 2$ (blue) and for $k = 20$ (yellow), for $p = 0.15$ and systems size $N = 100$. The curves display the best fit to the cumulative distribution corresponding the Generalized Extreme Value probability density function: $F(x, c, \mu, \sigma) = \exp(-(1 + c(\frac{x-\mu}{\sigma}))^{-1/c})$ for $\frac{x-\mu}{\sigma} < -1/c$, where c ($\neq 0$) is the shape parameter, μ is the location and σ is the scale parameter. The scale σ for the blue curve (fit to data for $k = 2$) is 2.16, and for the yellow curve (fit to data for $k = 20$) is 23.52, indicating that the distribution is much more spread out for higher k.

The cumulative distribution function (cdf) of the maximum population density x_{max}, denoted by $F(x_{max})$, is estimated. The results are displayed in Fig. 5.7. It is evident that the cumulative distribution is well fit by the cdf corresponding to the Generalized Extreme Value probability density function. Notice that the scale σ of the best fit cdf for $k = 2$ is 2.16, and for $k = 20$ is 23.52. This indicates that the distribution is much more spread out for networks which couple over larger neighborhoods.

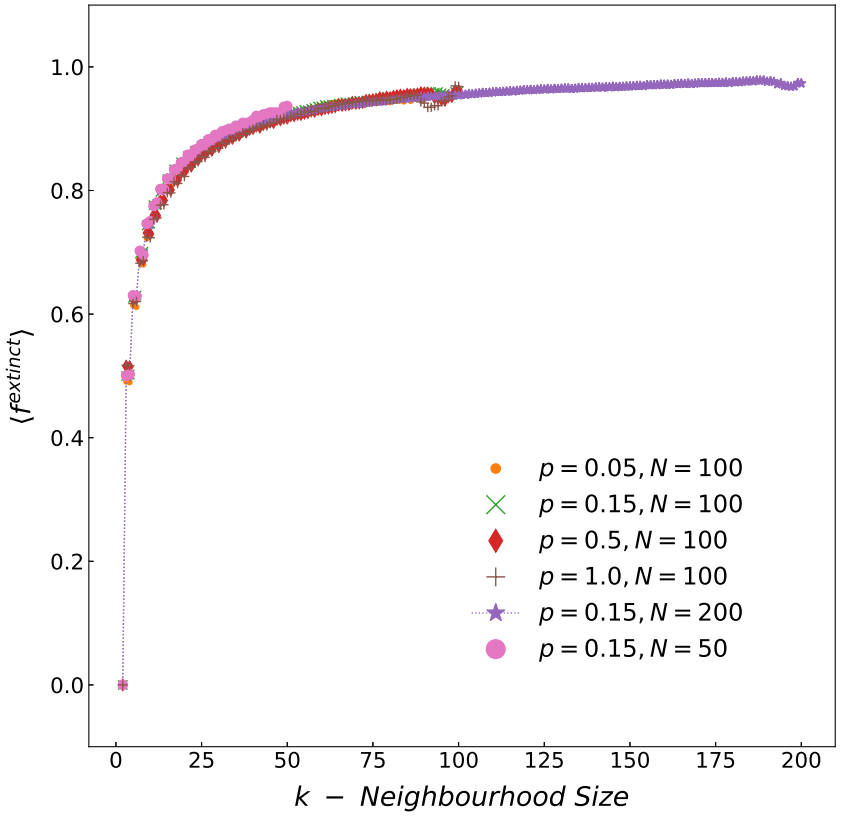

Figure 5.8: Average fraction of near-extinct nodes, denoted by $\langle f_{extinct} \rangle$ (see text for definition), for different neighbourhood sizes k. Results for network size $N = 100$ with $p = 0.05, 0.15, 0.5, 1.0$, and network sizes $N = 200$ and $N = 50$ with $p = 0.15$, are displayed with different symbols given in the key.

Lastly, the population patches where the population density has depleted severely are observed. Since it is clearly evident from the temporal patterns of the sites in the network that extreme local growth in patches occurs at the expense of other patches which are driven to near-extinction, a good indicator of the extreme local variation of populations would be the number of near-extinct sites that emerge in the network. So the fraction of near extinct nodes in the network at time t is calculated, denoted by $f_t^{extinct}$, where a

near-extinct node is one whose population density is less than some low threshold value, i.e. $x_t^i < x_{threshold}$, with $x_{threshold}$ chosen to be 10^{-5} without loss of generality. The average fraction of such near-extinct sites, $\langle f^{extinct} \rangle$, are estimated by sampling over 10^3 time steps (post transience) and 10^2 random initial states. It is evident from Fig. 5.8 that there is a very sharp transition from $\langle f^{extinct} \rangle = 0$ to a large finite $\langle f^{extinct} \rangle$ at $k \to 0$. Therefore, in the presence of coupling, for the smallest possible coupling neighbourhood ($k \sim 2$) the number of near-extinct sites jumps significantly and constitutes the majority of the network sites. Also notice that the data from networks of different sizes and different fractions of random links ($0 < p < 1$) collapse to the same curve. This indicates that this behaviour is universal for networks of varying sizes and topologies. It also indicates that the size of the coupling neighbourhood k is important for $\langle f^{extinct} \rangle$, not the relative size of the neighbourhood k/N. This feature is similar to our observations for $\langle x_{max} \rangle$ for small k.

To complement this analysis, we observe the the population densities at the patches which are intermittently growing explosively. It is clearly evident from Fig 5.9 that $\langle f^{active} \rangle$ decreases with k as a power law. Also notice that the data from networks of different sizes N and different fractions of random links ($0 < p < 1$) collapse close to the same curve. This indicates that this behaviour is quite universal for networks of varying sizes and topologies. It also indicates that the size of the coupling neighbourhood k is important for $\langle f^{active} \rangle$, not the relative size of the neighbourhood k/N. This feature is similar to our observations for $\langle x_{xmax} \rangle$ for small k.

5.4 Extreme Events in Biomass Production

The next focus of this study is on the temporal patterns of emergent collective behaviour of the network, by exploring the time evolution of an important collective quantity, the biomass $B(t)$. The time series of the biomass for different neighbourhood sizes is shown in Figs. 5.10. It is clear that the biomass displays some extremely high values at certain points in time when the coupling neighbourhood k is sufficiently large, i.e. as the coupling neighbourhood k increases, there are more instances of large deviations of the biomass from the mean, namely more extreme events. The top panel in Fig. 5.10 shows the evolution of biomass of a system of completely uncoupled population patches ($k = 0$), and it is clear that there are *no* extreme events in the large window of time displayed. However, for larger k there is a suppression of activity interrupted by random bursts of explosive biomass generation (cf. second panel of Fig. 5.10 displaying $B(t)$ for a network

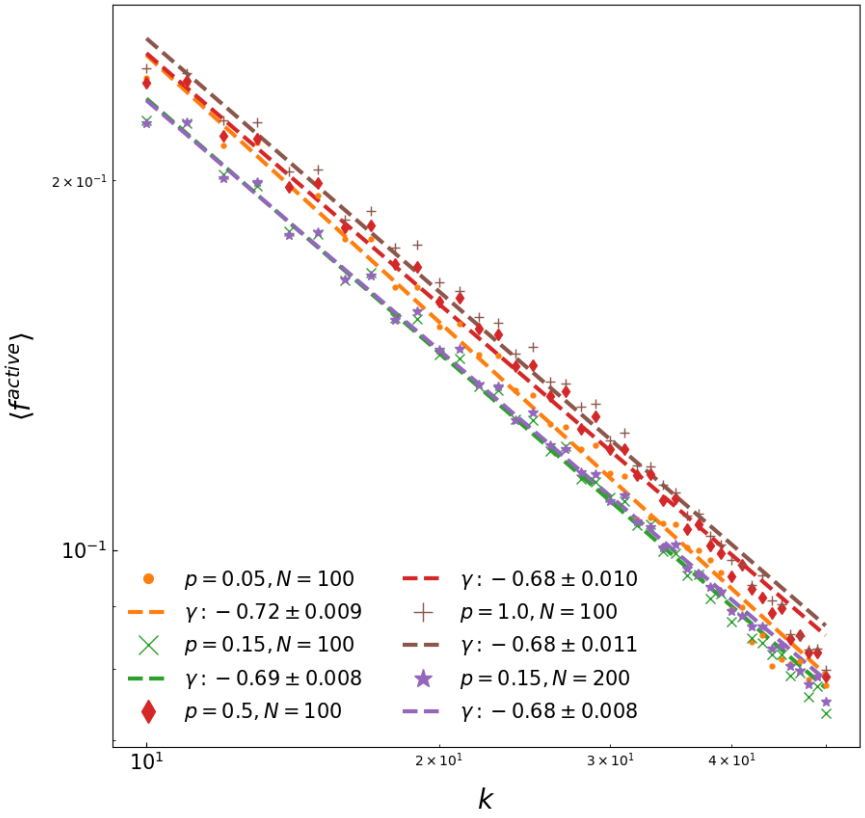

Figure 5.9: Dependence of the average fraction of active nodes, denoted by $\langle f^{active}\rangle$ (see text for definition), on different neighbourhood sizes k, for networks of different sizes N and with different fractions of random links p. Clearly, $\langle f^{active}\rangle \sim k^{-\gamma}$. The values of γ obtained from the best fit using the least square method are in the range $0.68 - 0.72$ for different N and p. The γ values, along with the uncertainty in their estimates, are listed in the key.

with coupling neighborhood $k = 50$).

This qualitative observation is further corroborated quantitatively through the distribution $P(B)$ of the biomass in Fig. 5.11. It is evident that the distribution is close to a Gaussian distribution when the coupling neighborhood k is very small, such as the case of $k = 2$ shown in the figure. Note that a Gaussian distribution is expected from a set of uncoupled sites evolving from random initial conditions, according to the chaotic map given by Eq.5.1. So when the coupling neighborhood is small, the network is similar to a system of uncoupled populations. Specifically, at these low k values the distribution of biomass is narrowly peaked at a value around $2N$, indicating that on an average the sites have population densities close to 2. As the coupling neighborhood increases, the

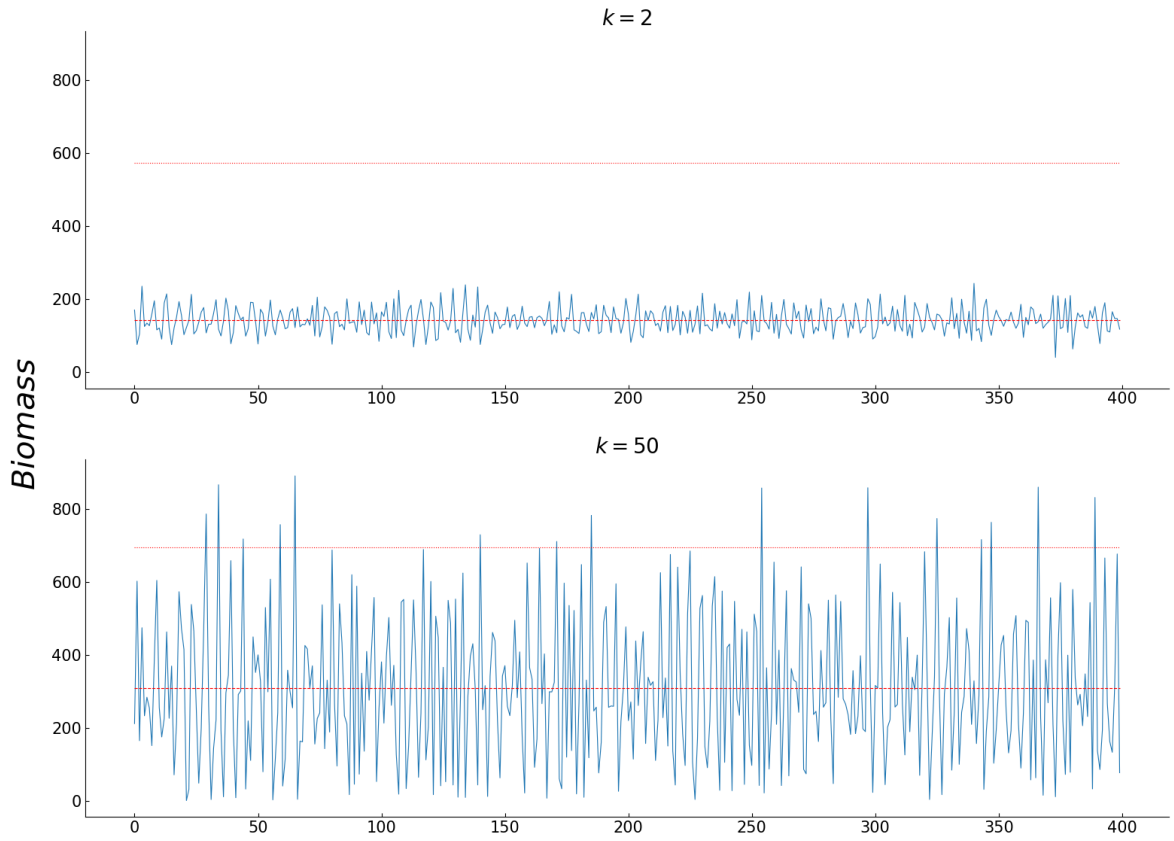

Figure 5.10: Time evolution of the total biomass $B(t)$, (cf. Eqn. 5.4) over 400 time steps (post transience), for neighbourhood sizes $k = 2$ and $k = 50$, on a network of size $N = 100$ with a fraction of random links (rewiring probability) $p = 0.15$. The red dashed line marks the mean value of biomass $\bar{B}$, and the red dotted line indicates 3σ above the mean. Clearly the biomass values deviate much more significantly from the mean when k is larger. The line indicates the value $\langle B(t)\rangle + 3\sigma$, and marks the *Extreme Events* regime.

distribution becomes heavy tailed and stretches towards high values of B, indicating that there is enhanced probability of obtaining very high biomass at certain points in time. For instance, for $k = 20$, the distribution suggests that even $B \sim 600$ has significant probability of occurence. For $k = 80$ the tail of the distribution stretches beyond $B \sim 1000$. Also notice that the distribution develops significant weight at very low biomass. This implies that the probability of obtaining large biomass is correlated with the probability of obtaining B close to zero. Namely, the explosive total population densities at points in time is interspersed with episodes of all sites falling to very low population densities.

A quantitative estimate of the propensity of extreme biomass events is calculated. In order to gauge the probability of encountering an extreme event in a large window of time, the following measure is defined (with no significant loss of generality): an "extreme

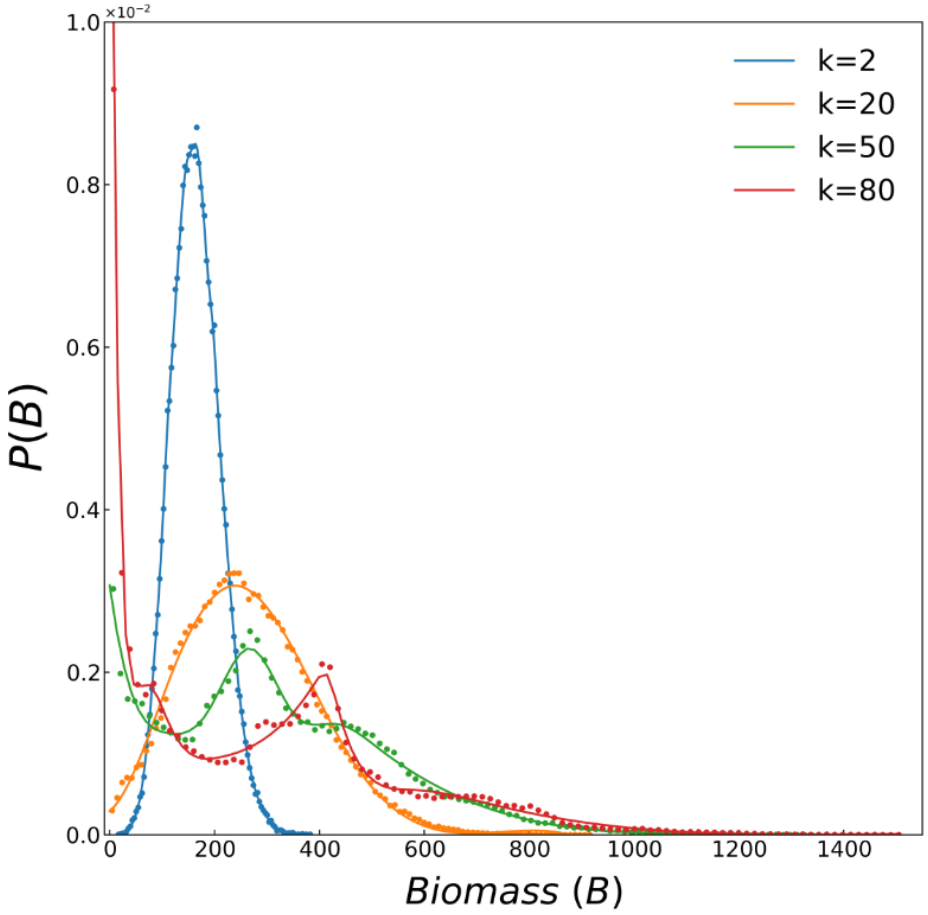

Figure 5.11: Probability distribution $P(B)$ of the biomass B (cf. Eqn. 5.4), obtained by sampling over long time periods and random initial states. Here system size $N = 100$, $p = 0.15$, and $k = 2, 20$ and 80.

event" is one that is more than three standard deviations away from the mean. The system is allowed to evolve over a long period of time and the number of such events is counted, after transience. The number of extreme B values, scaled by the length of the time window under consideration, denoted by $P_{\mathrm{B}}^{\mathrm{XE}}$ in Fig. 5.12, provides an estimate of the frequency of extreme biomass events. Fig. 5.12 shows this quantity for different sizes of the relative size of the coupling neighborhood. Clearly, the probability of encountering an extreme event increases approximately linearly with k/N, up to $k/N \sim 0.9$. This result holds for different fractions of random links p and system sizes N, as evident through the collapse of the data for varying p and N on to a broadly similar trend. Further, for $0.9 < k/N < 1$ there is a sharp jump in $P_{\mathrm{B}}^{\mathrm{XE}}$, i.e. close to the global coupling limit the system shows an enhanced propensity for extreme biomass production. Interestingly however, the exact global coupling limit, where the system attains full symmetry in the dynamical equations and the random links do not have any effect on the dynamics as the

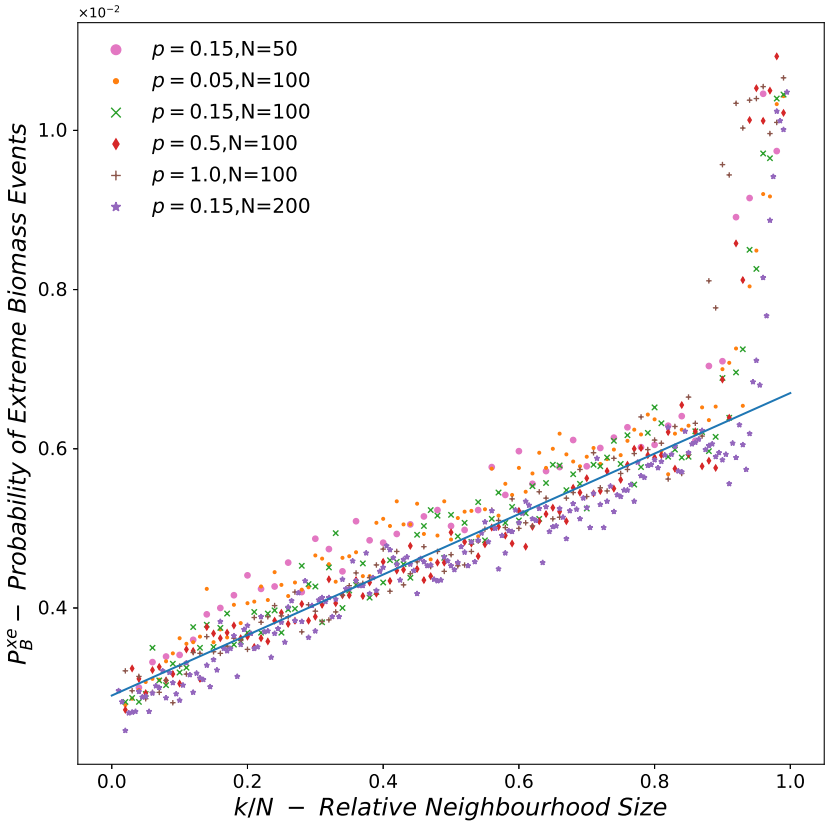

Figure 5.12: Dependence of the probability of extreme biomass events, $P_{\mathrm{B}}^{\mathrm{XE}}$ (see text for definition), on relative size of the coupling neighbourhood k/N. The probability is estimated by sampling 10^3 time steps (post transience), evolved from 10^2 random initial states. Here network size $N = 100$, with fraction of random links p is equal to 0.05 (yellow), 0.15 (green) and $p = 0.5$ (red). The best linear fit is indicated by lines in yellow (for $p = 0.05$), green (for $p = 0.15$) and red (for $p = 0.5$).

coupling is all-to-all, shows singular behaviour: all extreme events are again suppressed, and $P_{\mathrm{B}}^{\mathrm{XE}} \sim 0$ at $k = N$.

The probability distribution $P(T_{int})$ of the time intervals between two successive extreme events, denoted by T_{int}, is shown in Fig. 5.13. It is evident from the figure the time intervals are well described by Poissonian distributions. This implies that successive extreme events are essentially uncorrelated events, and there is no temporal pattern to the occurence of the extreme events. The consequence of this observation is that it would be difficult to anticipate such events.

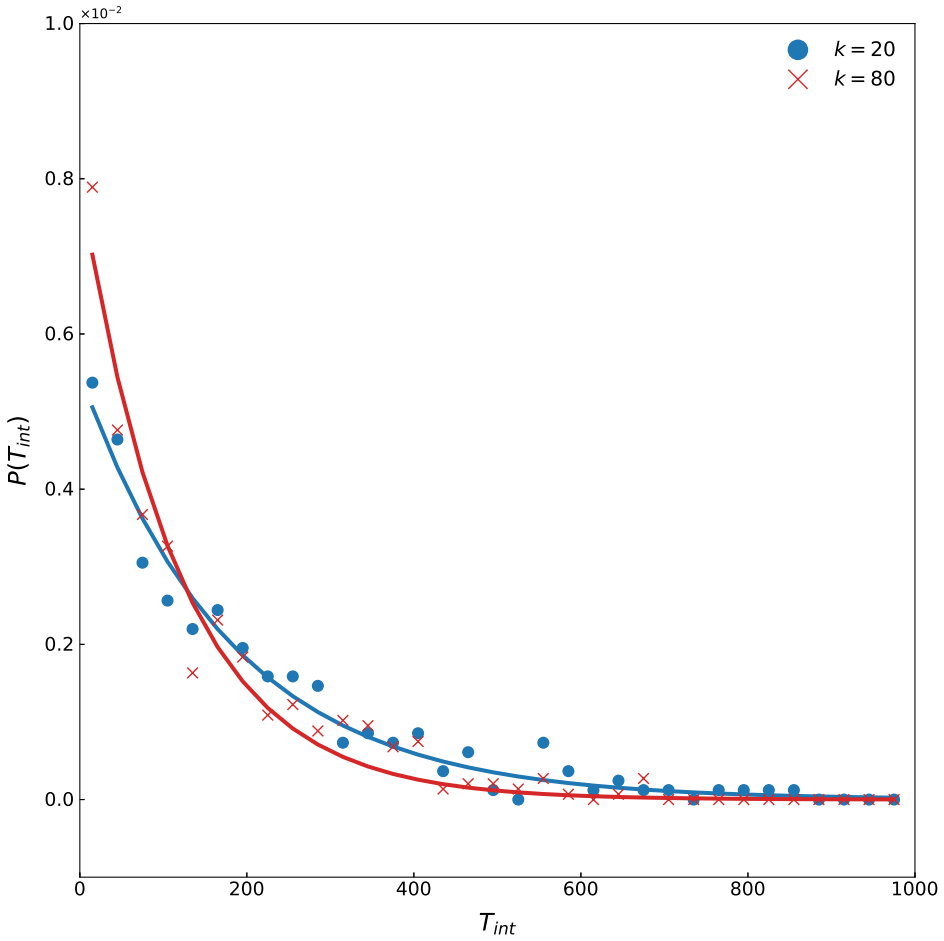

Figure 5.13: Probability distribution $P(T_{int})$ of the time intervals between two successive extreme biomass production events, T_{int}, for coupling neighbourhood sizes $k = 20$ and $k = 80$. The solid lines show the best fit line to exponential decays.

5.5 Special limiting cases

We observe the behaviour of the population patches when they are connected as a regular a ring, which is the limiting case of $p = 0.0$. Fig 5.14 shows the behaviour of the ring network, initialized randomly and evolving in time. Localized clusters of population patches are visibly growing in an explosive fashion, with some of them going into the regime of extreme events.

We also observe the probability of extreme events in space $P_{\mathrm{S}}^{\mathrm{XE}}$ for the case of the ring topology. It is evident from Fig 5.15 that for small k, $P_{\mathrm{S}}^{\mathrm{XE}}$ undergoes a very sharp transition at k/N close to zero, as well as attains a similar maxima, to the small-world topologies. However, the power-law scaling behaviour of $P_{\mathrm{S}}^{\mathrm{XE}}$ with k/N was not observed for larger relative neighbourhood sizes.

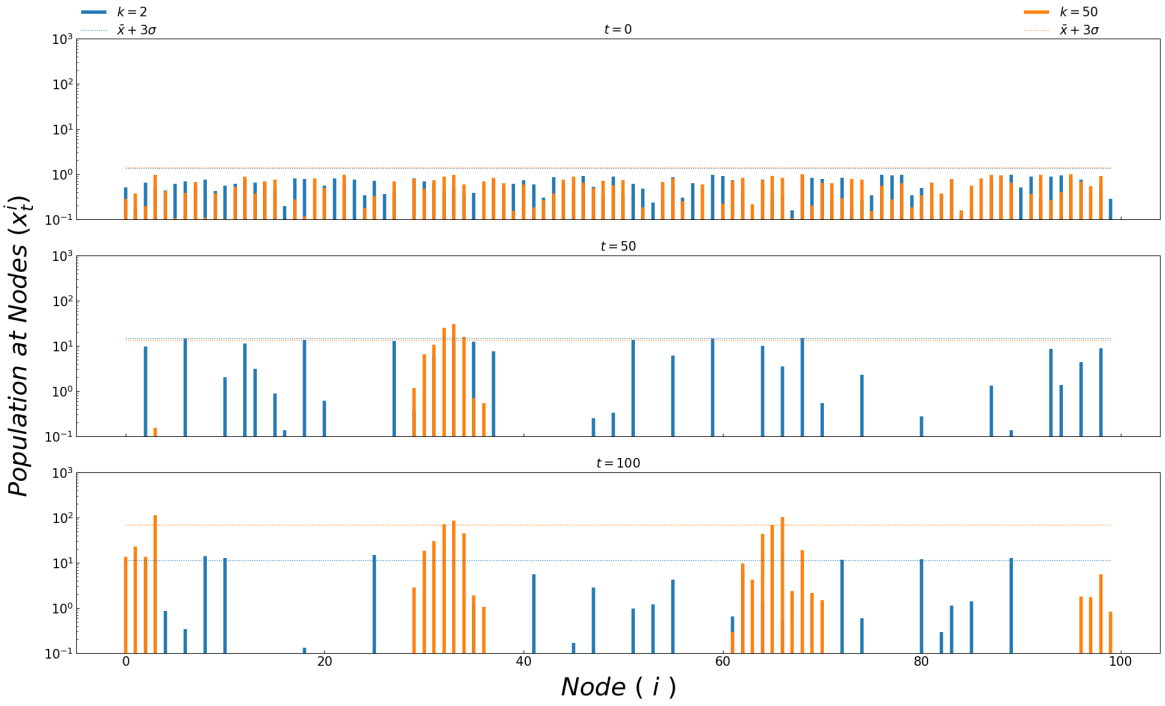

Figure 5.14: Population densities x_t^i, $i = 1, \ldots N$, where system size $N = 100$, at different times $t = 0, 50, 100$. The initial state x_0^i is randomly distributed over the range $(0 : 1]$. The dotted line marks the $3\sigma_t$, where σ_t is the standard deviation of the population densities at time t. Here we have a ring of populations, with only nearest neighbour connections and no random links ($p = 0.0$). The size of the coupling neighbourhood is $k = 2$ (denoted in blue) and $k = 50$ (denoted in yellow). Note that the population densities are shown on a *log-scale*. So it is evident that the maximum emergent population density is still at least an order of magnitude larger than that in the initial state. Owing to the local nature of connections, clusters of bursting patches are observed.

We further explore the temporal collective behaviour of the system, by observing the dynamics of the biomass $B(t)$ in time. Fig 5.16 makes it clear that the system displays extreme biomass growth, intermittently in time, similar to our observations for small-world networks.

The other limiting case we explore is the case of global, or all-to-all coupling, that is $k = 100$. In this scenario, each node is connected to every other node, and therefore each node has the same neighbourhood (which is the entire network). Therefore the feedback received by every node is identical. As can be seen in Fig 5.17 , in this case, we found that all the population patches grew and fell together, and all extreme events get suppressed. The suppression of extreme events was observed not only in space, but also in time. Fig 5.18 shows the time evolution of the biomass in the globally coupled case, and it is clear that the biomass does not deviate from the mean beyond the 2σ limit.

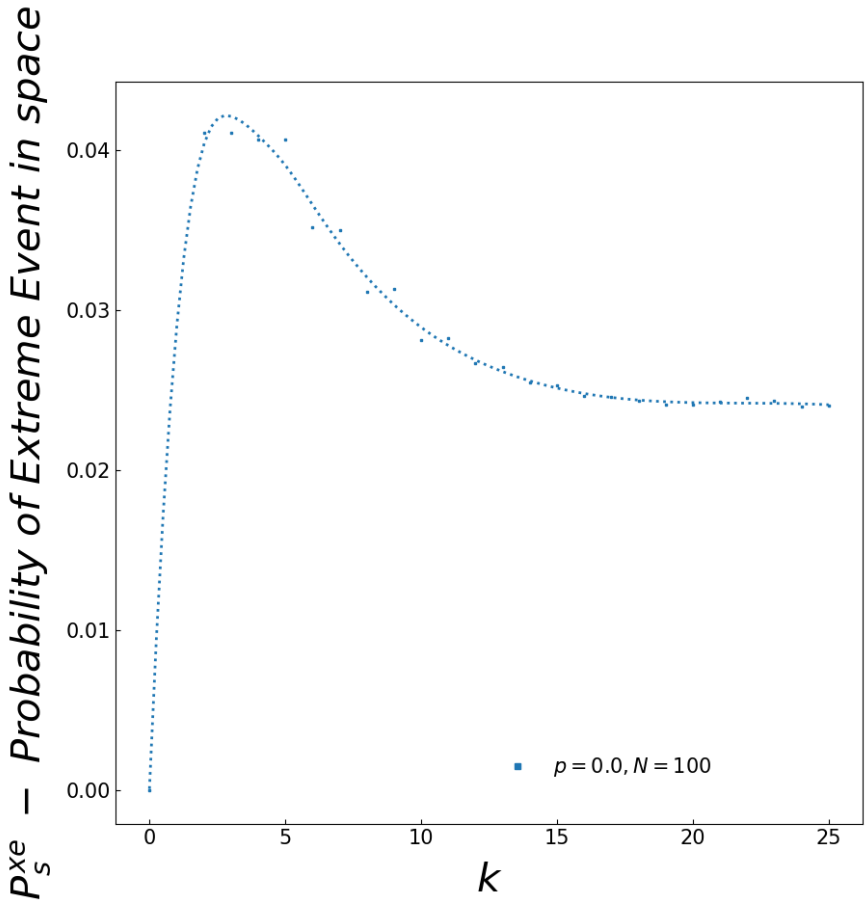

Figure 5.15: Dependence of the probability of extreme events in space $P_{\mathrm{S}}^{\mathrm{XE}}$ (see text for definition) on the relative neighbourhood size k/N. Here network size $N = 100$, with no random links, that is $p = 0.0$. The figure shows $P_{\mathrm{S}}^{\mathrm{XE}}$ for $k/N \leq 0.2$, clearly indicating a sharp transition at $k/N \to 0$.

5.6 Discussions

To summarise, in this work we considered a network of populations modelled by the prototypical chaotic Ricker map (Eq. 5.1), relevant to population growth of species with non-overlapping generations, whose growth rates are influenced by the local mean field of its neighbourhood. This form of parametric coupling has not been adequately explored, compared to the usual diffusively coupled systems. We examined the dynamics and distribution of the local populations, as well as the total biomass. We found the following counter-intuitive and interesting emergent behaviour in the system: When the range of coupling is sufficiently large, namely when enough neighbouring populations influence the growth rate of a population, the system yields extremely large biomass values that are very far from the mean. These extreme events are relatively rare and uncorrelated

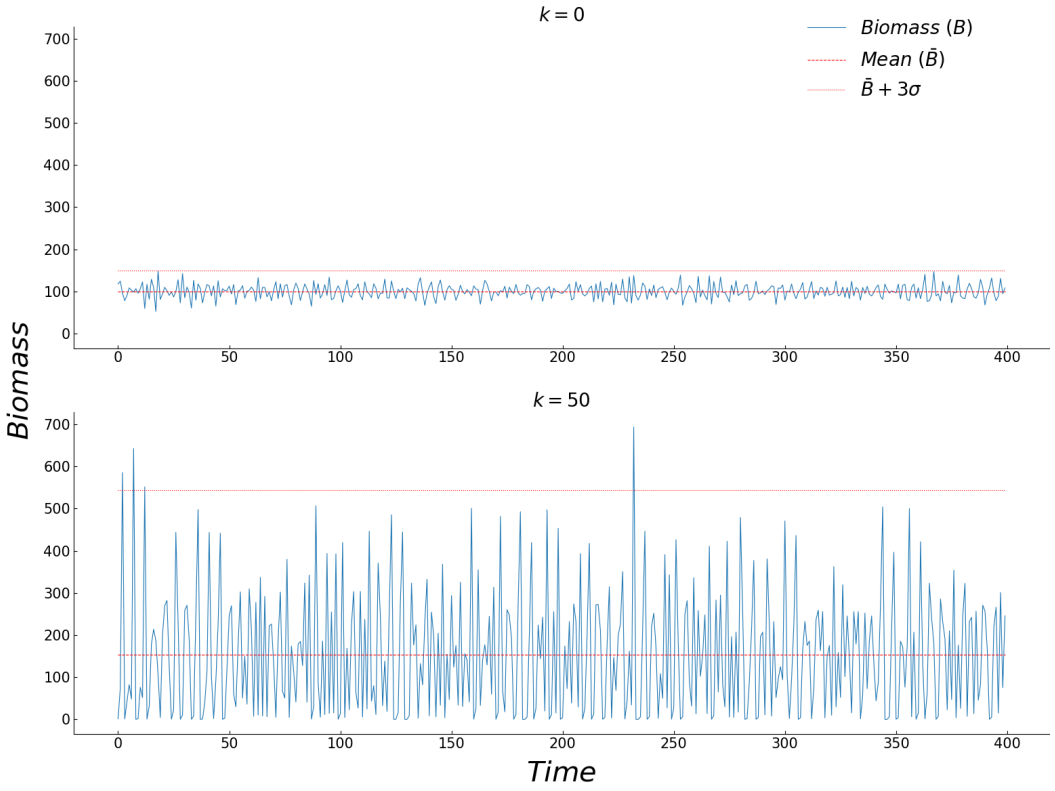

Figure 5.16: Time evolution of the total biomass $B(t)$, (cf. Eqn. 5.4) over 400 time steps (post transience), for neighbourhood sizes $k = 2$ and $k = 50$, on a network of size $N = 100$ with no random links, i.e. $p = 0.0$. The red dashed line marks the mean value of biomass $\bar{B}$, and the red dotted line indicates 3σ above the mean. Clearly the biomass values deviate much more significantly from the mean when k is larger. The line indicates the value $\langle B(t) \rangle + 3\sigma$, and marks the *Extreme Events* regime.

in time, even though this system is completely deterministic and there is no external stochastic influence. We also find that at any point in time, large population densities emerge in a few patches, and this extremely large and relatively rare explosive growth in space is analogous to an extreme event in space. Interestingly, a similar form of parametric coupling has been explored in the context of models of income distributions of individuals on a regular network of deterministic economic agents [56]. So the rare and sudden extreme growth reported in our work also has potential relevance to such economic systems. Thus we suggest a new mechanism for the emergence of extreme events in coupled chaotic systems, in both time and space.

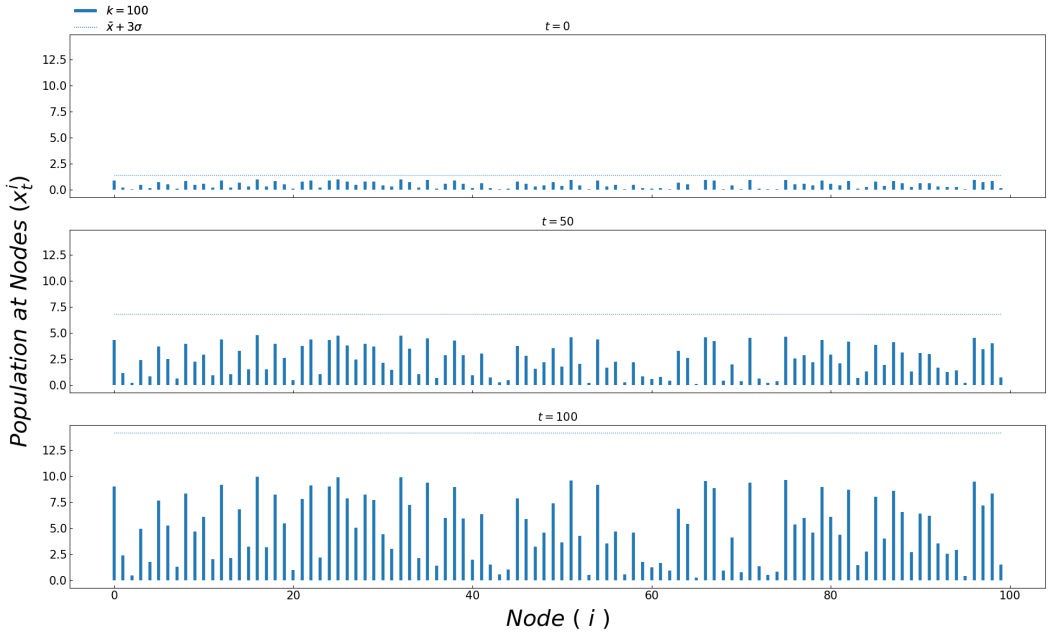

Figure 5.17: Population densities x_t^i, $i = 1, \ldots N$, where system size $N = 100$, at different times $t = 0, 50, 100$. The initial state x_0^i is randomly distributed over the range $(0 : 1]$. The dotted line marks the $3\sigma_t$, where σ_t is the standard deviation of the population densities at time t. The size of the coupling neighbourhood is $k = 100$ (globally coupled). So it is evident that the maximum emergent population density evolves almost in synchrony, largely maintaining their initial differences.

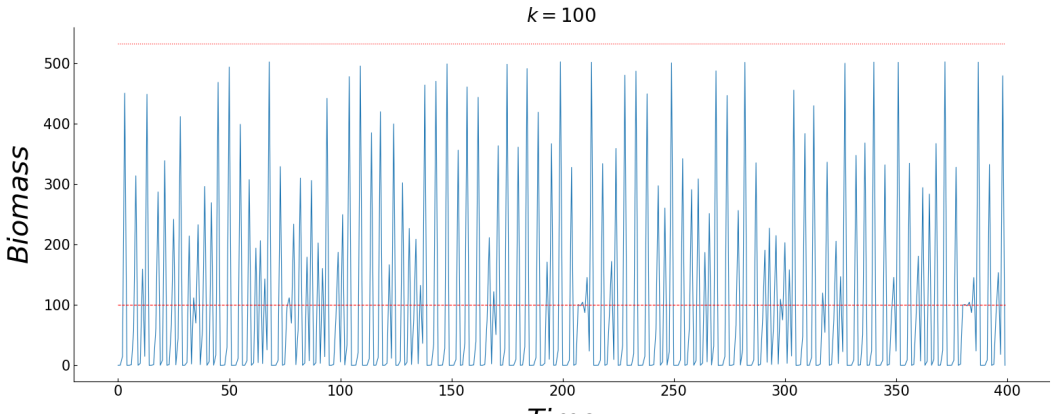

Figure 5.18: Time evolution of the total biomass $B(t)$, (cf. Eqn. 5.4) over 400 time steps (post transience), for neighbourhood size $k = 100$ (globally coupled), on a network of size $N = 100$. The red dashed line marks the mean value of biomass $\bar{B}$, and the red dotted line indicates 3σ above the mean. Clearly the biomass values do not deviate significantly from the mean. The line indicates the value $\langle B(t) \rangle + 2\sigma$.

Chapter 6

Conclusion

The work presented in this thesis is motivated by the advent of novel modeling approaches to understand the emergent collective dynamics of complex systems. The focus of the problems has been numerical experimentation and analysis of dynamics on spatially extended systems. This approach has revealed a rich diversity of behaviours which are pervasively observed, although the underlying mechanisms of their generation has largely eluded explanation. The research work in this thesis provides analysis and characterization of these emergent behaviours, arising from the interplay of local dynamics and the form and topology of coupling, in complex dynamical systems.

In the first problem that was explored, we present a model of a non fatal infection spreading across a population within a bounded region. The dynamics of infection at the individual level was represented by the SIRS model, where a susceptible (S) individual becomes infected by infected individuals (I) in its immediate neighbourhood, and then proceeds deterministically to the refractory phase (R) which provides them with temporary immunity, at the end of which they become susceptible again. We observe the impact of a heterogenous initial condition, with a mixture of individuals at different phases of the disease and located randomly, on the asymptotic persistence of infection in the population. The interplay of deterministic dynamics at the individual level with the randomness of locations, owing to the locality of the interactions, reveals interesting emergent phenomena from the system.

The persistence of infection in the population was studied under increasing heterogeneity in the partitioning of the population into different disease compartments, as well as increasing heterogeneity in the phases of the disease among individuals within a compartment. Our main observation was that a uniform distribution of phases in the population

led to the burnout of the infection in the population, and the population evolves to a homogenous state with all individuals becoming susceptible. However, the presence of even a single infected individual in a sufficiently mixed distribution of individual phases, leads the population to evolve to a dynamic steady state with persistent spatiotemporal oscillations, or waves, of infection being generated and spreading across the system. We characterize the basin of these asymptotic states, and investigate the effects of further randomizing the phases within each disease compartment. We find qualitatively similar results for such controls, leading us to the the conclusion that heterogeneity in the initial state enables the persistence of spatiotemporal oscillations of infection in such systems.

In the following study we investigated the role of synchronization of the disease phases on the persistence of infection in the system presented above. We not only explored synchronization in the asymptotic and global context, but we also defined and observed the synchronization of disease phases in the initial few time steps of the system's evolution, as well as in local patches. The motivation behind this approach was to explore whether early transient local synchronization could act as a consistent precursor to the presence or absence of infection in the asymptotic state of the population, thus providing an early warning signal and enabling us to anticipate the final state of the system. We demonstrated clear correlations between low synchrony and high probabilities of persistent infection, and established the effectiveness of utilizing transient local synchronization as a measure of the future persistence of infection in the population.

So far, we had been implementing a uniformly random distribution of initial phases for our investigations of the spreading of infection in a population. Subsequently, we studied the impact of segmenting the population into distinct communities, with varying densities of infected sub-populations, on the asymptotic prevalence of infection. We found that even when the average density of infection is too high to sustain persistent oscillations (when distributed uniformly in space), the community structure enabled certain spatially distinct parts of the system to support persistent oscillations, which eventually spread across to the rest of the population, thus attracting it to an asymptotically persistent state. We also observed that the spatial spreading patterns of infection are distinct in each community. Instead of homogenising over time, the communities maintained signatures, akin to some memory, of their initial states. This observation is especially surprising, in context of the temporal behaviour of the communities, namely the average fraction of the infected sub-population in each community, which show striking similarities.

The first three studies on the spatiotemporal dynamics of an infection spreading across a population in a closed region, have revealed very interesting and counter intuitive

emergent phenomena. Although the model is very simple in terms of the individual dynamics as well as the form of interaction between the elements, it is readily applicable in the broad context of critically damped excitation relaxation oscillators, spread out in space and interacting with each other. Such examples are ubiquitous in their presence in biological systems, from cardiac tissues to neurons. The observed asymptotic states are reminiscent of many dynamical behaviours which are found in such real-world systems, but which have proven to be exceptionally tricky to model and analyze.

Certain possible modifications to, and generalizations of, the system described above will surely reveal a richer, wider gamut of complex dynamical phenomena. For instance, motivated by the variability of immune responses of individuals to a certain disease, one such modification could be the inclusion of variability in the timescales of each oscillator in the system. This could establish the importance of the ratio of the lengths of the infectious and refractory phases, to the total length of the disease cycle, in determining the collective emergent behaviour of the system. Another possible aspect of the system that may be investigated is the impact of mobility on the persistence of infection. Allowing the oscillators to move in space as random walkers, and interacting only when they are within a certain radius of each other, could reveal interesting patterns and mechanisms of spreading and sustaining the oscillations of the infected sub-population in the system.

In a final study, we investigated the effect of a novel form of coupling on a network of one dimensional chaotic population maps. The form of coupling is motivated by indirect interactions between isolated patches where a population resides, via the environment. We modeled the impact of these indirect interactions between such patches by reinterpreting the map as a combination of two distinct terms - one for growth, and the other as a nonlinear feedback term to suppress growth. The interplay of these two terms leads to the unimodal nature of the dynamical map at the individual scale. We modified the feedback term at each node to reflect the indirect interactions with their neighbours, by including feedback not only from a node to itself, but also from its neighborhood. We observed that this form of coupling leads to a very asymmetric state of the overall system, where the activity at certain nodes gets suppressed, and a few nodes show explosive activity, going well beyond the average populations present in the network. We investigated the impact of gradually increasing the coupling neighborhood for each node, and it was found that suppression of activity occurred for a larger fraction of the nodes, along with increase in the extent of explosive activity at fewer and fewer nodes. After analyzing the spatial distributions, as well as the biomass distributions over time, we concluded that this emergent behaviour is akin to the generation of extreme events, in both space and time. Thus we found a novel mechanism for the generation of extreme events in a

network of chaotic populations.

Although we established the robustness of our results for unimodal maps in the interval $[0, \infty)$ in the study elucidated above, it is imperative to generalize this notion of parametric coupling, and extend it to systems with multiple state variables, as well as continuous time systems. A rigorous definition of the notion of the *feedback term* utilized in the above investigation, needs to be developed. This study has, figuratively, opened a door towards analyzing how cross-coupling of state variables from neighbouring dynamical units, provides a mechanism for the generation of extreme events. It would be interesting to explore new and original coupling forms that directly modify the *parameters* of the dynamical elements of a complex system, based on inputs from their neighborhood. Such models, if fitted to real-world data, would provide deep and enduring insights into the underlying cause and effect relationships present in complex systems such as ecosystems, which usually elude intuitive understanding.

In conclusion, through these studies, apart from revealing and characterising a range of interesting dynamical regimes shown by these spatially extended models, we have established that such models provide an inventory of very effective tools to investigate and analyze the rich dynamics demonstrated by such systems. The results and insights from the simple models analyzed in these studies provide a basis to understand and model many real-world systems.

Bibliography

[1] Edward N Lorenz. Deterministic nonperiodic flow. *Journal of the atmospheric sciences*, 20(2):130–141, 1963.

[2] Chiranjit Mitra, Anshul Choudhary, Sudeshna Sinha, Jürgen Kurths, and Reik V Donner. Multiple-node basin stability in complex dynamical networks. *Physical Review E*, 95(3):032317, 2017.

[3] RM May. Simple mathematical models with complicated dynamics. *Nature*, 261(1):976, 1979.

[4] Yoshiki Kuramoto and Ikuko Nishikawa. Statistical macrodynamics of large dynamical systems. case of a phase transition in oscillator communities. *Journal of Statistical Physics*, 49(3-4):569–605, 1987.

[5] Daniel M Abrams and Steven H Strogatz. Chimera states for coupled oscillators. *Physical review letters*, 93(17):174102, 2004.

[6] James P Crutchfield and Kunihiko Kaneko. Phenomenology of spatio-temporal chaos. In *Directions In Chaos—Volume 1*, pages 272–353. World Scientific, 1987.

[7] Per Bak, Chao Tang, and Kurt Wiesenfeld. Self-organized criticality: An explanation of the 1/f noise. *Physical review letters*, 59(4):381, 1987.

[8] Kunihiko Kaneko. Overview of coupled map lattices. *Chaos: An Interdisciplinary Journal of Nonlinear Science*, 2(3):279–282, 1992.

[9] TM Janaki, Sudeshna Sinha, and Neelima Gupte. Evidence for directed percolation universality at the onset of spatiotemporal intermittency in coupled circle maps. *Physical Review E*, 67(5):056218, 2003.

[10] Duncan J Watts and Steven H Strogatz. Collective dynamics of 'small-world' networks. *nature*, 393(6684):440, 1998.

[11] Albert-László Barabási, Erzsebet Ravasz, and Tamas Vicsek. Deterministic scale-free networks. *Physica A: Statistical Mechanics and its Applications*, 299(3-4):559–564, 2001.

[12] Colin McEvedy. The bubonic plague. *Scientific American*, 258(2):118–123, 1988.

[13] Martin M Kaplan and Robert G Webster. The epidemiology of influenza. *Scientific American*, 237(6):88–107, 1977.

[14] Andrew Cliff and Peter Haggett. Island epidemics. *Scientific American*, 250(5):138–147, 1984.

[15] Erik M Rauch, Hiroki Sayama, and Yaneer Bar-Yam. Dynamics and genealogy of strains in spatially extended host–pathogen models. *Journal of Theoretical Biology*, 221(4):655–664, 2003.

[16] Cristopher Moore and Mark EJ Newman. Epidemics and percolation in small-world networks. *Physical Review E*, 61(5):5678, 2000.

[17] Robert M May and Alun L Lloyd. Infection dynamics on scale-free networks. *Physical Review E*, 64(6):066112, 2001.

[18] Romualdo Pastor-Satorras and Alessandro Vespignani. Epidemic dynamics and endemic states in complex networks. *Physical Review E*, 63(6):066117, 2001.

[19] Anna Litvak-Hinenzon and Lewi Stone. Spatio-temporal waves and targeted vaccination in recurrent epidemic network models. *Journal of the Royal Society Interface*, 6(38):749–760, 2008.

[20] Quan-Xing Liu, Rong-Hua Wang, and Zhen Jin. Persistence, extinction and spatio-temporal synchronization of sirs spatial models. *Journal of Statistical Mechanics: Theory and Experiment*, 2009(07):P07007, 2009.

[21] Sitabhra Sinha, Jari Saramäki, and Kimmo Kaski. Emergence of self-sustained patterns in small-world excitable media. *Physical Review E*, 76(1):015101, 2007.

[22] Marcelo Kuperman and Guillermo Abramson. Small world effect in an epidemiological model. *Physical Review Letters*, 86(13):2909, 2001.

[23] Prashant M Gade and Sudeshna Sinha. Dynamic transitions in small world networks: Approach to equilibrium limit. *Physical Review E*, 72(5):052903, 2005.

[24] Vivek Kohar and Sudeshna Sinha. Emergence of epidemics in rapidly varying networks. *Chaos, Solitons & Fractals*, 54:127–134, 2013.

[25] CJ Rhodes and RM Anderson. Dynamics in a lattice epidemic model. *Physics Letters A*, 210(3):183–188, 1996.

[26] James M Greenberg and SP Hastings. Spatial patterns for discrete models of diffusion in excitable media. *SIAM Journal on Applied Mathematics*, 34(3):515–523, 1978.

[27] Herbert W Hethcote. Qualitative analyses of communicable disease models. *Mathematical Biosciences*, 28(3-4):335–356, 1976.

[28] Cagri Ozcaglar, Amina Shabbeer, Scott L Vandenberg, Bülent Yener, and Kristin P Bennett. Epidemiological models of mycobacterium tuberculosis complex infections. *Mathematical Biosciences*, 236(2):77–96, 2012.

[29] David JD Earn, Pejman Rohani, Benjamin M Bolker, and Bryan T Grenfell. A simple model for complex dynamical transitions in epidemics. *science*, 287(5453):667–670, 2000.

[30] Michelle Girvan, Duncan S Callaway, Mark EJ Newman, and Steven H Strogatz. Simple model of epidemics with pathogen mutation. *Physical Review E*, 65(3):031915, 2002.

[31] JD Murray. Mathematical biology (biomathematics, vol. 19) 2nd corr. ed, 1993.

[32] Leah Edelstein-Keshet. *Mathematical models in biology*. SIAM, 2005.

[33] Vidit Agrawal, Promit Moitra, and Sudeshna Sinha. Emergence of persistent infection due to heterogeneity. *Scientific reports*, 7:41582, 2017.

[34] Alun L Lloyd and Robert M May. Spatial heterogeneity in epidemic models. *Journal of theoretical biology*, 179(1):1–11, 1996.

[35] Changsong Zhou, Jürgen Kurths, Zoltán Neufeld, and István Z Kiss. Noise-sustained coherent oscillation of excitable media in a chaotic flow. *Physical review letters*, 91(15):150601, 2003.

[36] Faisal Naqib, Thomas Quail, Louai Musa, Horia Vulpe, Jay Nadeau, Jinzhi Lei, and Leon Glass. Tunable oscillations and chaotic dynamics in systems with localized synthesis. *Physical Review E*, 85(4):046210, 2012.

[37] Gordon K Moe, Werner C Rheinboldt, and JA Abildskov. A computer model of atrial fibrillation. *American heart journal*, 67(2):200–220, 1964.

[38] Gil Bub, Alvin Shrier, and Leon Glass. Global organization of dynamics in oscillatory heterogeneous excitable media. *Physical review letters*, 94(2):028105, 2005.

[39] Pak-Ming Lau and Guo-Qiang Bi. Synaptic mechanisms of persistent reverberatory activity in neuronal networks. *Proceedings of the National Academy of Sciences*, 102(29):10333–10338, 2005.

[40] David JD Earn, Pejman Rohani, and Bryan T Grenfell. Persistence, chaos and synchrony in ecology and epidemiology. *Proceedings of the Royal Society of London. Series B: Biological Sciences*, 265(1390):7–10, 1998.

[41] Katia Koelle and John Vandermeer. Dispersal-induced desynchronization: from metapopulations to metacommunities. *Ecology Letters*, 8(2):167–175, 2005.

[42] D Sornette, S Albeverio, V Jentsch, and H Kantz. Extreme events in nature and society, 2005.

[43] Jane Lubchenco and Thomas R Karl. Extreme weather events. *Phys. Today*, 65(3):31, 2012.

[44] Kristian Dysthe, Harald E Krogstad, and Peter Müller. Oceanic rogue waves. *Annu. Rev. Fluid Mech.*, 40:287–310, 2008.

[45] DR Solli, C Ropers, P Koonath, and B Jalali. Optical rogue waves. *Nature*, 450(7172):1054, 2007.

[46] Ryan Kinney, Paolo Crucitti, Reka Albert, and Vito Latora. Modeling cascading failures in the north american power grid. *The European Physical Journal B-Condensed Matter and Complex Systems*, 46(1):101–107, 2005.

[47] Fabrizio Lillo and Rosario N Mantegna. Power-law relaxation in a complex system: Omori law after a financial market crash. *Physical Review E*, 68(1):016119, 2003.

[48] Vimal Kishore, MS Santhanam, and RE Amritkar. Extreme events on complex networks. *Physical review letters*, 106(18):188701, 2011.

[49] Gerrit Ansmann, Rajat Karnatak, Klaus Lehnertz, and Ulrike Feudel. Extreme events in excitable systems and mechanisms of their generation. *Physical Review E*, 88(5):052911, 2013.

[50] William E Ricker. Stock and recruitment. *Journal of the Fisheries Board of Canada*, 11(5):559–623, 1954.

[51] Sitabhra Sinha and Sudeshna Sinha. Evidence of universality for the may-wigner stability theorem for random networks with local dynamics. *Physical Review E*, 71(2):020902, 2005.

[52] Anshul Choudhary and Sudeshna Sinha. Balance of interactions determines optimal survival in multi-species communities. *PloS one*, 10(12):e0145278, 2015.

[53] Timothy Killingback, Gregory Loftus, and Bala Sundaram. Competitively coupled maps and spatial pattern formation. *Physical Review E*, 87(2):022902, 2013.

[54] Tomislav Stankovski, Tiago Pereira, Peter VE McClintock, and Aneta Stefanovska. Coupling functions: universal insights into dynamical interaction mechanisms. *Reviews of Modern Physics*, 89(4):045001, 2017.

[55] V Balakrishnan, Catherine Nicolis, and Grégoire Nicolis. Extreme value distributions in chaotic dynamics. *Journal of Statistical Physics*, 80(1-2):307–336, 1995.

[56] JR Sánchez, J González-Estévez, R López-Ruiz, and MG Cosenza. A model of coupled maps for economic dynamics. *The European Physical Journal Special Topics*, 143(1):241–243, 2007.